



HUNGARIAN UNIVERSITY OF AGRICULTURE
AND LIFE SCIENCES

IMPROVEMENT OF KNEE PROSTHESIS
GEOMETRY

TÉRDPROTÉZIS GEOMETRIA JAVÍTÁSA

PhD dissertation

by
Kheireddine Zehouani

DOI: 10.54598/002110

Gödöllő
2022

Doctoral school

Denomination: Mechanical Engineering PhD School

Science: Biomechanical Engineering Sciences

Leader: Prof. Dr. Gábor Kalácska, DSc
Institute of Technology
Hungarian University of Agriculture and Life Sciences,
Szent István Campus, Gödöllő, Hungary.

Supervisor: Dr. István Oldal
Institute of Technology
Hungarian University of Agriculture and Life Sciences,
Szent István Campus, Gödöllő, Hungary.

CONTENTS
CONTENTS

NOMENCLATURE AND ABBREVIATIONS.....	6
1. INTRODUCTION AND OBJECTIVES.....	8
1.1. Introduction	8
1.2. Research objectives	10
2. LITERATURE REVIEW.....	11
2.1 Knee joint geometry	11
2.1.1. <i>Anatomical description of the knee</i>	11
2.1.2. <i>Ligaments</i>	14
2.2. Knee prosthesis	17
2.2.1. <i>Total knee replacement</i>	18
2.2.2. <i>Formal prosthesis</i>	18
2.2.3. <i>Tibial prosthesis</i>	18
2.2.4. <i>Patella prosthesis</i>	18
2.3. Knee kinematics	19
2.3.1. <i>Tibiofemoral motion</i>	20
2.4. Description of the calculations employed in the ADAMS model	22
2.4.1. <i>Movement of the femorotibial joint out of the plan sagittal</i>	23
2.4.2. <i>Synthesis of joint movements</i>	25
2.4.3. <i>Reverse dynamics analysis</i>	26
2.4.4. <i>Optimization of muscle strength</i>	28
2.4.5. <i>Contact forces</i>	28
2.5. Summary of literature review evaluation	31
3. MATERIAL AND METHODS	34
3.1. Femur	34
3.2. Patella	34
3.3. Tibia	35
3.4. The movements of the knee	36
3.4.1. <i>Knee flexion</i>	36
3.4.2. <i>Knee rotation</i>	36
3.5. Ligaments (springs)	37
3.6. Machines	37
3.6.1. <i>Machine for measurement of the knee prosthesis</i>	37
3.7. ADAMS program	40
3.8. The Virtual Multibody Model	40
3.8.1. <i>Femur axis</i>	41
3.8.2. <i>Tibia axis</i>	42
3.8.3. <i>Patella axis</i>	42
3.8.4. <i>Cylindrical joint</i>	43
3.8.5. <i>Motion of the geometry</i>	44
3.8.6. <i>Friction</i>	44
3.8.7. <i>Principal components knee motion</i>	45
3.9. Boundary conditions for the simulation	45
	44

3.10.	Block diagram showing the applied steps of the multibody virtual model created in the ADAMS software.....	46
4.	RESULTS AND DISCUSSION.....	47
4.1.	The virtual multibody model M1.....	47
4.1.1.	<i>Simulation of the multibody model M1 in different range of rotation.....</i>	48
4.1.1.1	<i>Simulation of the multibody model M1 at the position of 25°.....</i>	48
4.1.1.2	<i>Simulation of the multibody model M1 at the position of 50°.....</i>	49
4.1.1.3	<i>Simulation of the multibody model M1 at the position of 100°.....</i>	51
4.1.2.	<i>Experimental measurement result for test machine of the hungarian university of agriculture engineering and Life Science.....</i>	51
4.1.3.	<i>Comparing the results of the current study of the numerical measurement method and the experimental measurement result for the Hungarian University of Agriculture Engineering and Life Science test machine.....</i>	51
4.2.	The virtual multibody model M2.....	54
4.3.	Developing the kinematic motion of multibody model for the knee prosthesis geometry.....	59
4.4.	Developing the new prosthesis geometry.....	69
4.4.1.	<i>Boundary conditions for the simulation</i>	72
4.4.2.	<i>Simulation of the multibody model in different positions.....</i>	72
4.4.2.1	<i>Simulation of the multibody model at the position of 25°.....</i>	72
4.4.2.2	<i>Simulation of the multibody model at the position of 50°.....</i>	73
4.4.2.3	<i>Simulation of the multibody model at the position of 100°.....</i>	74
4.4.3.	<i>Comparing the current study results of the new multibody numerical measurement with a previous results from my previous multibody model.....</i>	75
5.	NEW SCINTIFFIC REULTS.....	81
6.	CONCLUSIONS AND SUGGESTIONS	82
7.	SUMMARY	83
8.	APPENDICES	85
	A1. Bibliography	85
	A2. Publication related to the dissertation	90
9.	ACKNOWLEDGEMENT	93

NOMENCLATURE AND ABBREVIATIONS

NOMENCLATURE AND ABBREVIATIONS

F_{PF}	Patellofemoral compression force (N)
F_{tf}	Tibiofemoral compression force (N)
F_q	Quadriceps tendon force (N)
F_s	Friction force (N)
F_N	Normal force (N)
F_h	Hamstring muscle force (N)
F_{GR}	Measured ground reaction force (N)
$F_{extension}$	Extension torque (Nm)
$F_{flexion}$	Flexion torque (Nm)
BW	Body weight force (N)
D_h	Moment arm of hamstrings muscle (mm)
D_{pl}	Moment arm of patellar tendon (mm)
D_r	Moment arm for external force (mm)
M_q	Moment arm of the quadriceps force about the patellofemoral contact point (cm)
M_{act}	Moment arm of the patellar tendon force about the patellofemoral contact point (cm)
M_{eff}	Actual moment arm of patellar tendon about the tibiofemoral contact point (cm)
d	Moment arm of the net knee moment in case of standard squat (m)
L_{eff}	Effective moment arm of quadriceps tendon (mm)
M_N	Net knee moment (m)
$g(\alpha)$	Approximate function of F_{pt}/F_q ratio (-)
$k(\alpha)$	Approximate function of F_{pf}/F_q ratio (-)
$C_{1-2-3-4}$	Constants for approximate functions (-)
l_{10}	Length of the tibia (cm)
l_{30}	Length of the femur (cm)
l_1	Intersected length of the axis of tibia and the instantaneous line of action of the BW (cm)
l_3	Intersected length of the axis of femur and the instantaneous line of action of the BW (cm)
l_p	Length of the patellar tendon (cm)
l_t	Perpendicular length between the tibia and the tibial tuberosity (cm)
l_f	Perpendicular length between the femoral axis and the line of action of quadriceps tendon force (cm)
λ_1	Dimensionless, intersected tibia length function (-)
λ_3	Dimensionless, intersected femur length function (-)
λ_p	Dimensionless length of patellar tendon (-)
λ_t	Dimensionless thickness of shin (-)
λ_f	Dimensionless thickness of thigh (-)
α	Flexion angle of the knee (°)
β	Angle between the patellar tendon axis and the tibial axis (°)

NOMENCLATURE AND ABBREVIATIONS

γ	Angle between the axis of tibia and the line of action of the BW force ($^{\circ}$)
δ	Angle between the axis of femur and the line of action of the BW force ($^{\circ}$)
φ	Angle between the tibial axis and tibiofemoral force ($^{\circ}$)
ρ	Angle between the patellar tendon and the patellar axis ($^{\circ}$)
ε	Angle between the patellar axis and the femoral axis ($^{\circ}$)
Ψ	Angle between the quadriceps tendon and the femoral axis ($^{\circ}$)
ξ	Angle between the quadriceps tendon and the patellar axis ($^{\circ}$)
ϕ	Dimensionless function of the angle between the axis of tibia and the line of action of the BW force (-)
θ	Flexion of femur relative to the tibial axis ($^{\circ}$)
θ_q	Quadriceps force angle with respect to tibial axis ($^{\circ}$)
θ_p	Patellar axis angle with respect to tibial axis ($^{\circ}$)
η_{1-2-3}	Patellar rotation, twist and tilt ($^{\circ}$)
τ	Change in patellofemoral mechanism angle ($^{\circ}$)
ϑ^m	Angular acceleration (1/s ²)
x_c	Position of center of gravity in the x direction (m)
y_c	Position of center of gravity in the y direction (m)
z_c	Position of center of gravity in the z direction (m)
t	Constant for t-tests (-)
r^2	Linear correlation coefficient between the original and modelled data values (-)
d_{b1}	Basic circle of the driving gear (m)
d_{b2}	Basic circle of the driven gear (m)
V_1	Contact velocity of the driving gear (m/s)
V_2	Contact velocity of the driven gear (m/s)
ω_1	Angular velocity of the driving gear in the contact (1/s)
ω_2	Angular velocity of the driven gear in the contact (1/s)
x	Sliding-rolling ratio (-)
ρ_{r-s}	Rolling-sliding ratio (-)
\vec{r}_{ci}	Displacement vector describing the path of the contact points (m)
\vec{r}_{CMF}	Displacement vector of the center of mass regarding the femur (m)
\vec{r}_{CMT}	Displacement vector of the center of mass regarding the tibia (m)
\vec{v}_{CMF}	Velocity vector of the center of mass regarding the femur (m/s)
\vec{v}_{CMT}	Velocity vector of the center of mass regarding the tibia (m/s)
$\vec{\omega}_{CMF}$	Angular velocity vector of the center of mass regarding the femur (1/s)
$\vec{\omega}_{CMT}$	Angular velocity vector of the center of mass regarding the tibia (1/s)
\vec{e}_{ci}	Tangential unit-vector of the contact path (-)
\vec{r}_{CF}	Displacement vector determining the contact point with respect to the center of mass of the femur (m)
\vec{r}_{CT}	Displacement vector determining the contact point with respect to the center of mass of the tibia (m)
\vec{v}_{CF}	Velocity vector of the contact point with respect to the center of mass of the femur (m/s)
\vec{v}_{CT}	Velocity vectors of the contact point with respect to the center of masses of the tibia (m/s)

NOMENCLATURE AND ABBREVIATIONS

v_{CFt}	Tangential velocity components in the contact point regarding the femur (m/s)
v_{CTt}	Tangential velocity components in the contact point regarding the tibia (m/s)
v_{CFn}	Normal velocity components in the contact point regarding the femur (m/s)
v_{CTn}	Normal velocity components in the contact point regarding the tibia (m/s)
S_{femur}	Arc length of femur (m)
S_{tibia}	Arc length of tibia (m)
μ_s	Static coefficient of friction (-)
μ_d	Dynamic coefficient of friction (-)
TKR	Total knee replacement
ACL	Anterior cruciate ligament
PCL	Posterior cruciate ligament
MCL	Medial cruciate ligament
LCL	Lateral cruciate ligament
SD	Standard deviation
COP	Center of pressure
COG	Center of gravity
ODE	Ordinary differential equations
DAE	Differential-algebraic equations
CCD	Charge-couple device

1. INTRODUCTION AND OBJECTIVES

1. INTRODUCTION AND OBJECTIVES

In this chapter, the importance of the research topic is presented along with this research's objectives.

1.1. Introduction

The knee joint is the largest joint in the human body and the joints most commonly affected by arthritis. Fig1.1. The knee joint is a hinge joint, meaning it allows the leg to extend and bend back and forth with a minimal side-to-side motion. It is comprised of bones, cartilage, ligaments, tendons, and other tissues. (Olinski et al., 2016). The human knee is a complex joint located between the leg and the thigh, below the body's center of gravity. It is often considered an organ of biological transmission comparable to a torque converter (Mesfar, 2005). In this context, mechanically, the articular surfaces are considered to support bearings. The muscles are the system's motor or brake organs, and the ligaments provide the link for transmission. The literature includes a multitude of research studies interested in studying the human knee joint. This work covers several aspects, such as the functioning, diagnosis, prevention and treatment of injuries. Their goal is to understand the biomechanics of the joint, predict potentially harmful loads and prescribe rehabilitation techniques. Just like experimental studies, numerical studies help in the prevention of injury and degeneration. In addition, an appropriately developed EF model is a powerful tool to predict the effects of the different parameters involved and provide information complex to obtain from experience. 3D planning of your total knee prosthesis: The new technology allows an ideal preparation and positioning of your knee prosthesis. Traditionally, preoperative planning is based on x-rays to determine the size and positioning of your prosthesis, Optimizing its implementation using 3-dimensional planning by computer and imaging—realization of tailor-made, personalized instruments. The new technology allows an ideal preparation and positioning of your knee prosthesis. Traditionally, preoperative planning has been based on x-rays to determine the size and positioning of your prosthetic knee. These x-rays give a two-dimensional image. The new technology uses MRI or CT scans of your knee to develop specific and unique instruments. These images are three-dimensional and, therefore, exact. The new technology allows the doctor to do a complete preoperative assessment and be more precise in the placement of your prosthesis. This technique also reduces bleeding, the duration of the operation and therefore the risk of intraoperative complications Fig. 1.1.

The human knee joint usually suffers progressive deterioration with time. The conventional cure of this issue is to replace it with an alternate knee by applying the prosthesis implant. The reason is that the process causes the abrasion of the different materials rather than just sliding or rolling. This study aims to develop the numerical measurement of the knee prosthesis's geometry, which fulfils the mechanical requirements of the human knee. The MSC.ADAMS programme was applied to demonstrate the movement of the human knee joint in terms of rotation and flexion. The changes between the condyles of the developed Multibody of the prosthesis related to the flexion angle ranging from 20–120° were investigated and presented. The boundary conditions were determined, and simulations performed using the ADAM's programme. An average value of 0.7 was reached for the slip ration, with the maximum getting up to 0.79. An angle between 110–120° for the flexion angle was obtained. It can be said that the application of the Multibody model saves

1. INTRODUCTION AND OBJECTIVES

Time as there is no involvement of the tibia and the femur as required for the knee prosthesis. More importantly, as the application of the test machine is omitted in our process, our model's approximations to a human knee are carried out directly. Without cost, several measurements for the knee prosthesis could be made and repaired. The study results provide the necessary insight for future tests regarding the movement of the knee joint.

1. INTRODUCTION AND OBJECTIVES

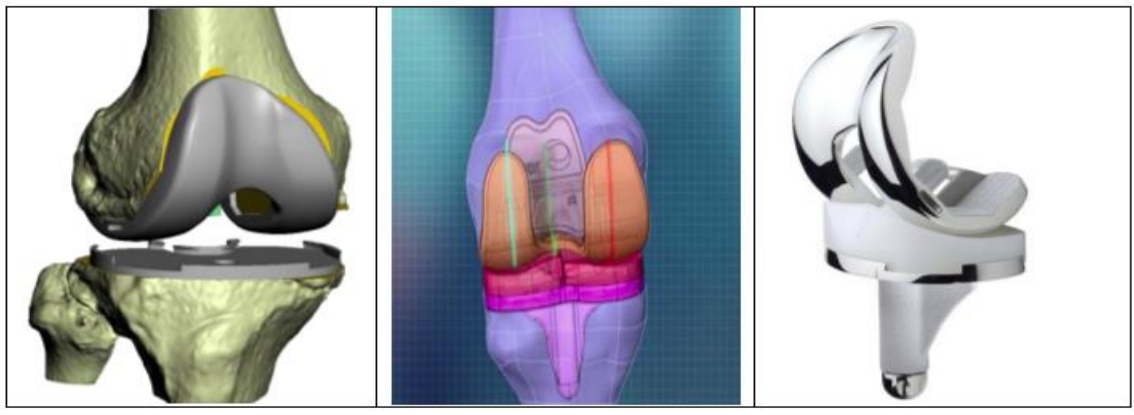


Fig 1.1: Knee prosthesis geometry

1.2. Research objectives

In this research, we will develop the numerical measurement of the knee prosthesis geometry, which fulfils the human knee's requirements mechanically. The objectives of this research can be described as follow:

- To create the new multibody model of the knee prosthesis geometry by using MSC.ADAMS program, within that model to develop the numerical measurement of the knee prosthesis geometry.
- To develop the kinematic motion of the multibody model for the knee prosthesis geometry and this part of the study will be making rotation for Multibody model like Balassa did that with his test machine at MATE university, and we will did the same study to compare our model with his results, with new method with fast result and lower cost.
- To develop the new geometry of the knee prosthesis to reach good results that it can be close to the range the normal human knee motion and will be that great results to reach it.

2. LITERATURE REVIEW

2.1. The knee joint

As I have already mentioned, the knee is the biggest and most complicated joint of the human body, making its movement complex. To study the knee joint movement, we need to know the knee joint's structure, anatomy, and basic functioning. (I use the knee joint and knee words as synonyms for each other).

2.1.1. Anatomical description of the knee

The knee is the largest and most complicated joint in the human body (Bull et al., 2008; Z. KHEIREDDINE, 2019). The knee is a joint connecting the femur (thigh bone), patella (knee cap) and tibia (shin bone). The fibula, connected to the tibia, also forms part of the knee joint. Fig. 2.1 and Fig. 2.2 shows us the main components of the knee joint. In humans, the knees support almost the entire body's weight and are therefore very vulnerable to injury and the development of osteoarthritis.

Osteoarthritis is the abnormal wearing of the cartilage covering the joints and decreasing synovial fluid, which acts as a lubricant for the joints. This results in low-grade inflammation of the joints, which leads to pain and can significantly affect a person's quality of life. For instance, simple tasks like walking or climbing stairs can become difficult. The knee movement can be separated into two significant articulations within the knee, the tibiofemoral articulation and the patellofemoral articulation.

Currently, knee replacement surgery is performed on a large number of people throughout the world. Modern technologies would be required to contribute to this subject within the near future. This means that techniques used for virtual prototyping of mechanical systems must be extended to advanced biomechanical systems to meet the specifications and demands (Ardestani et al., 2015; Katona et al., 2015; Price et al., 2018; Zanasi, 2011)(Bull et al., 2008).

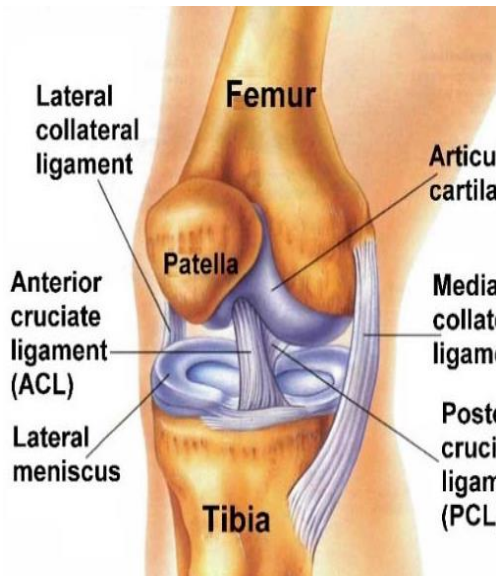


Fig. 2.1 Visible cruciate ligaments for human knee joint (Olinski et al., 2016)

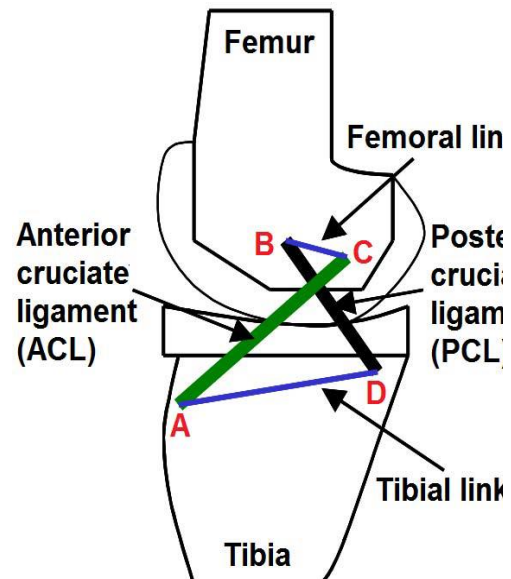


Fig. 2.2 Crossed four-bar mechanism for the left knee (Olinski et al., 2016).

The human knee is a joint that joins the leg to the thigh. From an anatomical point of view, this complex structure consists of two joints: the tibiofemoral joint, which provides the connection between the femur and the tibia, and the patellofemoral joint, which describes the movements of the patella concerning the tibia (Gill, 2016). The tibiofemoral joint is made up of several non-congruent surfaces; the femoral condyles as well as the Tibial plateau. The latter comprises two glenoid cavities: the medial glenoid cavity and the lateral glenoid cavity (Postolka et al., 2020). In the plateau's central part, these cavities straighten out to form the massive Tibial spine (Fig. 2.3). This massive creates a pivot of rotation which engages in the intercondylar notch (which separates the two femoral condyles).

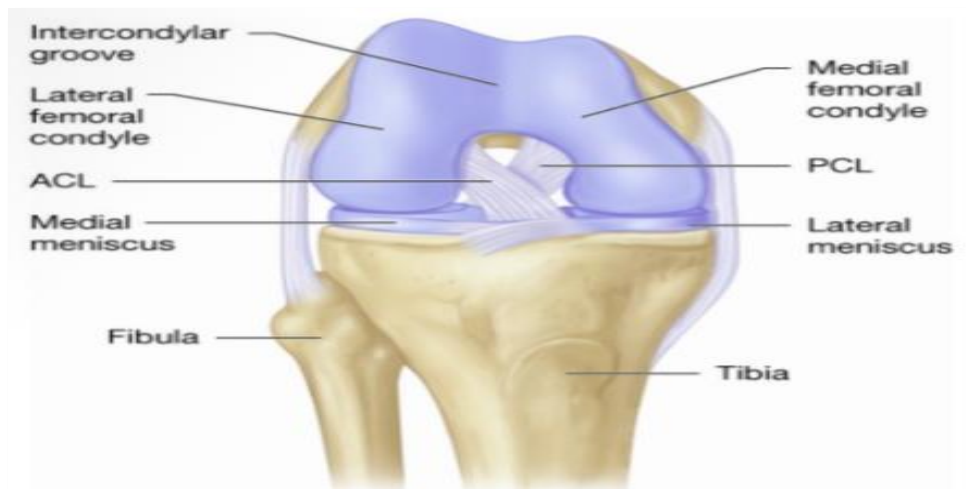


Fig.2.3 The Distal Articulation Components of the femur.

2. LITERATURE REVIEW

Each of the tibiofemoral joint surfaces is covered by layers of the cartilage of varying thicknesses, between which are interposed the menisci (placed between the tibia and the femur). The cohesion of this joint is ensured by a set of ligaments as well as by the patella. We distinguish the anterior cruciate ligament (ACL), the posterior cruciate ligament (PCL), the medial collateral ligament (LCM) and the lateral collateral ligament (LCL). The former two help with anteroposterior stability and flexion-extension, and the latter two provide lateral stability (Percy, 1999). As the femur flexes, an additional contact takes place through the layers of cartilage between the femur and the kneecap. Figs 2.3 and 2.4, respectively, show the different constituents and movements (mainly flexion and extension movements combined with rotations in other planes) of the knee joint.

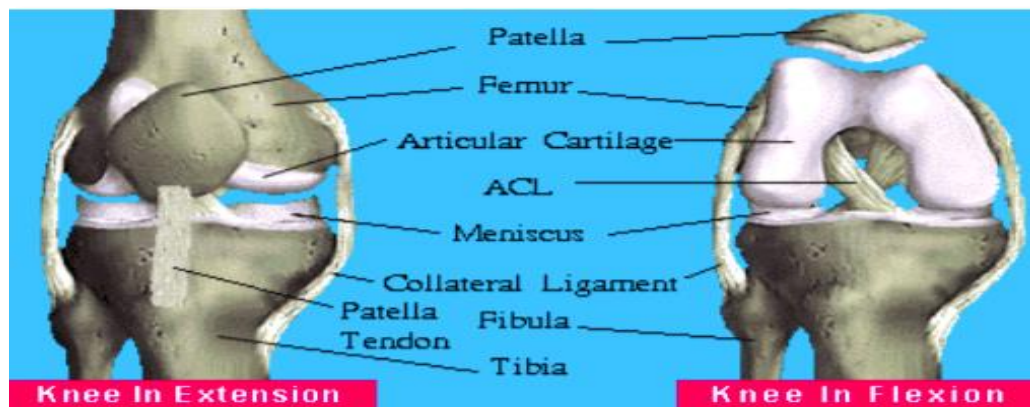


Fig 2.4: Right knee fully extended (left) and flexed (right).

The most efficient process for correcting deformities in the leg and removing pains associated with the knee, and enabling sanctionative patients to resume traditional daily activities is Total knee replacement (TKR) surgery. Since the primary TKR surgery was performed in 1968, enhancements with different materials and methods have drastically increased this method's effectiveness (Bert, 2005; Bull et al., 2008; Phruetthiphat et al., 2021; Vince, 2014).

The proper handling of degenerative abrasion in the knee joint is currently one of the essential orthopedic problems. The appropriate solution for this issue is to remove and replace it with a prosthesis. Unfortunately, no perfect knee prosthesis can replace the original knee because of the knee kinematics' complexity.

During the various daily activities, this joint is exposed to significant loads and movements, which may in some cases exceed the mechanical capacities of its components. Several previous works have mentioned that the compressive force on the knee joint varies from 2 to 4 times the weight of the human body in daily activities such as walking, climbing stairs, etc. (Richards and Higginson, 2010; Sciences et al., 2019). These forces can reach even 11 times the body weight during the practice of particular sports activities (football, skiing, etc.). These heavy loads are responsible for the injuries and pain observed in the knee joint, such as torn meniscus, ruptured ligaments, and osteoarthritis (OA). The latter affected more than 27 million Americans

2. LITERATURE REVIEW

(Christiansen et al., 2012; Richards and Higginson, 2010) and about 4.4 million Canadians (13% of the population) in 2010. This is expected to reach 10.4 million by 2040 for Canadians or 25.6% of the population (Barber et al., 2016). The total economic burden of osteoarthritis is expected to reach \$ 405.1 billion in 2020 (AAFC, 2011). When it comes to problems with anterior cruciate ligament injuries, the American Orthopedic Association (AOS) has reported that approximately 95,000 people have been affected each year. This has led surgeons to perform 50,000 procedures to repair this ligament. This clearly shows that the pathologies are pretty numerous in the human knee, and the treatment sometimes requires a surgical intervention either to repair or to implant.

The knee designates a joint of the lower limbs connecting the leg to the thigh and supporting the weight of the body. It involves three bones, the femur, the tibia and the patella, through three joints, the patellofemoral joint (FP) and the double joint femorotibial (FT), bicondylar. At the distal end of the femoral epiphysis, the femoral trochlea articulates with the posterior surface of the patella. The anterior region of the knee is thus formed by the soft tissues and the patella, located in front of the knee joint, while the posterior region of the knee or popliteal is placed behind the joint. It is a synovial joint whose lubrication is provided by synovial fluid. Cartilage, a thin avascular and non-innervated elastic tissue, protects the bone, ensures the sliding of the articular surfaces easily against each other as well as the fluidity of the movements of the knee. There are two types of articular cartilage, the fibrous cartilage at the level of the menisci and the hyaline cartilage. An extremely low coefficient of friction allows resistance to high compression and tension forces in the lower limbs.

The two main elements that make up cartilage are the matrix and the chondrocyte. The matrix is composed of a network of rigid type II fibrillar collagen fibers which form a solid framework. Inside this collagen network, certain molecules called proteoglycans retain water molecules by a hydrophilic effect.

The chondrocyte is the only cell type of articular cartilage. In adults and under physiological conditions, it is a resting cell that functions in autarky and anaerobically, nourishing itself by imbibition from the synovial fluid. The architecture of cartilage is thus complex and accounts for its biomechanical capacities (Guillemin et al., 2011).

The frontal stability of the knee is ensured by two extra-articular ligaments, an internal lateral ligament and an external lateral ligament. Sagittal stability is provided by two intra-articular cruciate ligaments, forming the pivot of the knee, the anterior cruciate ligament (ACL) and the posterior cruciate ligament (PCL).

Each knee has two menisci, an internal meniscus and an external meniscus. Made up of cartilage, they are interposed between the femur and the tibia in order to stabilize the knee. The different structures of the knee are shown in Fig 2.5 (Id, 2021).

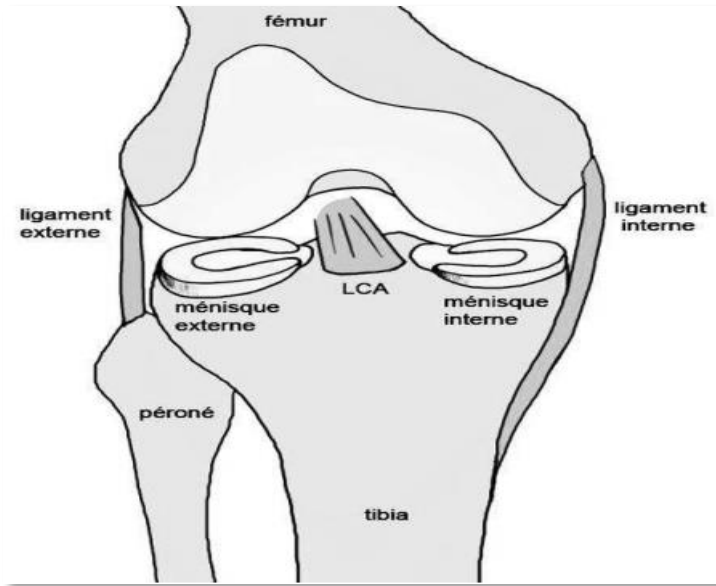


Fig 2.5: Right knee, front view(Id, 2021).

2.1.2. Ligaments

The element that connects the femur and tibia is the ligaments (Imhauser et al., 2017). There are four main ligaments in the knee joint, the lateral and medial collateral ligaments (LCL and MCL) and the posterior and anterior cruciate ligaments (PCL and ACL). These are presented in (Fig 2.6). The ligaments work together to stabilize the knee joint and play a crucial role in its kinematics. The LCL and MCL are attached on the sides of the joint and are responsible for the joint's side-to-side stability. The ACL lies to the front, in the center of the knee joint, and restricts the tibia's anterior movement relative to the femur. The PCL restricts the tibia's rearward movement relative to the femur and lies to the knee joint's back.

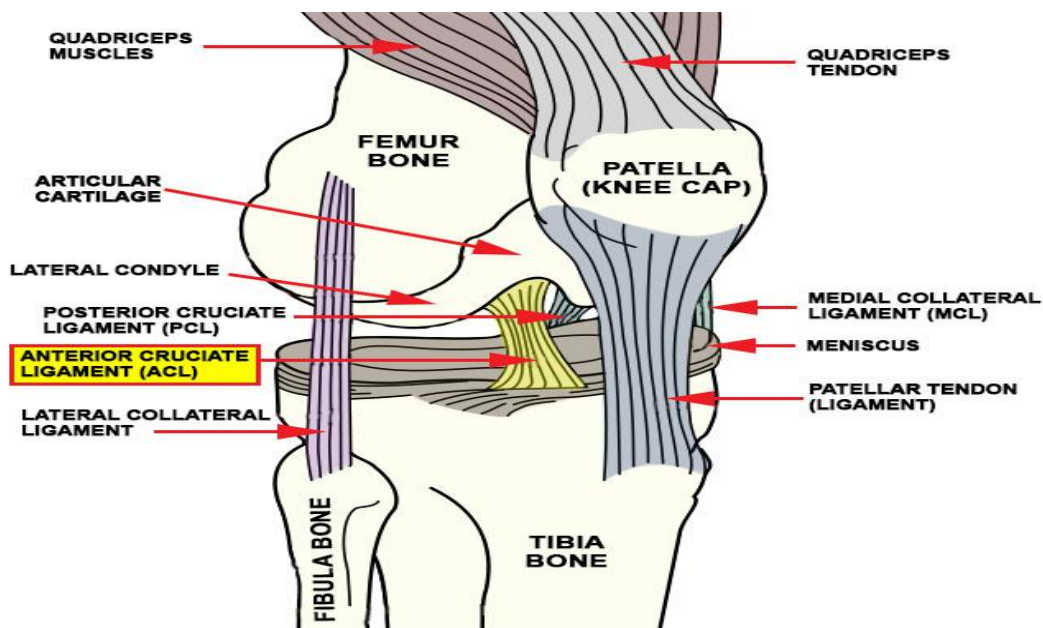


Fig 2.6. Main components of the knee ligaments (Imhauser et al., 2017).

2. LITERATURE REVIEW

Ligaments are bands of connective tissue that are fibrous, elastic and whitish. All of these ligament structures help maintain good joint kinematics (Weiss, 2014). Indeed, the ligaments limit the abnormal movements of the joint while ensuring the maintenance of the bone parts in their physiological position. Normal. Four main ligaments contribute to the relative movement of the tibial-femoral joint; the anterior cruciate ligament (ACL), the posterior cruciate ligament (PCL), the collateral ligament medial (LCM) and lateral collateral ligament (LCL) (Fig 2.6). One of the main characteristics of these ligaments is their excellent resistance to different loads. Therefore, depending on the loading conditions, one or a combination of these ligaments work as a primary restriction in the joint's stability. In addition, the anatomical geometry of these ligaments and the location of their insertion sites (Fig 2.6) have an essential role in joint mobility and stability (Weiss, 2014).

The anterior cruciate ligament (ACL), located in the middle of the knee, is characterized by a width that varies from 7 to 12 mm and an intra-articular length of 32 mm on average (Petersen and Sekiya, 2006). It connects the posterior part of the lateral aspect of the intercondylar notch at the anterior part of the tibial spine (Fig 2.11). This ligament, formed by long and aligned fibers, prevents excessive posterior movement of the femur relative to the tibia. It can be divided into the anteromedial bundle (AM) and the poster lateral bundle (PL). The first is the largest and longest bundle. Kummer and Yamamoto (1988) measured the intra-articular length of the PL bundle of 50 corpses and reported a length of 17.8mm. Furthermore, several cadaveric studies have shown that the PL beam plays a more critical role than the AM beam in ensuring rotational stability (Gabriel et al., 2004; Steckel et al., 2007).

The posterior cruciate ligament (PCL) is located just behind the ACL. It is inserted at the level of the upper half of the medial surface of the intercondylar notch and on the posterior part of the tibial spine (Figure 2-7). Its primary role is to prevent movement of excessive posterior tibia concerning the femur (Steckel et al., 2007). The average length and thickness of the LCP are respectively 38 ± 4 mm and 13 ± 1 mm (Bonasia et al., 2018). It comprises two principal bundles: the posteromedial bundle (PM) and the anterolateral bundle (AL). All Like the ACL bundles, each of these bundles is stretched into positions different from the knee's range of motion (Of et al., 1996).

The medial collateral ligament (MCL) represents a broad, fibrous, flattened band (an average length of 100 to 120 mm). It extends from the top of the internal condylar tuberosity to the medial aspect of the tibia, also attaching to the inner periphery of the medial meniscus (Fig 2.7). It resists internal and external rotations, but its most outstanding contribution is to the overall stiffness of the joint under valgus moments (K. Markolf, Mensch, & Amstutz, 1976; Nielsen, Rasmussen, Ovesen, & Andersen, n.d.). The lateral collateral ligament (LCL) is an almost circular cross-section (an average length of 50mm). It originates from the external condylar tuberosity and ends on the lateral aspect of the fibula head (Fig 2.7). However, this ligament has no anatomical link with the meniscus. external(Price et al., 2018).

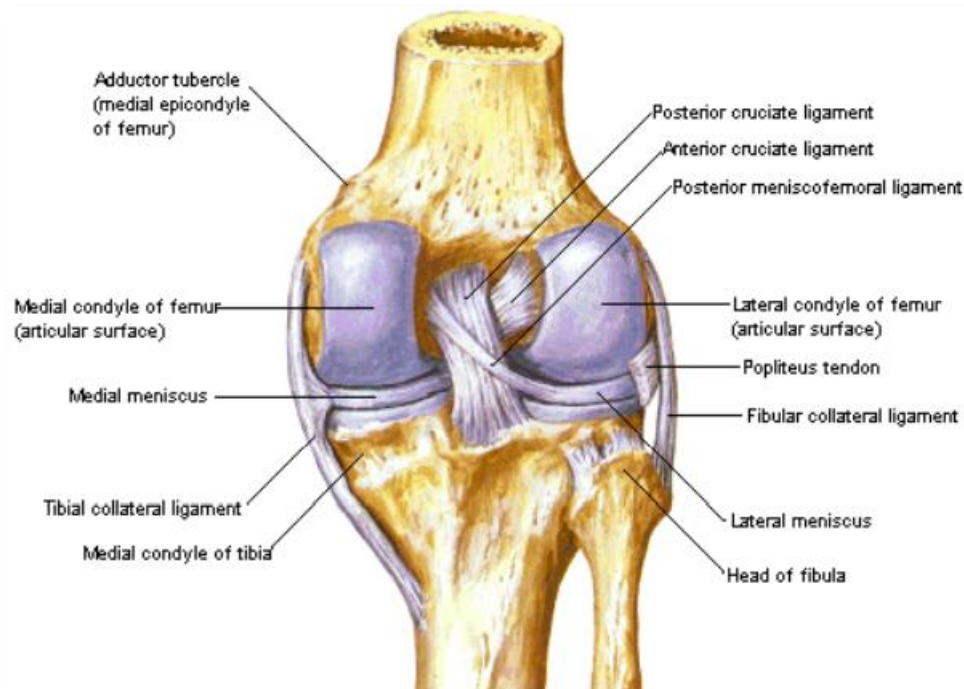


Fig 2.7 Cruciate ligaments (LCA, LCP) and collaterals (LCM, LCL)

Besides these four ligaments, there are other ligaments in the human knee. Namely, the two patellofemoral ligaments (internal and external patellar fins) and the patellar ligament connect the kneecap to the tibia (often called the patellar tendon because it pursues muscle action). Therefore, these ligaments can play a more or less important role in the stability of the joint. Indeed, some studies have mentioned the importance and the potential role of the internal patellar fin in the stability of the patella (Nomura et al., 2000).

To understand the mechanical behavior of knee ligaments, several studies have been carried out to determine the value of different mechanical parameters such as modulus of elasticity, maximum deformation, the energy density at break and maximum stress (Mommersteeg et al., 1996). By examining in vitro three human knees from male donors, (Jones and Grimshaw, 2010) determined the stress-strain curve (Fig 2.8) of the cruciate ligaments (ACL and PCL), the lateral collateral ligament (LCL) and patellar tendon (PT). In this curve, the stiffness increases with the applied stress. This observation was explained later by (Popescu, 2009). According to them, ligaments are tissues similar to cords that connect the femur to the tibia. At large deformations, the waviness of the fibers decreases and therefore, the stiffness increases significantly.

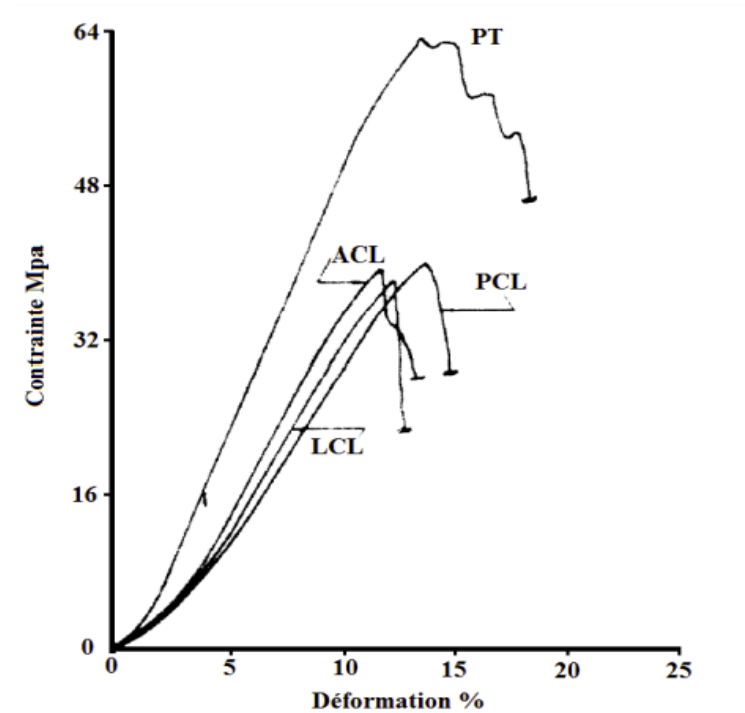


Fig 2.8 Stress-strain curve for the different ligaments: cruciate ligaments (ACL and PCL), lateral collateral ligament (LCL) and patellar tendon (PT) (Feder and Levy, 1992).

4.4 Knee prosthesis

Prosthetic knee replacement is now a mature surgical technique as widely used as total hip replacement. It is primarily intended for patients suffering from knee osteoarthritis when it becomes debilitating and painful and no longer responds to conservative medical and physiotherapeutic treatments. Even in the long term, its results are excellent in patients 70 years of age or older. They can still be improved in younger and more active patients requiring more extended and more intense implants. Infection, aseptic loosening and implantation defects are the most common complications. (Kheireddine and Oldal, 2021) There are currently three forms of knee prostheses allowing the replacement and resurfacing of worn or destroyed compartments:

- The total prosthesis addresses the three compartments of the knee: internal femorotibial, external and patellofemoral.
- The uni-compartmental prosthesis for the internal or external femorotibial compartment.
- The patellofemoral prosthesis. In 1965, the first so-called hinged prostheses appeared. Then, at the end of the 1970s, modern so-called sliding, semi-constrained prostheses appeared; the femoral and tibial parts are independent, but their design ensures stability.

Perfect PTG should be compatible with normal knee function and remove any instability resulting from the pre-existing pathology. It should also have little exposure to wear and tear and have an optimal fixation. To date, all the TKGs represent compromises. Although the prostheses used to strive to meet these requirements, to varying degrees, depending on the situation individual, restoring normal knee function appears to be the most challenging goal to achieve, many questions remain unanswered. So, it is not established that it is possible or even desirable to restore normal kinematics after PTG.

2.2.1. Total knee replacement

The total prosthesis replaces all of the worn cartilage. It is a set of components mechanical which replaces the normal joint, ensuring the same rotational movements and slip like a normal knee. Three-compartment prostheses are made up of three different implants.

2.2.2. Femoral prosthesis

It is fixed on the femur, which will be subjected to significant friction forces and is most often made of a chromium-cobalt alloy (in these mechanical conditions, this alloy is the best tolerated one).

2.2.3. Tibial prosthesis

Which even includes two parts:

- A horizontal metal plate, usually made of titanium for elasticity reasons, anchored in the tibia.
- A removable polyethylene tray is fixed in the metal tray.

2.2.4. Patella prosthesis

It covers the posterior surface of this bone. It included a metal part cemented in the bone on which was fixed a zone of polyethylene friction. Experience has shown that this prosthesis should be eliminated because the polyethylene wedged between two metal surfaces wears out quickly. Fig 2.9 Surgeons are reverted to a patellar prosthesis entirely in polyethylene. Some do not put a prosthesis patella and are satisfied with femoral and tibial prostheses.

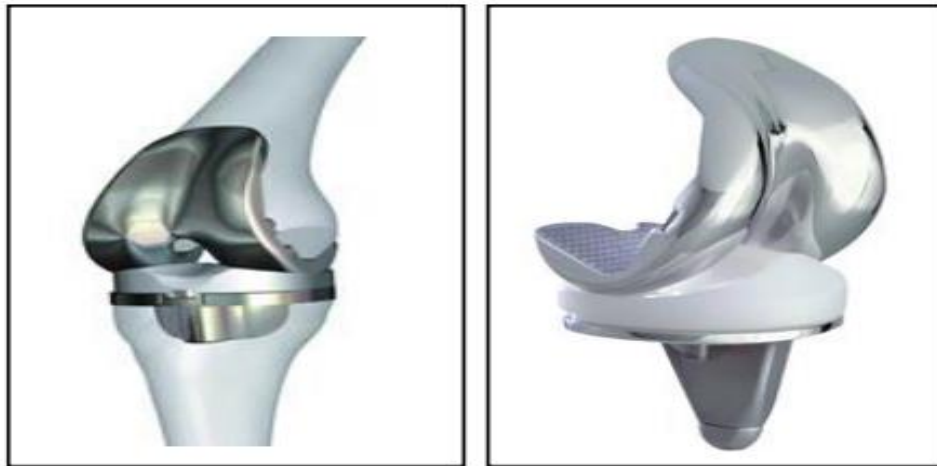


Fig 2.9 Total knee replacement

2.3. Knee kinematics

Fig 2.10 shows us 6 degrees of freedom for the knee joint. It is important to note that the knee joint is not a pure hinge joint but moves with a complex set of translations and rotations in all six degrees of freedom (Komdeur et al., 2002). During normal Flexion of the knee, tibiofemoral motion is a combination of sliding and rolling motions between the contacting tibia and femoral condyles. The motion is constrained by the bones' geometry, as well as the menisci and the muscular attachments via ligaments and tendons. The knee can only reach full extension with a small amount of external tibial rotation on the femur. This is due to the fact that the medial condyle is typically in the order of 12 mm longer than the lateral condyle. This tibial rotation is known as the 'screw home' mechanism, and it allows the knee to be held in full extension without undue fatigue of the surrounding muscles (Komdeur et al., 2002). Therefore, the shapes of the articulating surfaces in the knee are the most important factor when dealing with knee movement.

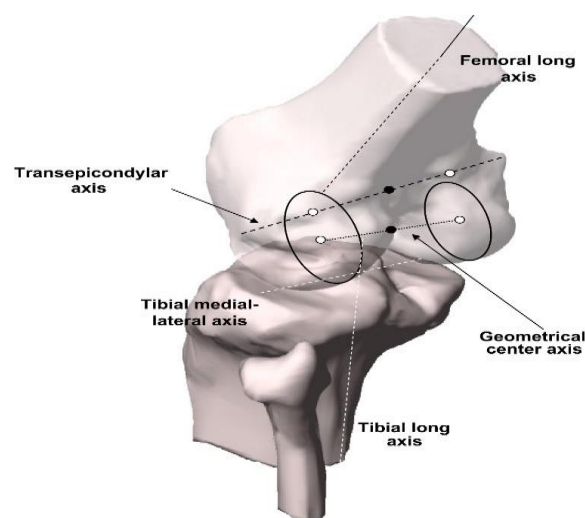


Fig 2.10. Reference directions for knee movement (Komdeur et al., 2002).

2.3.1. Tibiofemoral motion

The posterior condyles' geometry was the first circular and roughly the same size in 1836 by Weber and Weber (Freeman and Pinskerova, 2005). This hypothesis has been used in numerous kinematics-related studies (Freeman and Pinskerova, 2005; Niitsu, n.d.; Williams and Logan, 2004), and is still very popular today. Proposes that the flexion arc can be divided into three segments. The mode of articulation differs for each portion as the shape of the condyle changes. The active functional arc is the portion ranging from about 20° to 120°. This part is known as the Flexion Facet (FFC). The (screw-home) arc stretches from 20° to full extension and is also known as the Extension Facet (EFC). The third portion is known as the passive arc and stretches from about 120° to full Flexion. The three portions are shown in Fig 2.11.

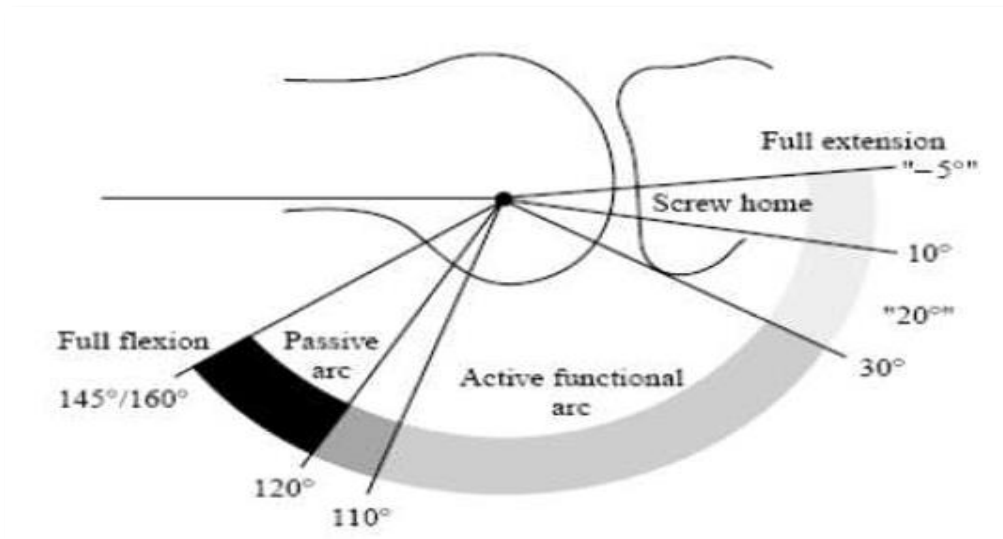


Fig 2.11. The three arcs of Flexion (Freeman and Pinskerova, 2005).

The knee joint has six degrees of freedom, as is shown in Fig 2.12. It is important to note that the knee joint is not a pure hinge joint but moves with a complex set of translations and rotations in all six degrees of freedom (Lenz et al., 2021; Postolka et al., 2020). During normal Flexion of the knee, tibiofemoral motion is a combination of sliding and rolling motions between the contacting tibia and femoral condyles. The motion is constrained by the geometry of the bones and the menisci and the muscular attachments via ligaments and tendons. The knee can only reach full extension with a small amount of external tibial rotation on the femur. This is due to the fact that the medial condyle is typically in the order of 12 mm longer than the lateral condyle. This tibial rotation is known as the 'screw home' mechanism, and it allows the knee to be held in full extension without undue fatigue of the surrounding muscles (Lenz et al., 2021). The shapes of the articulating surfaces in the knee are the most important factor when dealing with knee movement.

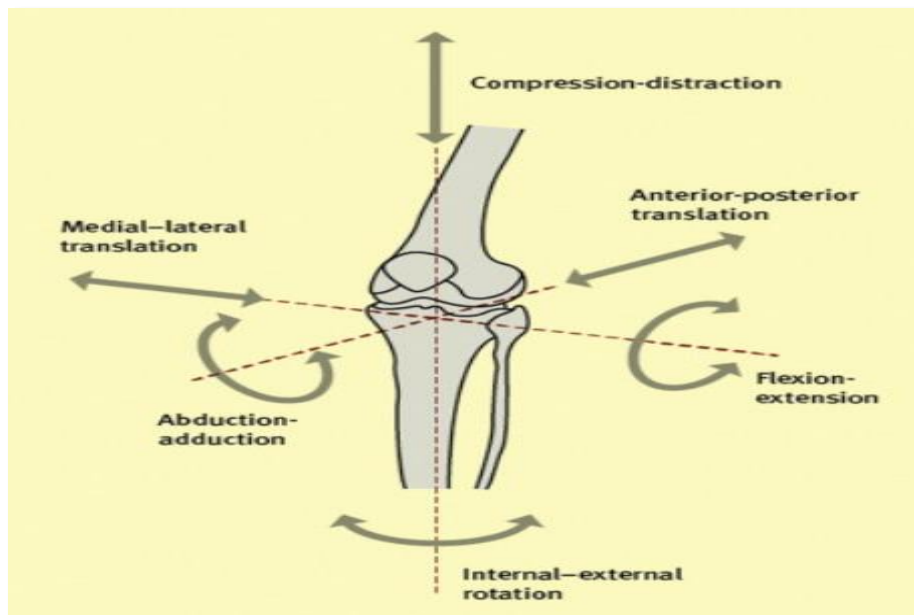


Fig 2.12 Reference directions for knee movement (Lenz et al., 2021)

The experimental poses of each participant's tibia and patella with respect to their femur from the MRIs at approximately 0° , 7° , 15° and 25° of TFJ flexion angle (Fig.2.13) (Barzan et al., 2019). The anatomical landmarks identified in the MRI-reference 0° position, and used to create the initial SCSs, were identified on the corresponding registered bones at 7° , 15° and 25° positions (Fig.2.13b–e). These landmarks were used to create the bones' SCSs and six-degrees-of-freedom kinematics at the four TFJ flexion angles. To ensure that the same fibers within each ligament were chosen, the transformation matrices aligning the SCSs in the MRI-reference pose to the SCSs in 7° , 15° and 25° flexion angles were computed and used to derive the ligaments' attachment points in all poses. For each model, ligaments' lengths were computed as Euclidean distance between the attachment points at all four different poses. The Root-Mean-Square Errors (RMSEs) between each participant's predicted and MRI-measured TFJ, PFJ and ligament kinematics were computed for each kinematic model and averaged across the four TFJ flexion angles. Ninety-five per cent confidence intervals (CI) were also computed. A one-way repeated measures Analysis of Variance (ANOVA) with a priori contrasts were performed to determine differences in the average RMSE between each kinematic model at each TFJ and PFJ degree of freedom and ligament length ($\alpha = 0.05$). Kinematic data were not normally distributed according to Shapiro-Wilk test results. Therefore, Statistical non-Parametric Mapping (SnPM) was used to assess the models' outputs (Pataky et al., 2016). Subsequently, the resulting average kinematic curves from the three models were compared to determine if significant differences existed between the curves at any TFJ flexion angle (Society et al., 2020). To this end, thirty-three nonparametric one dimension two-tailed paired t-tests were conducted on the TFJ and PFJ kinematics, taking into consideration the dependency of all points of each TFJ Flexion ROM ($\alpha = 0.05$) to calculate the critical threshold (t^*) (Penney et al., 2011). There was no correction for multiple hypothesis testing. All SnPM analyses were performed in Matlab using the open-source SPM1D

code (Paelinck, 2018). Additionally, the similarity of the pattern of the TFJ and PFJ kinematic curves from the three models with those from published kinematics was examined using Pearson's correlation (q).

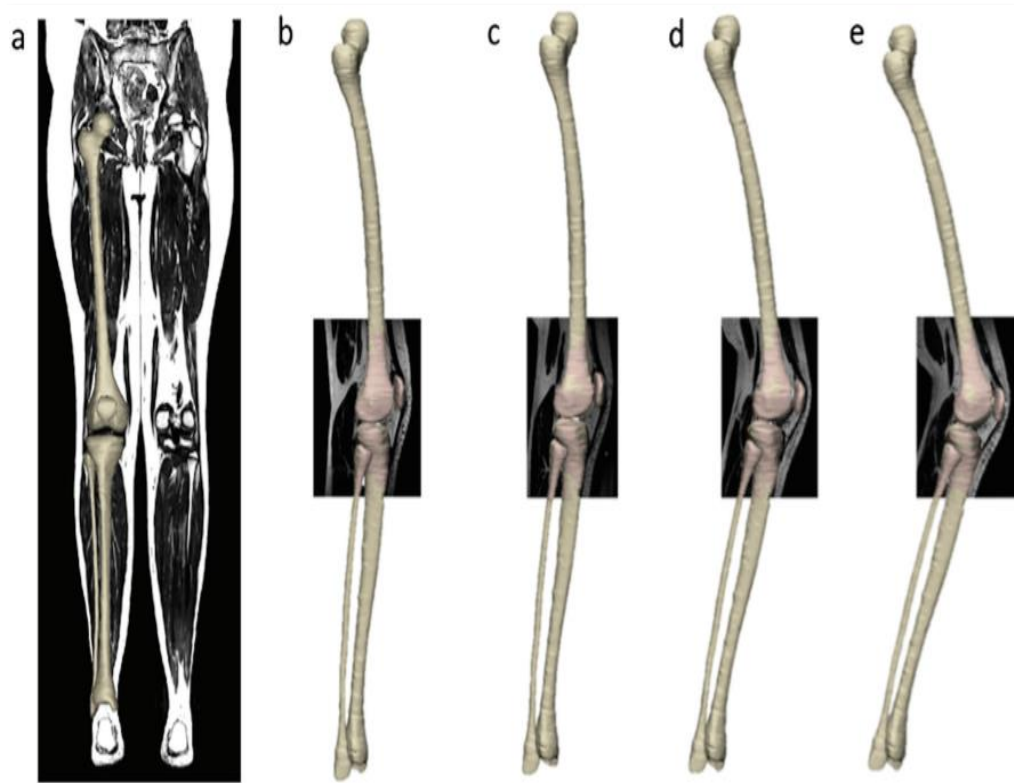


Fig 2.13. Example of full-length bone segmentation from the full lower limb MRI scan (a). Example of bone segmentation from the regional MRI scans at approximately 0°(b), 7°(c), 15° (d) and 25° (e) of TFJ flexion and registration of these bones to the full-length bones (b, c, d, e) (Barzan et al., 2019).

2.4 Description of the calculations Employed in the ADAMS Model

In this part, we will only focus on the movement of the knee in the sagittal plane. The femorotibial joint is made up of several joint surfaces that slide and roll over each other. In this shot, the movement of the knee is called the rolling-sliding motion. This movement is the composition of a rotation and a translation. Fig 2.13 illustrates this type of movement. In the case of pure sliding (see Fig 2.14 (a)), the friction between the femur and the tibia is low enough that the point of contact does not vary during flexion. This case corresponds to a pivot connection. In the case of pure bearing, Fig 2.14 (b), during flexion, the friction between the condyles of the femur and the tibial plateau is large enough to prevent slippage. In this case, there is a displacement of the point of contact, which depends only the flexion angle and diameter of the condyles.

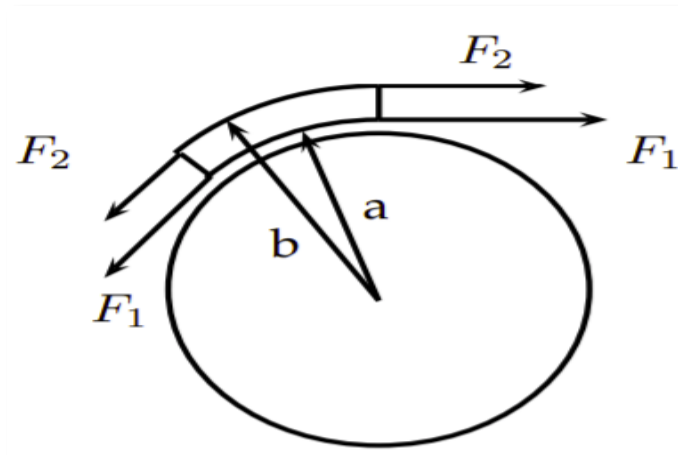


Fig 2.14 Simplified representation of the lengthening of the lever arm of the extensor system of the knee due to the patella (Klein and Sommerfeld, 2014).

Finally, the rolling-sliding case, shown in Fig 2.15 (c), corresponds to the anatomical movement observed with the human joint. In this case, the point of contact is displaced between the tibia and the femur. However, this displacement remains lower than in the case of pure bearing ($l_1 < l_2$). During the flexion of the knee, we observe the three successive movements. For bending less than 20° , the joint performs pure rolling. From 20 to 140° , the joint performs a rolling-sliding motion.

Finally, beyond 140° of flexion, the movement observed is a pure sliding movement, so there is no longer any movement of the point of contact between the tibia and the femur Fig 2.2. This complex movement brings several exciting properties to the knee joint. Thus, a pure rolling or pure sliding movement would limit the articular movement, Figs 2.15. 2.16 illustrates these two behaviors. It is observed that pure rolling causes dislocation of the knee for a flexion angle less than the maximum flexion angle of the knee. The case of pure sliding limits joint movement by early contact between the femur and the tibial plateau. The rolling-sliding movement, therefore, explains the significant joint movement observed in humans. Another attractive property provided by the knee joint movement is that it limits joint wear compared to pure sliding.

2.4.1 Movement of the femorotibial joint out of the plan sagittal

In addition to the rolling-sliding motion presented in the sagittal plane, we observe different rotations in the other planes. Thus, during the transition from full flexion to full knee extension, we observe a rotation of 10° to 15° in the horizontal plane.

2. LITERATURE REVIEW

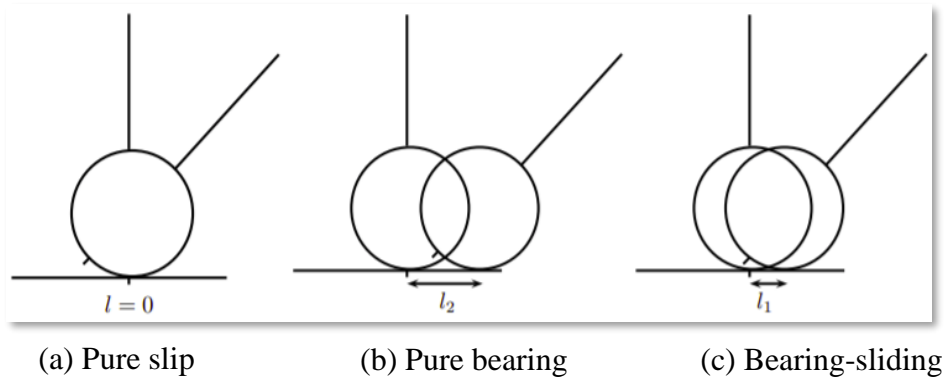


Fig 2.15 Illustration of the rolling-sliding movement (Klein and Sommerfeld, 2014)



Fig 2.16 Side view of the knee in extension and flexion (Subit, 2005).

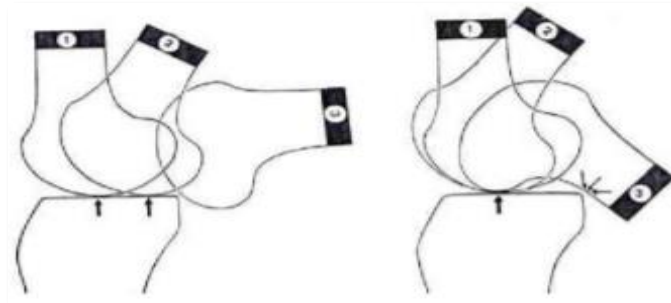


Fig 2.16 Illustration of the extreme behavior in the event of pure rolling or pure sliding (Klein and Sommerfeld, 2014).

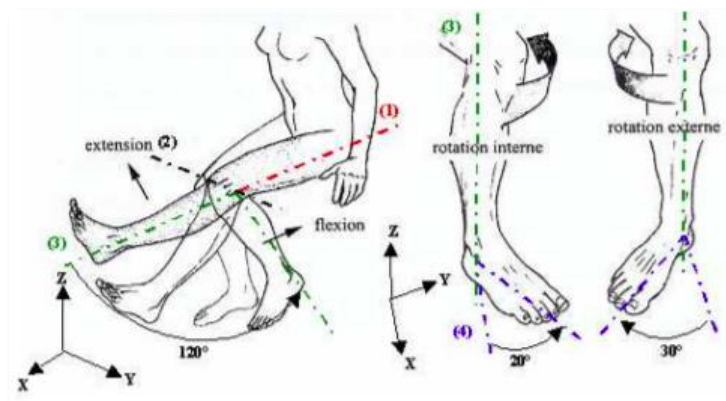


Fig 2.17 The possible movements of the knee (Lepoutre, 2007).

This degree of freedom is due to the non-symmetry of the condyles of the femur in the sagittal plane. This rotation provides more excellent stability when fully extending the knee, allowing for upright standing. In addition, we can observe a movement called varus-valgus of low amplitude in the frontal plane. The shapes of the condyles and tibial glenoid cause a varus-valgus movement of the tibia of about 10° . We see that the patella makes a sliding movement on the trochlea during these movements, which helps to ensure anteroposterior stability. These possible movements in and out of the sagittal plane show that modelling the knee by one or more pivot links does not consider all the knee movements. It should be noted that the majority of bipedal robots use knee joints with a single degree of freedom in rotation. The knee joint is made up of the femorotibial joint and its functional assembly with the patellofemoral joint. Indeed, the patella slides in the throat of the trochlea. Ligaments hold it on the femur and tibia (Fig 2.18). Its essential role is to allow flexion and extension movements of the knee.

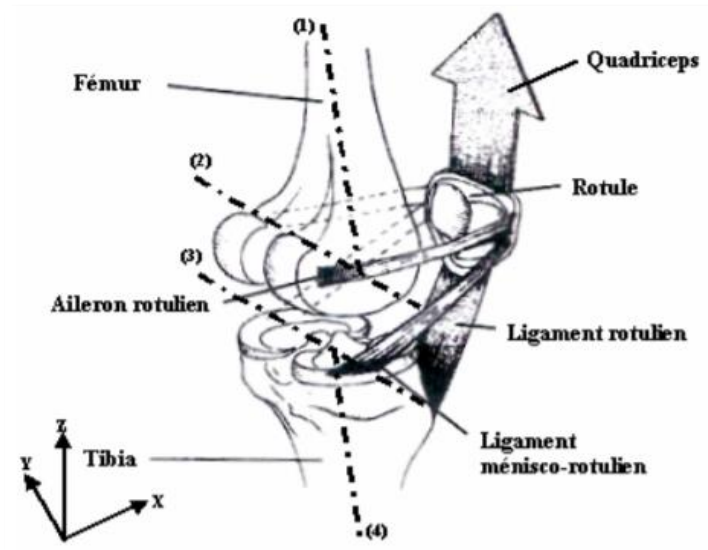


Fig 2.18 The patella and its fixation on the knee (after Calais Germain, 1986);
 (1): longitudinal axis of the femur, (2): axis of the condyles, (3): axis of the tibial plates, (4): longitudinal axis of the tibia.

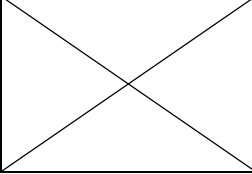
2.4.2. Synthesis of joint movements

The Synthesis of the physiological angular deflections of the main joints of the knee is summarized in Table 1.

Table 1: Angular amplitudes of the joints of the knee joint.

	Angular amplitudes along the antero-posterior axis (X)	Angular amplitudes following the Medio lateral axis (Y)	Angular amplitudes following the vertical axis (Z)
Hip	Max adduction: 30° Max abduction: 45°	Flexion max : 120° Extension max : 20°	Max internal rotation: 30° Max external rotation: 60°

2. LITERATURE REVIEW

Knee		Flexion max : 120° Extension max : 0°	(Knee flexed) Max internal rotation: 20 ° Max external rotation: 30 °
------	---	---	---

The physiological range of motion will characterize the pathological range in the analysis of our results.

2.4.3. Reverse dynamics analysis

Once the kinematic problem is solved, the Lagrange dynamics equations solve the inverse dynamics problem. To do this, we admit d'Alembert's principle, stating that for a given body (i), the sum of the difference between the external forces (\vec{F}_i) and the inertial forces ($m_i\vec{a}_i$) for a virtual work following the generalized coordinates ($\delta\vec{q}_i$) is zero:

$$\sum_{i=1}^n (\vec{F}_i - m_i\vec{a}_i) \cdot \delta\vec{q}_i = 0 \quad (2.1)$$

$$\sum_{i=1}^n (M_i - I_i\alpha_i - \tilde{w}_i I_i w_i) \cdot \delta\vec{q}_i = 0 \quad (2.2)$$

In other words, between two simulation steps, we can consider that the system is in equilibrium. The same logic applies to the moments (Equation (2.2)). We can therefore reduce Equation (2.1) to a set of rigid bodies in equilibrium:

$$m_i\ddot{\vec{r}}_i = \vec{F}_i \quad (2.3)$$

$$I_i\dot{w}_i + \tilde{w}_i I_i w_i = T_i \quad (2.4)$$

Where I_i is the inertial tensor (in the total system) of the body and \tilde{w}_i is the antisymmetric matrix of the vector w_i , that is to say, that $\tilde{w}_i = w_i^T = -w_i$. Finally, the angular velocity (w_i) can be found from the rotational part of the generalized coordinates, so that:

$$w_i = 2\dot{p}_i p_i^{-1} \quad (2.5)$$

We can rewrite equations (2.3) and (2.4) in matrix form:

$$\begin{bmatrix} m_i & 0 \\ 0 & I_i \end{bmatrix} \begin{bmatrix} \ddot{\vec{r}}_i \\ \dot{w}_i \end{bmatrix} + \begin{bmatrix} 0 \\ \tilde{w}_i I_i w_i \end{bmatrix} = \begin{bmatrix} F_i \\ T_i \end{bmatrix} \quad (2.6)$$

$$M_i\alpha_i + b_i = g_i \quad (2.7)$$

And by generalizing for all the rigid bodies of the system, we find:

$$\begin{bmatrix} M_1 & & & \\ & M_2 & & \\ & & \dots & \\ & & & M_n \end{bmatrix} \begin{bmatrix} \alpha_1 \\ \alpha_2 \\ \dots \\ \alpha_n \end{bmatrix} + \begin{bmatrix} b_1 \\ b_2 \\ \dots \\ b_n \end{bmatrix} = \begin{bmatrix} g_1 \\ g_2 \\ \dots \\ g_n \end{bmatrix} \quad (2.8)$$

$$M\alpha + b = g \quad (2.9)$$

Interestingly, Equation (2.9) is often written in $M\ddot{q} = g$, thus allowing a direct relationship between kinematics and dynamics (Flores, 2008). In (2.10), g represents the set of forces and moments present in the system. These can be broken down into three groups: applied forces and moments (g^A), contact forces and moments (g^c) and muscle forces and moments (g^M). Since the first forces are known (these are the reaction forces and moments on the ground and any other external forces or moments applied to the model), while the last two are unknown, it is more practical to rewrite the problem as follows:

$$M\alpha + b - g^A = d \quad (2.10)$$

With $d = g^c + g^M$ In addition, it is considered that the kinematic constraints (scleronomas) anatomically represent non-muscular forces (ligamentous, geometric, etc.), while piloting constraints (rheonomas) represent the consequences of muscular forces. Thus, the joint contact forces are on the same axis as the kinematic stresses and are the same number as the kinematic stresses. On the contrary, the muscular forces generating the movement are not necessarily the same direction as the piloting constraints. Thus, it is more interesting to represent d by a matrix of directional coefficients (C), a function of the geometry of the muscles, multiplied by a matrix of amplitudes (f^M), representing the muscle strength of each muscle (Tørholm et al., 2000):

$$d = cf^M \quad (2.11)$$

Directional coefficients (C) are a set of unit vectors describing the line of action of muscles. We, therefore, separate the muscular line of action, found from the kinematics and insertion points of the muscles, from the amplitude of muscle force (f^M), found from the optimization process. Since the number of equations represented by equation (2.11) is greater than the number of degrees of freedom of the system, these can be reduced by a standard reduction method, such as Gauss-Jordan elimination, before be resolved to speed up the optimization process. This reduces the number of rows in the matrix to the number of unknowns in the system (Damsgaard, 2006).

2.4.4. Optimization of muscle strength

Although the AMS does not distinguish between reverse calculating dynamics and muscle optimization in its solving steps, a distinction has been made here since. However, these are two different steps from the point of view. The problem of muscle recruitment applied to the reverse dynamic is one of optimization. The objective function to be minimized:

$$(Gf^M) \quad (2.12)$$

Is subject to the constraints posed by the problem of inverse dynamics (see section 3.2.3):

$$Cf^M = d \quad (2.13)$$

Because muscles can only pull (not push), then:

$$f_i^M \geq 0 \quad (2.14)$$

AMS uses the min-max criterion as an objective function that minimizes the maximum level of muscle activation (Damsgaard, 2006; Tørholm et al., 2000; Wolf and Wartzack, 2018).

$$G(f^M) = \max \left(\frac{f_i^M}{F_i} \right) \quad (2.15)$$

Where f_i^M is the force of a particular muscle and where F_i is the maximum force that this same muscle can generate. This criterion tends to distribute the muscular effort on as many muscles as possible, which will work as little as possible.

2.4.5. Contact forces

A contact force (F_C), also called bone-to-bone force (Winter and Winter, 2013) or internal reaction force (Zatsiorsky and Motion, 2005), is, for a given joint, the result of muscle forces and moments (F_M) and reaction forces and moments (F_R) derived from reaction forces and moments on the ground:

$$F_C = F_R + F_M \quad (2.16)$$

However, solving the inverse dynamic with AMS (see section 2.4.3) is one of the variables calculated in the muscle optimization process (named g^c , since the forces are g^c the reaction forces 2.4.4). We can therefore extract these results from the simulations without any difficulty. Despite the great strides in biomechanics, there are surprising gaps in our understanding of the human body and how it works. For example, the knee joint is located at the center of a chain of motion that begins at the foot and connects to the pelvis at the end. But the relationship between the tibia and femur

provides few engineering limitations. Knee stabilization is achieved by operating several soft tissue structures. Details of how these structures function are still largely a mystery. Adams of MSC, a multibody dynamics simulation solution, can provide the right insights to help gain a better understanding of the inner workings of the knee. This section presents the kinematic calculations for the motion as a function of time and is automatically solved by the ADAMS programme. This section presents the kinematic calculations for the motion as a function of time and is automatically solved by the ADAMS programme. Because the multibody is considered solid, solid body kinematics is applicable. Therefore, the ratio of the sliding roll is determined only between the femur and the tibia. This is what was noticed that the patella does not appear in the account or the figures. The following equations (2.17)–(2.18) were used to determine the velocity at a point of the connecting femoral or tibial surfaces (Fig 2.20).

$$\bar{P}_C(t) = \bar{V}_{CMF}(t) + \bar{Q}_{CMF}(t) \times \bar{D}_{CMF}(t) \quad (2.17)$$

Where,

$$\bar{D}_{C1}(t) = \bar{D}_{CMF}(t) + \bar{D}_{CF}(t) \rightarrow \bar{D}_{CF}(t) = \bar{D}_{C1}(t) - \bar{D}_{CMF}(t) \quad (2.18)$$

By substituting Equation (2.17) into (2.18), we obtain:

$$\bar{P}_C(t) = \bar{V}_{CMF}(t) + \bar{Q}_{CMF}(t) \times (\bar{D}_{C1}(t) - \bar{D}_{CMF}(t)) \quad (2.19)$$

From Equation (2.19), we obtain (2.20) and (2.21):

$$\bar{V}_{CF}(t) = \bar{V}_{CMF}(t) + \bar{Q}_{CMF}(t) \times (\bar{D}_{C1}(t) - \bar{D}_{CMF}(t)) \quad (2.20)$$

$$\bar{V}_{CT}(t) = \bar{V}_{CMT}(t) + \bar{Q}_{CMT}(t) \times (\bar{D}_{C1}(t) - \bar{D}_{CMT}(t)) \quad (2.21)$$

The absolute coordinate system has determined velocities relating to the femur and tibia at the point of contact (Fig 2.19 and 2.20).

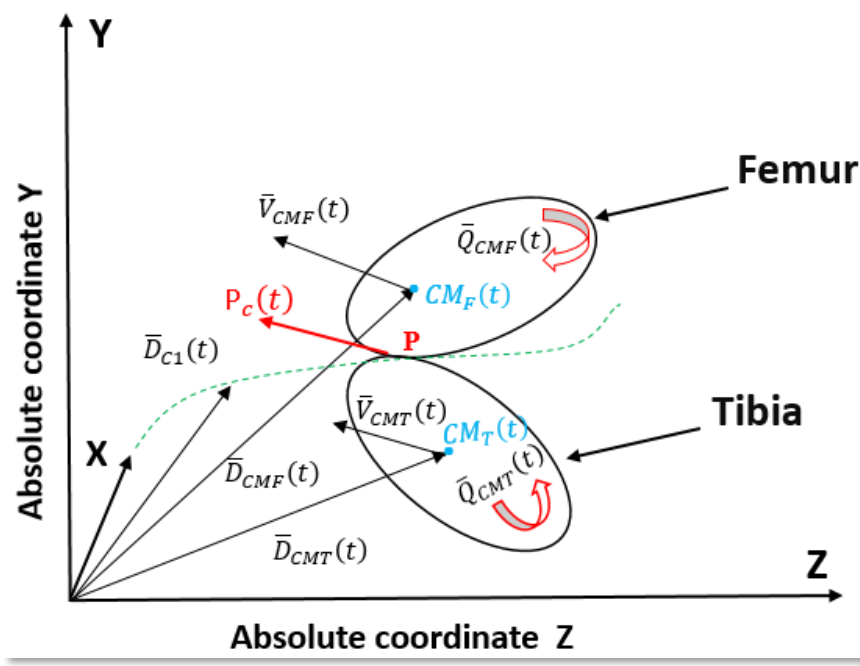


Fig 2.19 Kinematic of the knee prosthesis.

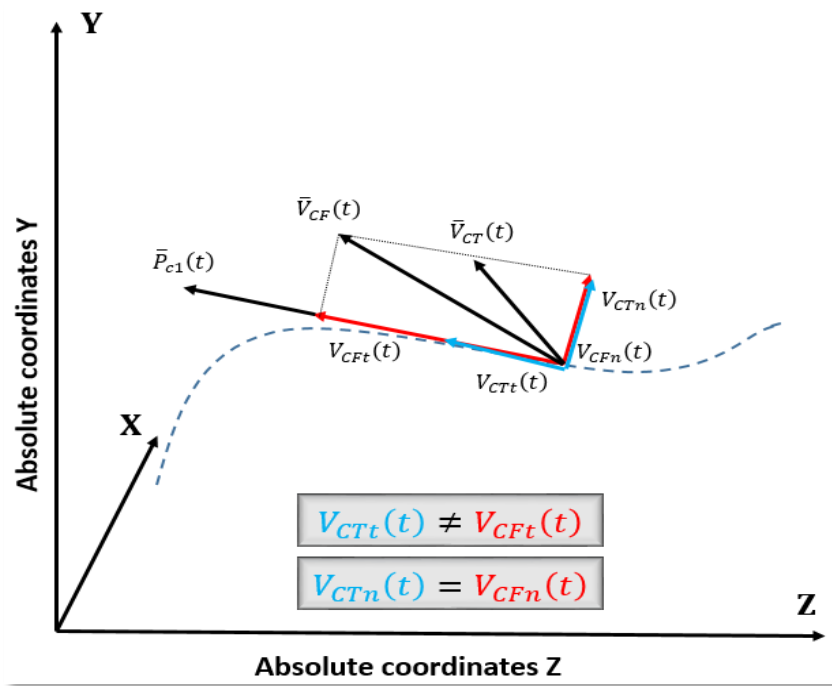


Fig 20. The motions of the tibia and femur at the contact point.

At the unit vector $\bar{P}_{c1}(t)$, we multiply Equations (2.20) and (2.21):

$$V_{CFt}(t) = \bar{V}_{CF}(t) \cdot \bar{P}_{c1}(t) = [\bar{V}_{CMF}(t) + \bar{Q}_{CMF}(t) \times (\bar{D}_{C1}(t) - \bar{D}_{CMF}(t))] \cdot \bar{P}_{c1}(t) \quad (2.22)$$

$$V_{CTt}(t) = \bar{V}_{CT}(t) \cdot \bar{P}_{c1}(t) = [\bar{V}_{CMT}(t) + \bar{Q}_{CMT}(t) \times (\bar{D}_{C1}(t) - \bar{D}_{CMT}(t))] \cdot \bar{P}_{c1}(t) \quad (2.23)$$

The tangential scalar components are justified only under the following condition (NAGY et al., 2015).

$$V_{CFn}(t) = V_{CTn}(t) \quad (2.24)$$

This indicates that the typical normal standard components of the femoral and tibia contact velocities should be the same. Otherwise, there would be a collision or separation of the two surfaces.

By combining scalar velocities over time, the length of the continuous arc concerning the femur and tibia can be calculated as follows:

$$S_{femur}(t) = \int V_{CFt}(t)dt = \int [\bar{V}_{CMF}(t) + \bar{Q}_{CMF}(t) \times (\bar{D}_{C1}(t) - \bar{D}_{CMF}(t))] \cdot \bar{P}_{C1} dt \quad (2.25)$$

$$S_{tibia}(t) = \int V_{CTt}(t)dt = \int [\bar{V}_{CMT}(t) + \bar{Q}_{CMT}(t) \times (\bar{D}_{C1}(t) - \bar{D}_{CMT}(t))] \cdot \bar{P}_{C1} dt \quad (2.26)$$

The sliding scroll ratio can be entered back by specifying the arc lengths on both connected bodies:

$$X(t) = \frac{\Delta S_{tibiaN}(t) - \Delta S_{femurN}(t)}{\Delta S_{tibiaN}(t)} \quad (2.27)$$

$$\Delta S_{femurN}(t) = S_{femurN}(t) - S_{femurN-1}(t) \quad (2.28)$$

$$\Delta S_{tibiaN}(t) = S_{tibiaN}(t) - S_{tibiaN-1}(t) \quad (2.29)$$

These rates show the differences increasing with the longest connected arc. The sliding rolling ratio is the difference between the distance travelled (ΔS_{tibiaN}) on the tibia and the additional distance travelled (ΔS_{femurN}) on the femur bone over the increased distance travelled (ΔS_{tibiaN}) on the tibia. N shows the arc length during the connection. Thus, we can conclude accurate calculations about the sliding and gradient features of motion. The sliding toll ratio that translates to zero means this is pure rolling. Regarding a ratio between 0–1, the movement turns into partial rolling and sliding. Determining the sliding roll ratio as a function of the bending angle is better than determining it as a function of time. We will explain what we have done with this sliding rolling ratio. First, the flexion angle (γ) was derived, adding the femur and tibia's angular velocities around the X-axis, and was set to an initial degree of 20° of squatting.

$$\gamma(t) = \int Q_{CMFx} \cdot dt + \int Q_{CMTx} \cdot dt + 20 \quad (2.30)$$

By defining a function, the flexion angle can alter the time, and rolling can be plotted in correlation with the flexion angle.

$$X(\gamma) = \frac{\Delta S_{tibiaN}(\gamma) - \Delta S_{femurN}(\gamma)}{\Delta S_{tibiaN}(\gamma)} \quad (2.31)$$

A case in point is the role of the menisci. It helps stabilize the knee by creating a cup for the femur to sit in. The menisci also act as a shock absorber spreading compression forces from the femur over a wider tibia area. However, there are still many things we still don't understand about the menisci. This is where MSC's Adams comes in.

2.5. Summary of literature review evaluation

The proper handling of degenerative abrasion in the knee joint is currently one of the essential orthopedic problems. The appropriate solution for this issue is to remove and replace it with a prosthesis. Unfortunately, no perfect knee prosthesis is available to replace the original knee because of the knee kinematics' complexity. Results for the kinematical design method of the knee prosthesis geometries by Balassa, 2019, compared to the normal human knee(Balassa, 2019), shows that the basic principle of their method was to move the two prosthetic components together according to the objective function of flexion and rotation of the knee prosthesis. The results showed a close match with the curve of the movement of the normal human knee. The test machine for measuring the prosthesis by(Balassa, 2019), was created by the Biomechanical Research Group of The Hungarian University of Agriculture Engineering and Life Science. With this machine, they made many different sizes of the prosthesis by using the 3D model of knee prosthesis. The developed prosthesis model was produced by the CNC milling technology (Balassa, 2019).The test machine is multipurpose, making it ideal for evaluating the knee prostheses. Its suitability for different types of loads is also significant. Unfortunately, in using the method of machine milling with 3D printing, designing and developing the knee prosthesis is time-consuming, and a high cost is incurred. Since it is a try and error method, and there is no predefined procedure, a significant quantity of knee prosthesis model material will be lost with these measurements (Chui et al., 2020; Zhou et al., 2020). Fekete et al. used the 3D computational model in the MSC.ADAMS software to examine the forces that connect the surfaces of the femur, tibia, and the patella. They applied the equilibrium equations by defining the forces relating to the femur, tibia, and the patella. In the end, they obtained the force functions as inputs for the isometric motions. However, the internal forces connecting the surfaces as a function for flexion were not investigated (Fekete et al., 2011; Quinlan et al., 2020; Zeng et al., 2020). The application of the MSC.ADAMS software for our study made use of the linear or non-linear ordinary differential equations simultaneously with the non-linear differential algebraic equations. To find a solution with these equations, an initial value is determined from which the final trajectory would be determined (Fekete et al., 2011). Thus, the appropriateness of using the ADAMS programme to design the knee prosthesis as a faster, more efficient and accurate procedure without having to go through the several tastings attempts to arrive at the appropriate design as done in the procedure by (Balassa, 2019).

2. LITERATURE REVIEW

This study aims to develop the numerical measurement of the knee prosthesis geometry by applying the MSC.ADAMS program. The forces that relate to the femur, tibia, and the patella would be investigated. The 3D CAD printing procedure will be applied to create the initial knee prosthesis, and then the ADAM software used to model and obtain the final product. The results would then be compared with the outcome from the 3D CAD model and CNC milling process, and the prosthesis results from a test rig. The proposed research is thus, to obtain the knee prosthesis by applying a more efficient procedure devoid of material and time wastage and minimize cost.

3. Material and methods

3.1. Femur

The femur is the longest bone in the body, and it alone constitutes the skeleton of the thigh. Extends from the hip to the knee. It presents an oblique direction towards the interior since the distance between the hips is more significant than between the knees. To partially compensate for the approach of the two femurs to the body axis, the tibias separate. The knee thus acquires the appearance of an angular joint outwards in the valgus. (Fig. 3.1).

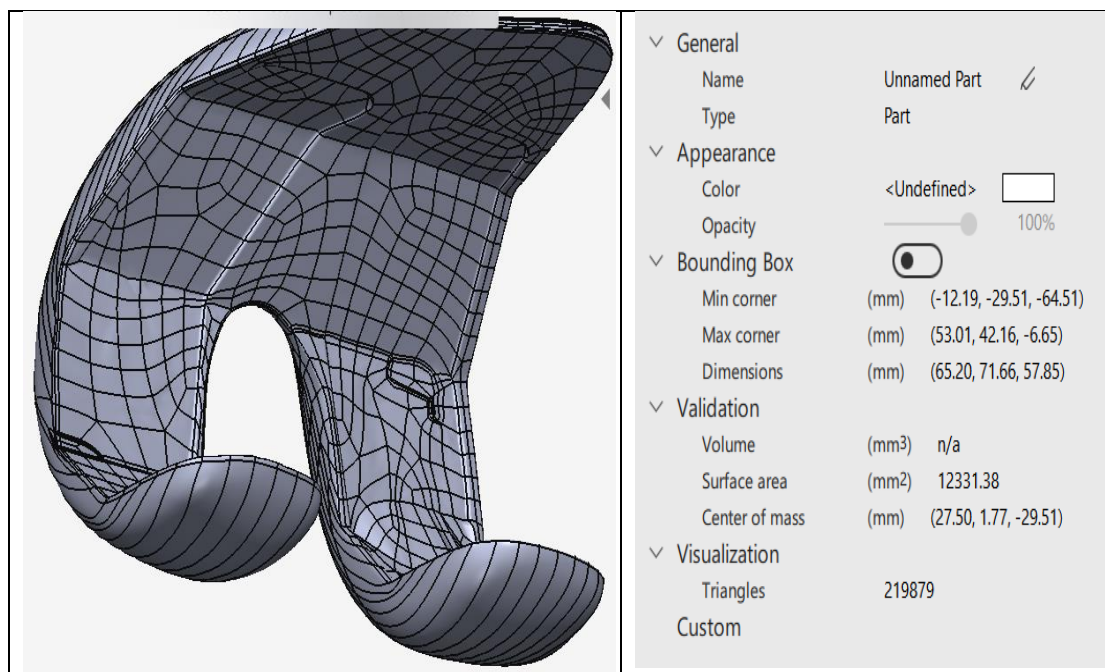


Fig. 3.1 Femur structure in Solidworks.

3.2. Patella

It is a flattened bone, rounded in appearance, or even oval, which extends downwards through its apex or the lower pole. It has two areas (Fig. 3.2):

- Anterior face, convex, which serves as a reflection pulley for the quadriceps and patellar tendons.
- Posterior surface. Oriented towards the joint's interior, it has two facets, internal and external, which contact the corresponding femoral condyles, adapting its concave shape to the convexity of the condyles.

3. MATERIAL AND METHODS

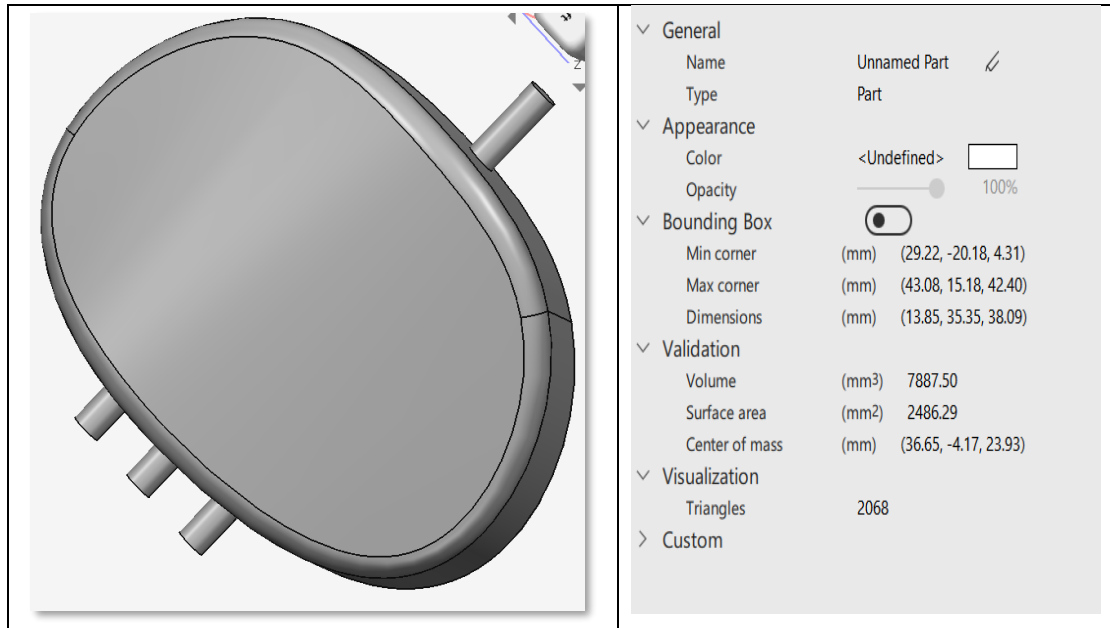


Fig.3.2 Patella structure in Solidworks.

3.3. Tibia

The tibia presents a flat surface that cannot receive the convexity of the condyles of the femur without the menisci which ensure articular congruence. These menisci provide stability and absorb the axial and rotational mechanical stresses of the knee. Together with the fibula, the tibia forms the skeleton of the leg. It supports the body weight and transmits the lines of force from the ankle to the knee.

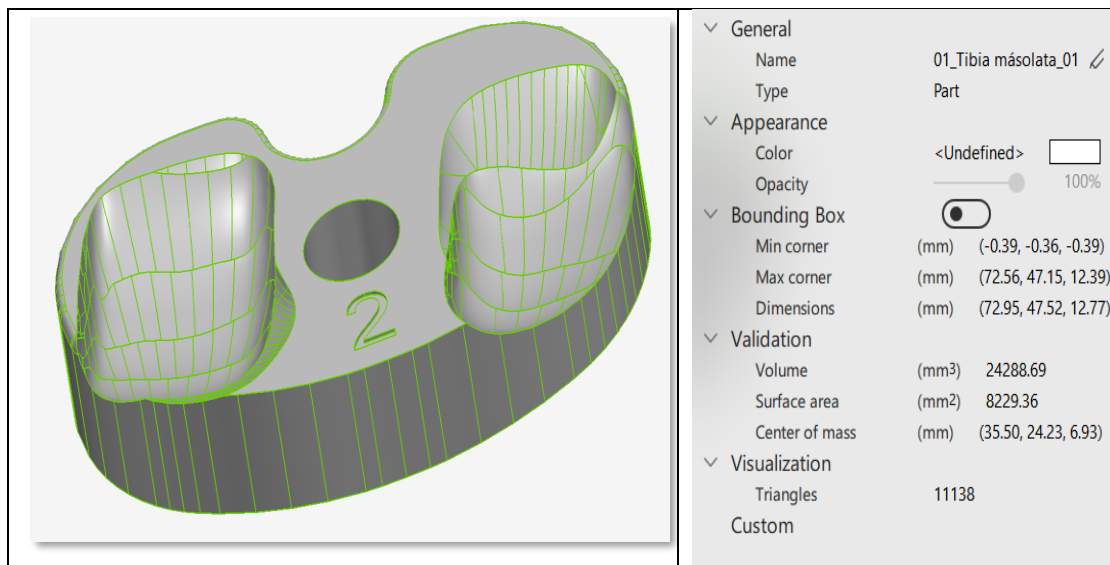
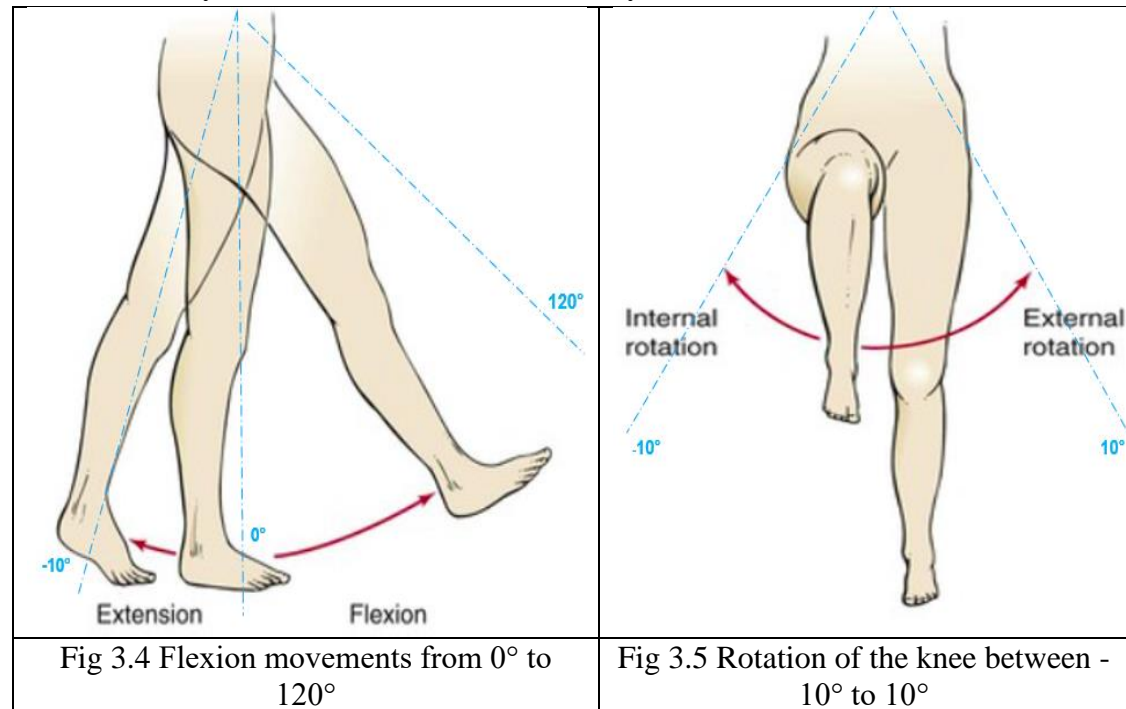


Fig 3.3. Tibia structure in Solidworks.

3.4. The movements of the knee

They are expressed above all in the profile plane (sagittal): flexion-extension, the amplitude of which goes from 0 to 140° of flexion. In extension, however, very flexible subjects called hyper axes can exceed 0° and go up to 15° of hyperextension, another movement is possible: rotation. The tibia can rotate on its axis by 30 to 60° in external rotation (mostly) and in internal rotation but only when the knee is in flexion.



3.4.1 Knee flexion

It requires the instantaneous combination of two movements: sliding rolling. Flexion causes the condyles to roll on the tibial plateau. However, the unfolding of the condyles is twice as long as that of the tibial plateaus. The succession of events takes place in several phases: rolling from 10 to 15° of flexion then association of sliding with rolling then at the end of the flexion only the sliding makes it possible to achieve the last degrees of flexion in thin and flexible people (140 to 160 °).

3.4.2 Knee rotation

When the knee is flexed the posterior part of the condyles is in contact with the middle portion of the glenoid. The massif of thorns is cleared of the indentation and therefore unblocked. The rotation causes one condyle to advance and the other to retreat on the tibial glenoid.

3.5. Ligaments (springs)

We create the springs between the femur and tibia by using the part of patella to replace the ligaments in the normal knee, so we add springs to fix the patella at the middle between the femur and tibia.

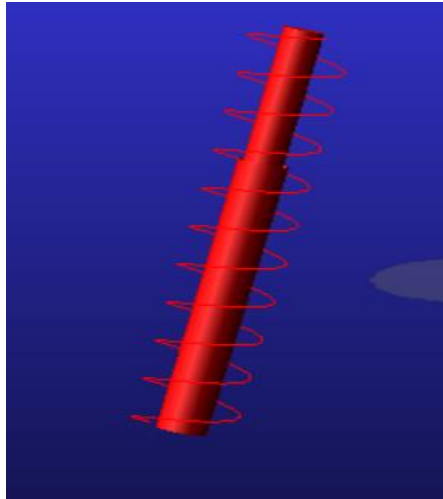


Fig.3.6 Spring in ADAMS program

3.6. Machines

3.6.1. Machine for measurement of the knee prosthesis

The test machine for measuring the prosthesis was created by the Biomechanical Research Group of MATE University (designed by Gabor Balassa). With this machine (Fig 3.7), they made many different prosthesis sizes by using the 3D model of knee prosthesis. The developed prosthesis model was produced by CNC milling technology.

The test machine is multipurpose, making it ideal for evaluating the knee prostheses. Its suitability for different types of loads is also significant.

Unfortunately, in using the method of machine milling with 3D printing, designing and developing the knee prosthesis is time-consuming, and a high cost is incurred. Furthermore, since it is a try and error method, and there is no predefined procedure, a significant quantity of knee prosthesis model material will be lost with these measurements.

3. MATERIAL AND METHODS

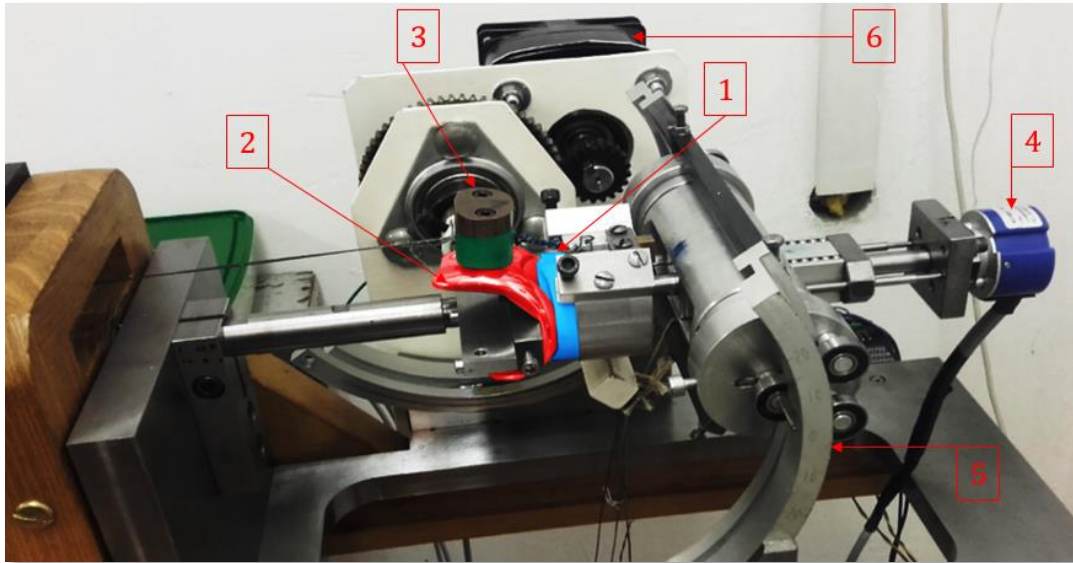


Fig 3.7. Machine for measurement of the knee prosthesis

1: Tibia

2: Femur

3: Patella

4: Rotation sensor

5: T-section guide track (-10 ° -+ 120 ° flexion range).

6: Stepper motor and gear transmission.

3. MATERIAL AND METHODS

3.6.2. A graph of Rotation against Flexion for the prosthesis developed with a test machine.

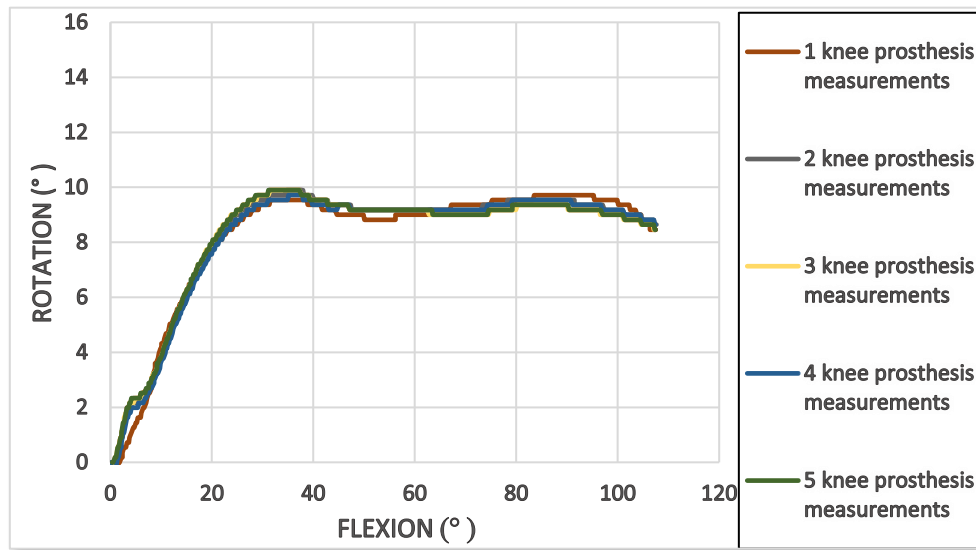


Fig 3.8 A graph of rotation against Flexion for the knee prosthesis was designed by Balassa and tested with their machine compared with the regular movement of the human knee (Balassa, 2019).

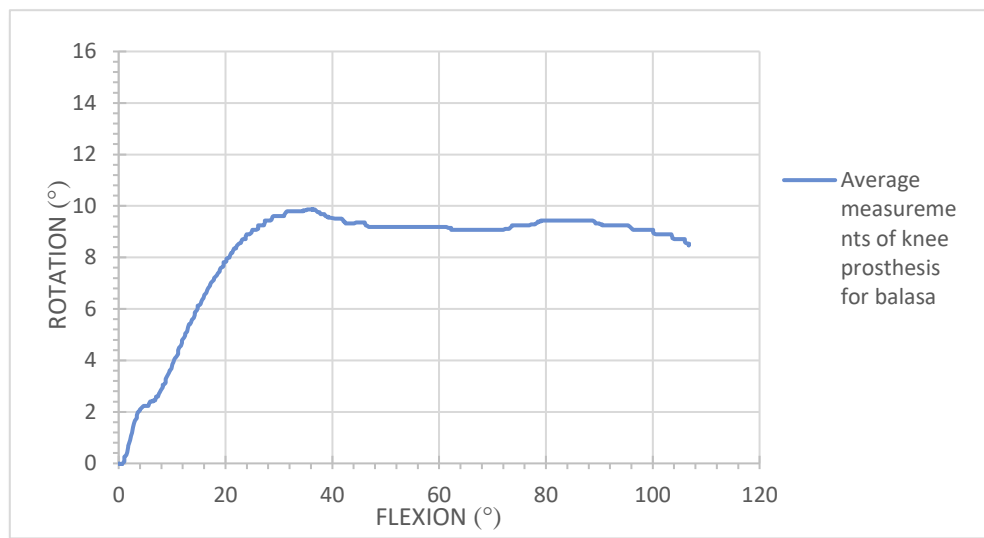


Fig 3.9. A graph of Rotation against Flexion for the prosthesis was developed with a test machine(Balassa, 2019).

These diagrams present a measurement of the test machine for the knee prosthesis geometry movements, and it is a good method, but unfortunately with this method, we will lose our time and money for creating the models and try it at the machine, that way we will replace this method with the new method by using a new virtual model method. Without losing money and time we can make the measurement of the knee prosthesis geometry and the results better than the test machine.

3.7. ADAMS Program

Adams is the most widely used multibody dynamics and motion analysis software in the world. Adams helps engineers study the dynamics of moving parts, how loads and forces are distributed throughout mechanical systems, and improve and optimize their products' performance (Hroncová et al., 2014). Utilizing multibody dynamics solution technology, Adams runs nonlinear dynamics in a fraction of the time required by FEA (Finite Element Analysis) solutions. In addition, loads and forces computed by Adams simulations improve the accuracy of FEA by providing a better assessment of how they vary throughout a full range of motion and operating environments. We used the MSC. Adams software environment to create a model (Fig. 4.1) for modelling and error analysis of the gear transmission mechanism. The model consists of solid bodies, the shaft is modelled by a geometric element "femur" "tibia" "patella" "springs" and the spur gearing is imported from the 3D parametric modelling software.

3.8. The Virtual Multibody Model

The virtual multibody model was created by applying the following procedures

- The general point motion was used to stabilize the distal femur, where all the coordinates are shown (Fig 3.10). This enables the distal femur to make a transitional movement along the y-axis.
- The cylindrical joint model was used to restrict the knee part to allow rotation around all axes (Fig 3.10). This enables the shin bone to conduct a natural rotation.
- We only considered the patellar tendon and the rectus femur in the numerical-kinematical model. Therefore, we create both of them as simple linear springs, as shown in (Fig 3.10).
- According to the literature, the rectal femoral stiffness modulus was determined between 25 and 100 N/mm, according to the literature (Frigo et al., 2010; Thelen et al., 2005). As an average value, we set it to 80 N/mm. With the stabilization factor set at 0.15 Ns/mm, for all the strings to prevent oscillations in the system, the patellar tendon was set to inextensible (Fig 3.10).
- According to Coulomb's law, contact restrictions are established concerning static and low dynamic friction coefficient ($\mu_s = 0.1$ $\mu_d = 0.085$) between the femur, tibia and patella, similarly to real joints (Fig 3.10). the kinetic relationship between systemic forces, frictional forces (F_n , F_s), and flexion angle is analyzed using this constraint.

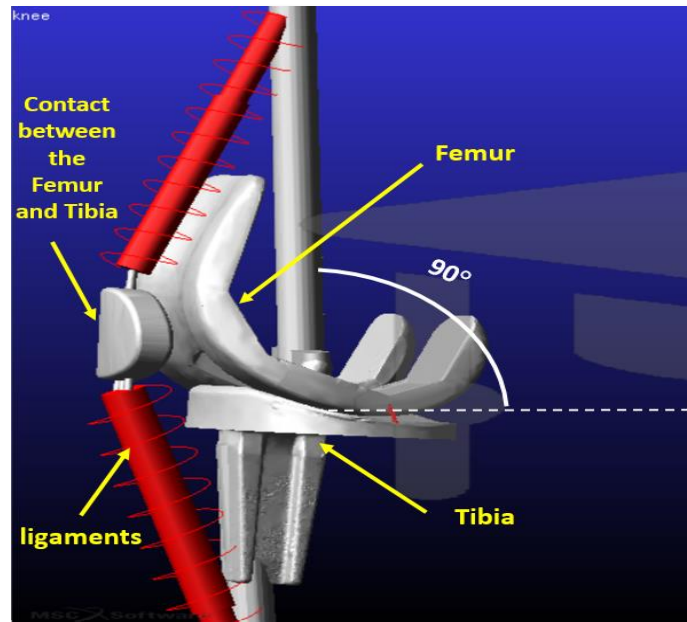


Fig 3.10. Our Multibody model in the MSC.ADAMS.

3.8.1 Femur axis

As we can see Fig 3.11, there are three main axis that apply to the movement of the femur, it begins with the X axis, which is responsible for the movement of the knee in a vertical direction, and this is what we call flexion of the knee prosthesis. And for the Y axis is responsible for the movements of the knee in a horizontal direction, and this is what we call rotation of the knee prosthesis, and for the axis Z is responsible for the gravity of knee prosthesis.

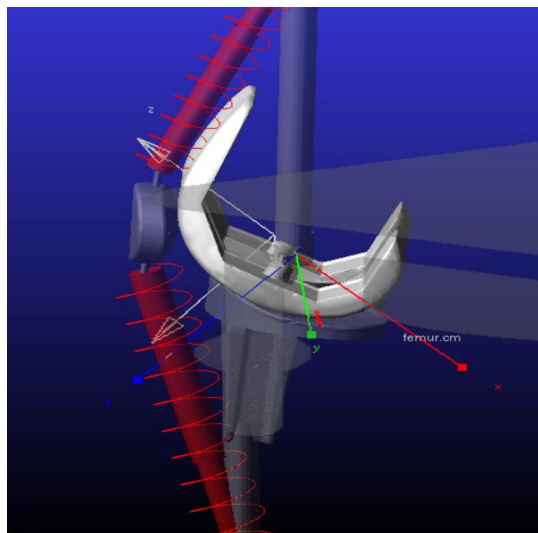


Fig. 3.11 femur axis (x, y, z)

3.8.2 *Tibia axis*

As we can see Fig 3.12, there are three main axis that apply to the movement of the Tibia, it begins with the Y axis, which is responsible for the movement of the knee in a vertical direction, and this is what we call flexion of the knee prosthesis in a negative direction compared to the Femur. And for the X axis is responsible for the movements of the knee in a horizontal direction, and this is what we call rotation of the knee prosthesis, and for the axis Z is responsible for the gravity of knee prosthesis.

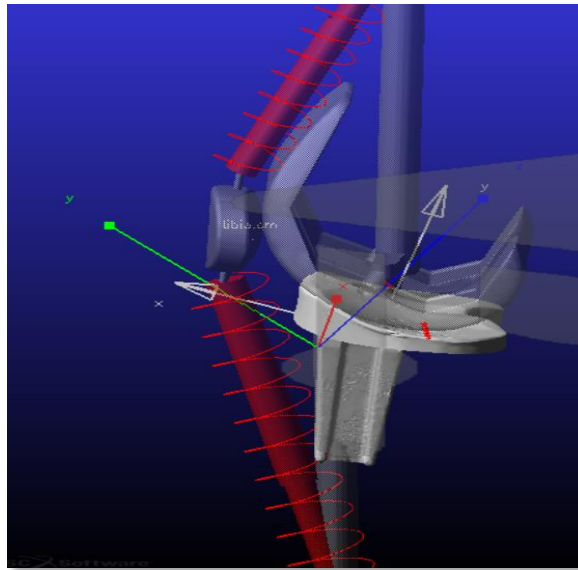


Fig. 3.12 tibia axis (x, y, z)

3.8.3 *Patella axis*

As we can see Fig 3.13, there are three main axis that apply to the movement of the femur, it begins with the X axis, which is responsible for the gravity of the knee prosthesis for the patella, and for the Y axis is responsible for the movement of the knee prosthesis in a vertical direction, and this is what we call flexion of the knee prosthesis, and for the X axis is responsible for the movement of the knee in horizontal direction, and this is what we call rotation of the knee prosthesis.

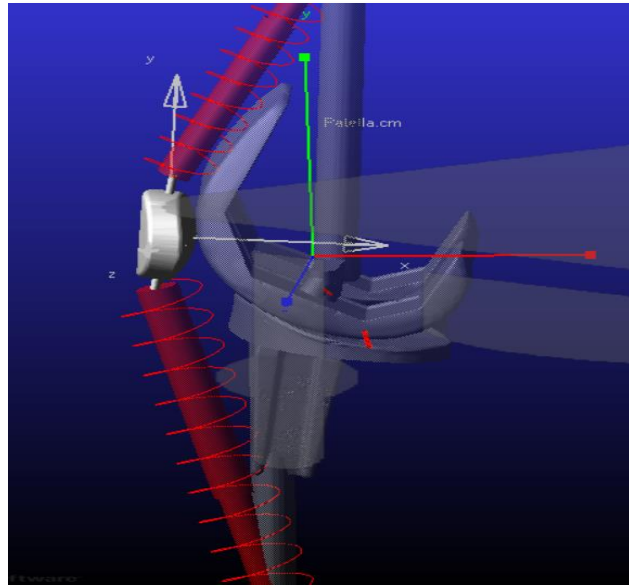


Fig.13. Patella axis (x, y, z)

3.8.4 Cylindrical joint

Fig3.14 it shows us a joint of rotation in proportion to the knee prosthesis, so we make it a cylinder to make it easier for us to move the femur and tibia in rotation side.

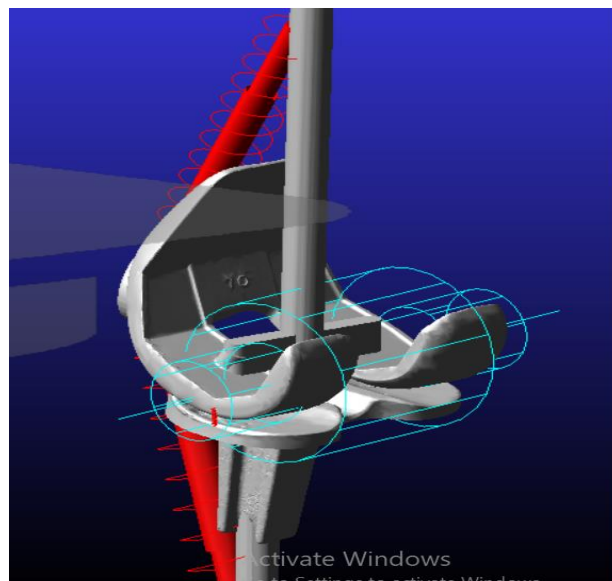


Fig 3.14 Cylindrical joint of the knee prosthesis in ADAMS program.

3.8.5 Motion of the geometry

This Fig 3.15 shows us the main direction of movement for the knee prosthesis geometry. And this described motion will allow us to correctly apply for our study to the knee prosthesis geometry of the rotation and flexion and friction.

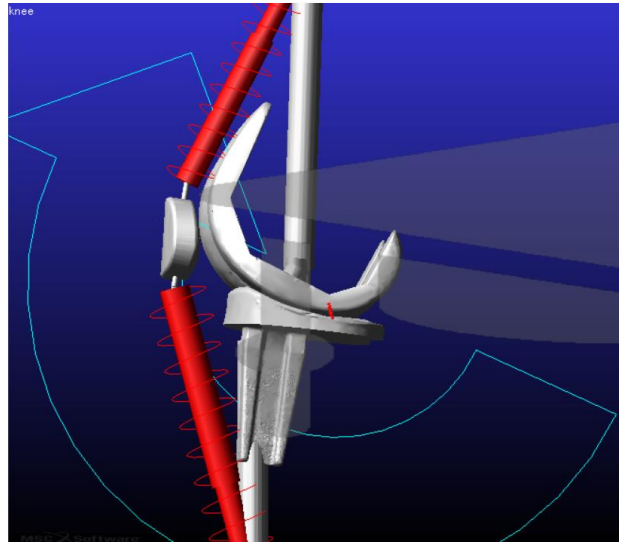


Fig 3.15 Motion direction of the knee prosthesis

3.8.6 Friction

Fig 3.16 shows us the place of friction in the ration of the knee prosthesis geometry, and it is applied to the knee bone, femur and tibia and patella. Because of this friction resulting from the loads of weights and serious sprains.

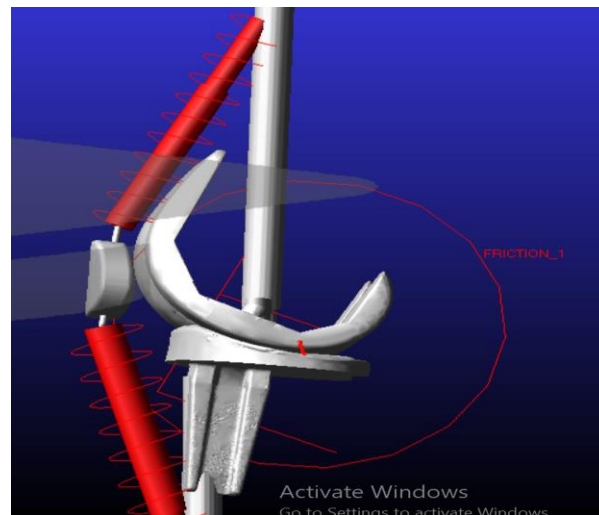


Fig 3.16 friction of the knee prosthesis

3.8.7 Principal components knee motion

As we note here Fig 3.17, the three most important things responsible for the movements of the knee are explained to us, without friction there is no knee prosthesis slip, and without a rotation joint there is no movement, and without a correct motion direction there is no correct study of the knee prosthesis geometry.

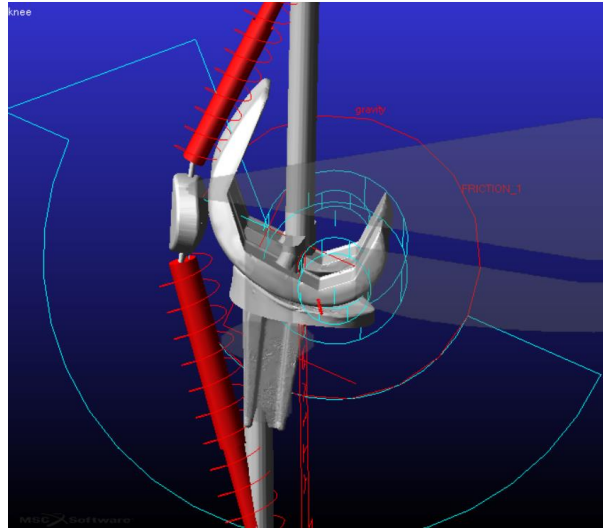


Fig 3.17 cylindrical joint, frication and motion

3.9. Boundary conditions for the simulation

After the geometrical model is obtained, the MSC.ADAMS program was used to build the multibody model. But, first, the following boundary conditions were applied to our model (prosthesis geometry):

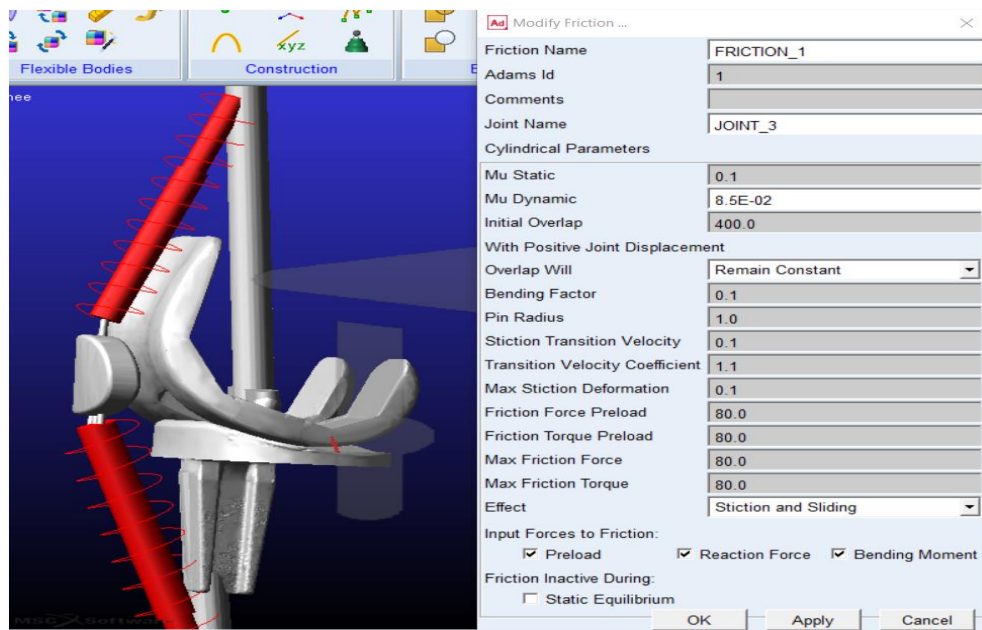


Fig 3.18. Parameters for friction Multibody model

3.10. Block diagram showing the applied steps of the multibody virtual model created in the ADAMS software.

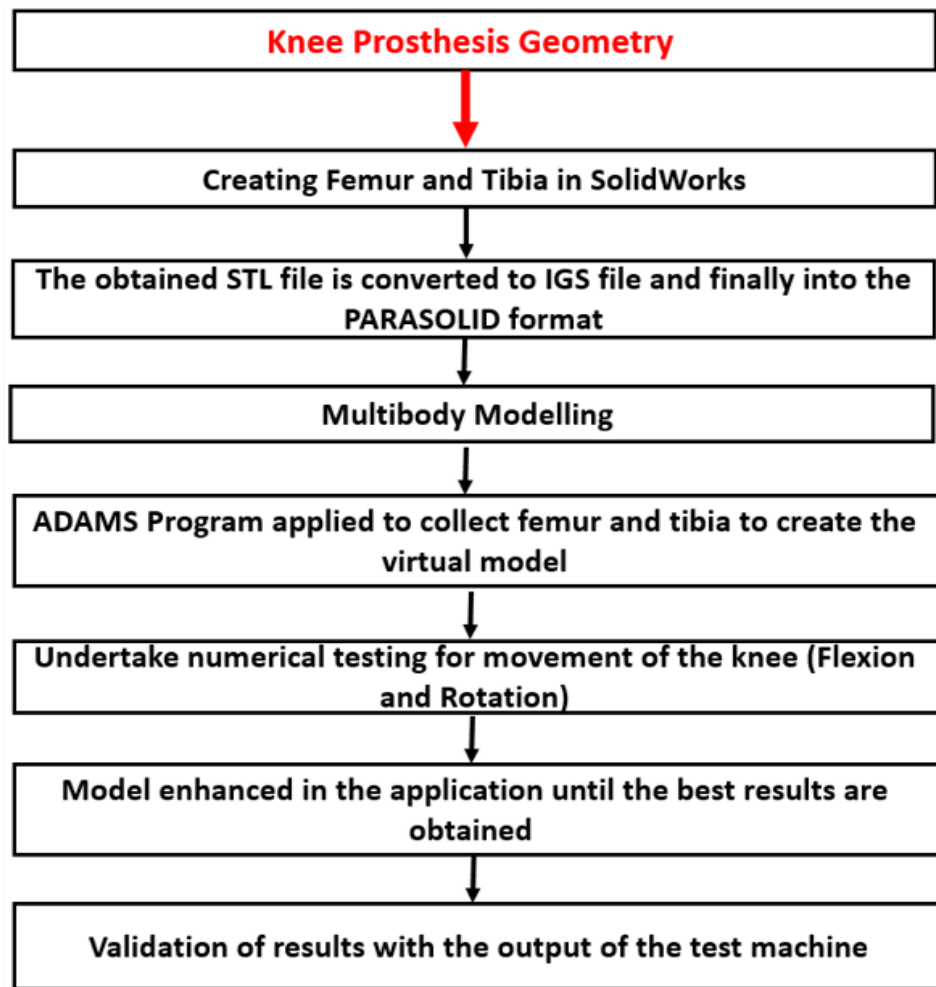


Fig 3.19. Block diagram showing the applied set

4. RESULTS And Discussion

This section presents the results and the accompanying discussions for the study

4.1. The Virtual Multibody M1

The ADAMS programme could compute the forces directly. At first, we saved it as PARASOLID, and we imported it into the MSC.ADAMS. The flexion angle was derived by combining the femur and tibia's angular velocities about the x-axis. This was done considering that the model was at 20° for the sliding and rolling at the start of the movement. The angles were divided into three to tackle the three-dimensional movement. The results are summarized in Fig. 4.1.

To be able to describe all the coordinates, we have restricted the distal femur by the general point motion, as shown in Fig 4.1. The knee model was restricted by a cylindrical joint, which allows the flexion process between a femur and tibia. Simple linear springs are designed as the boundary between the rectus femur and the patellar tendon as in (Frigo et al., 2010; Thelen et al., 2005).

According to Coulomb's law, the contact limitations between the femur and the patella tibia are established for low static and dynamic friction coefficients ($\mu_s = 0.1$ $\mu_d = 0.085$), similar to human joints (Merkher et al., 2006). On the femur distal, a force vector was created, as shown in Figure.4.1, and the value is set at 400 N. Whiles define it by a step function (A, x0, h0, x1, h1).

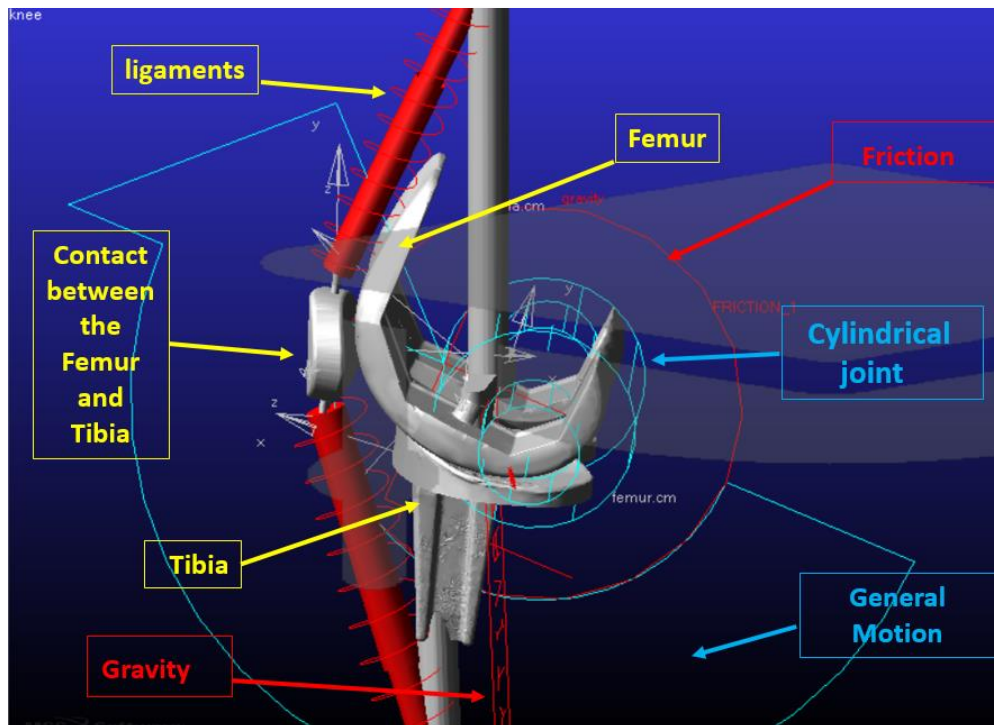
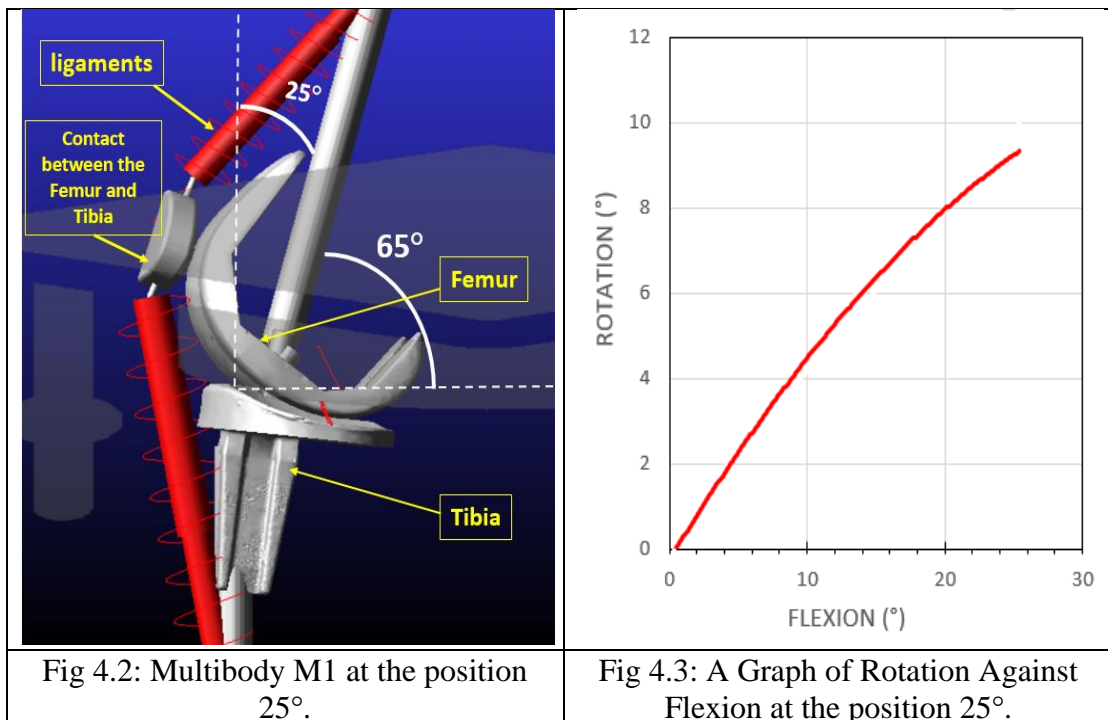


Fig 4.1. Our Multibody M1 in the MSC.ADAMS.

4.1.1. Simulation of the multibody M1 in different range of rotation

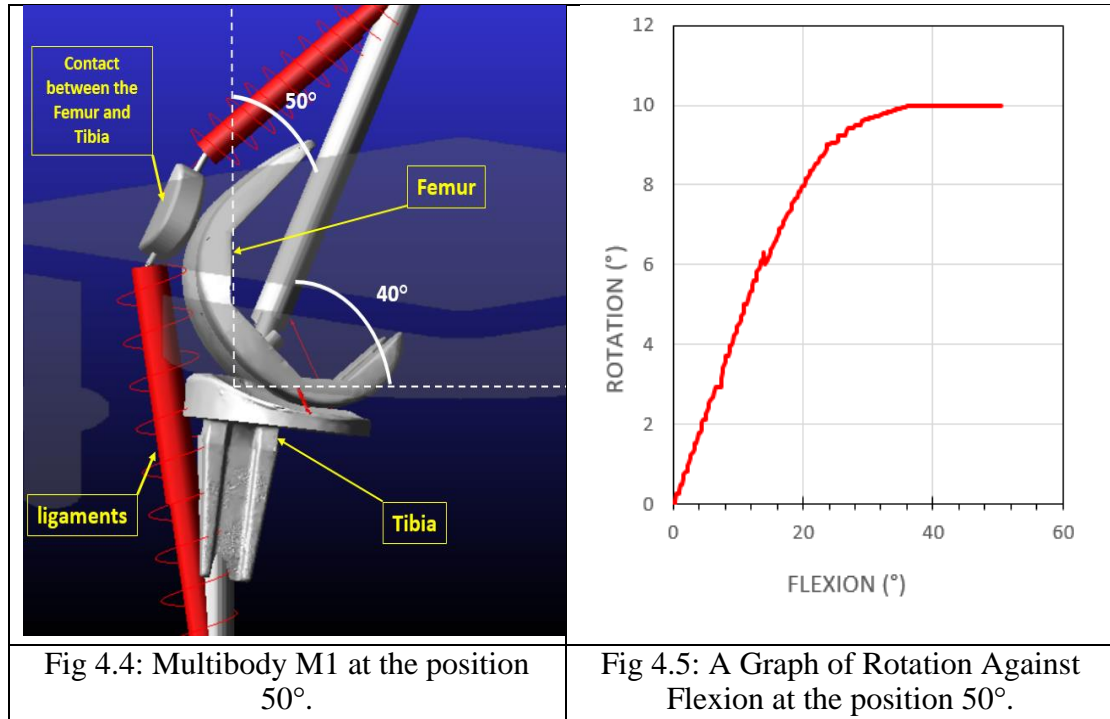
4.1.1.1 Simulation of the multibody model M1 at the position of 25°.

The simulated model is shown in Fig 4.2. The graph of rotation against flexion is illustrated in Fig. 4.3. It was noticed that the angle of rotation varies linearly with respect to the flexion. It was observed that the sudden increase in the rotational angle was offset by an increase in the angle of curvature. A sharp rise in the flexion angle till 25° was seen beyond the rotational angle of 20°. The maximum elevation of flexion against the angle of rotation was found to be 25°.



4.1.1.2. Simulation of the multibody M1 at the position of 50°.

The simulated model and the graphical representation of the rotational angle with flexion are depicted in Figs 4.4 and 4.5, respectively. It was observed that there was an increase in the degree of rotation (virtual axis) from 0° to 9.5°, whereas the flexion (horizontal axis) varies until 50°. Furthermore, the flexion angle's relative variation was five times bigger than the rotational angle, which indicates that the onset of sliding between the tibia and the femur in the knee occurs in the range of 20°-30° of flexion angle, which conforms to the movement range of the normal human knee.



4.1.1.3. Simulation of the multibody M1 at the position of 100°.

The pictorial representations of the model at the angles of 0° and 100° of Flexion are shown in Figs 4.6 and 4.7. The relationship between the angles of rotation and flexion is illustrated in Fig 4.8. It is observed that the sudden increase in the rotational angle was offset by an increase in the angle of curvature. A sharp rise in the flexion angle till 35° was seen beyond the rotational angle of 20°, which indicates the onset of sliding between the tibia and the femur in the knee. Similarly, the flexion angle in the range of 20°-30° originates the joint prone to rolling. In contrast, the rotational angle's stability for the flexion angle lies in the range of 30° to 110°. The increasing flexion angle indicates that the tendency of sliding is predominant.

4. RESULTS AND DISCUSSION

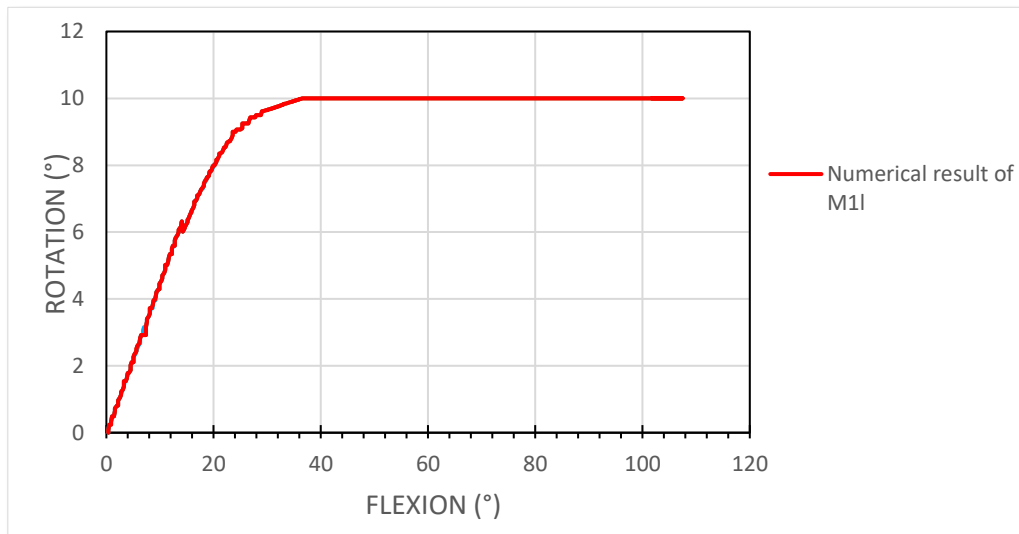
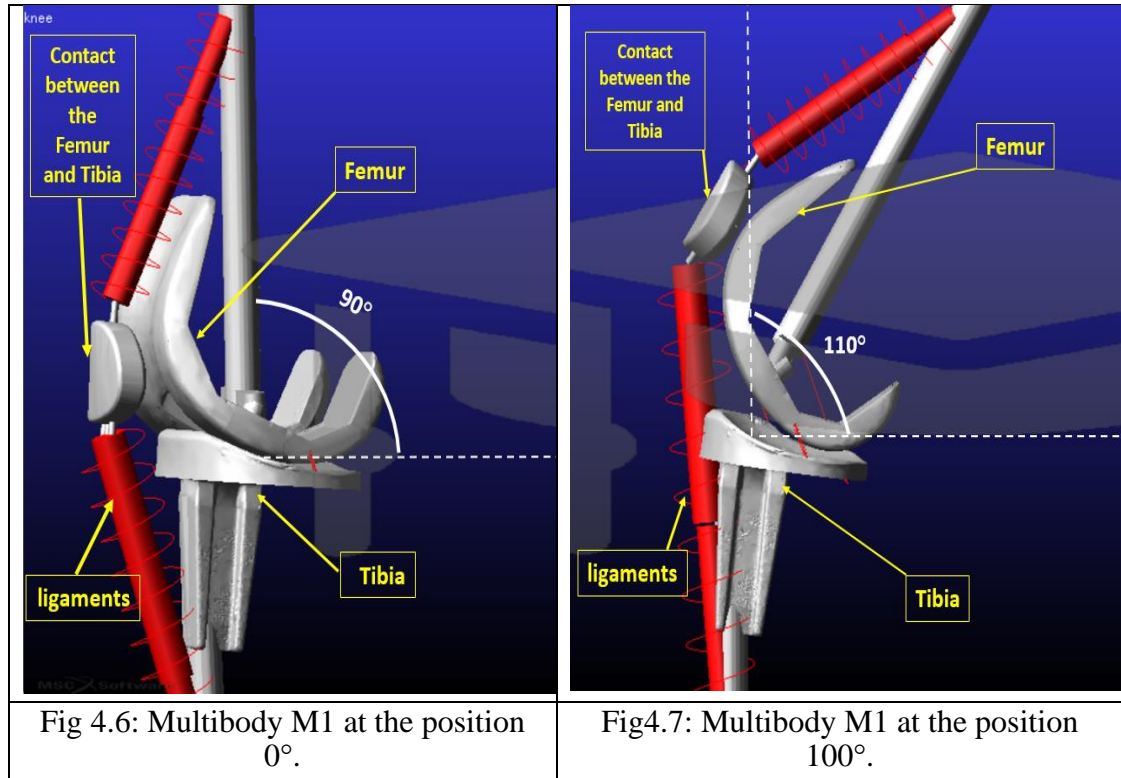


Fig 4.8. A graph of rotation against flexion of our virtual M1.

4.1.2. Experimental measurement result for test machine of The Hungarian University of Agriculture Engineering and Life Science.

The result shown in Fig 4.8 is essential as it is the bases for our numerical experimentation. The Hungarian University of Agriculture Engineering and Life Science research team developed several pros-thesis design methods initiated by (Balassa, 2019) by using the test machine they developed, as shown in Fig 3.7. It was mentioned by (Balassa, 2019) that the presented results (Figs 3.8 and 3.9) in his study was actually the best with respect to the closeness to the natural knee movement.

4.1.3.. Comparing the results of the current study of the numerical measurement method and the experimental measurement result for the Hungarian University of Agriculture Engineering and Life Science test machine.

In order to validate the results from the numerical studies, we compared our virtual numerical model with the prostheses joints that have been tested using with the test machine in the Hungarian University of agriculture engineering and life science. The average values are plotted together against the virtual numerical model, as shown in Fig 4.9. The close similarity between the two curves indicates that this virtual model can replace the measurement by the test machine of the Hungarian University of Agriculture Engineering and Life Science. It was also found that there was a rise in the angle of rotation as the flexion angle varied from 0° to 30°. Thus, a good agreement of value obtained from our model with other prosthetic joints is established in the flexion range of 30° to 110°. We noticed there are the close results between the proposed model and other prostheses. In this case, we were able to create a new model that enables us to make multiple measurements of a new model. As a result, we can change the materials made of artificial joints, more accessible, and obtain faster results without many calculations.

Table 2. Comparison between the virtual model procedure and the test machine.

Virtual model	Test machine
It saves time and material	Time-consuming and involves wastage of material.
It saves money because it is objectively focused	High cost incurred because it is a procedure of try and error
The Lack of transition in flection and rotation is used to simplify the geometry and diversity in motion, allowing our new virtual model to be more realistic.	This process cannot be applied with a test machine hence the inefficiency of the procedure.

4. RESULTS AND DISCUSSION

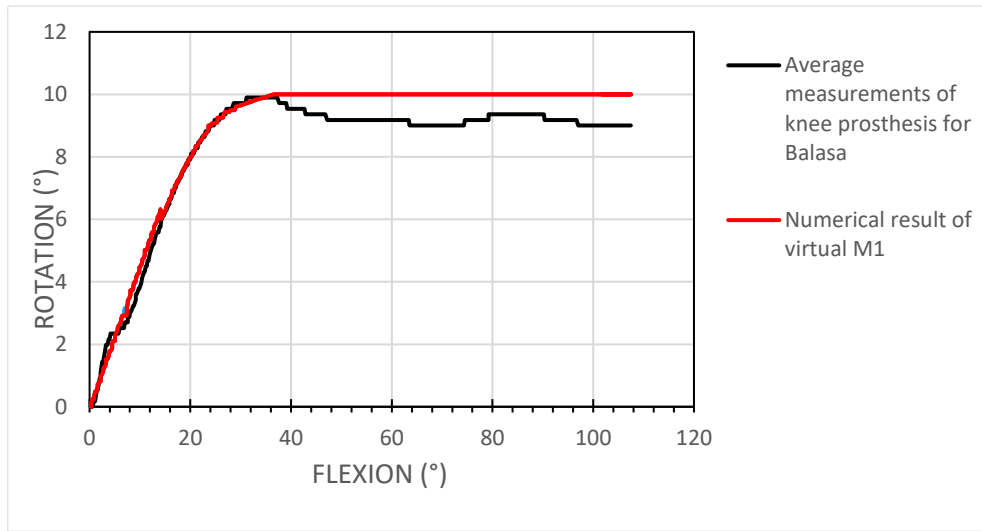


Fig 4.9. Verification results of our virtual M1 with the prosthesis developed with a test machine.

For calculate the error rate between the prosthesis measuermnt for the test machine and the multibody model (M1)Fig 4.10:

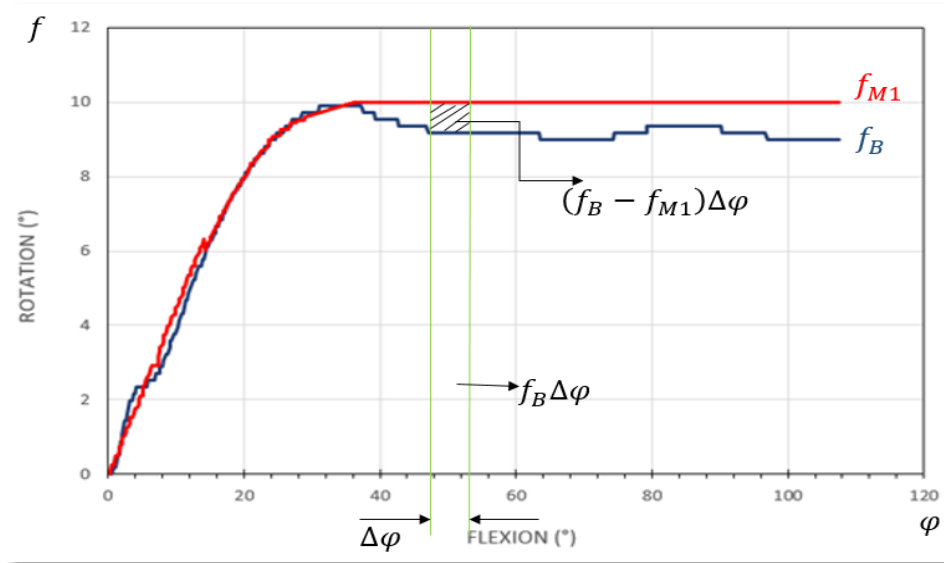


Fig 4.10 Normalized error between Balassa results and the Multibody model

As we can see (Fig4.10) the deferent between the measurements of the knee prosthesis for Balassa and numerical results of virtual model (M1) presented by $(f_B - f_{M1})\Delta\varphi$.

Calculate the error rate:

$$\Delta = \frac{\sqrt{\sum \left[\left(\frac{f_{M1} - f_B}{f_B} \right) \Delta\varphi \right]^2}}{\varphi} = \frac{\sqrt{58,25}}{106,02} = 0,072 = 7,2\% \quad (4.1)$$

4. RESULTS AND DISCUSSION

That is mean the error rate between the original multibody model and measurement of the knee prosthesis for Balassa: 7, 2%.

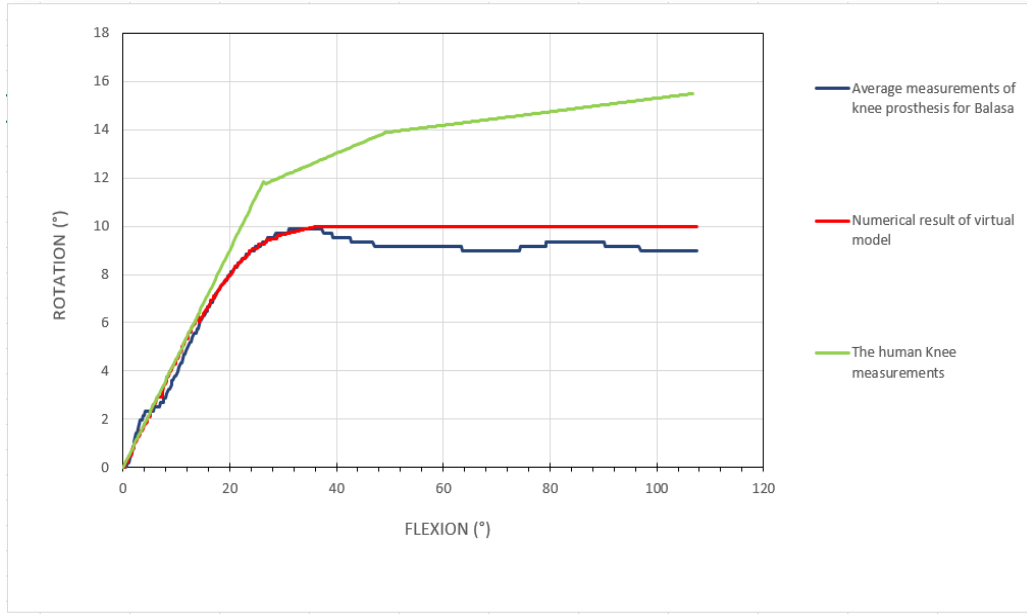


Fig 4.11 Verification results of our new virtual model with Balassa results and comparing with the human knee measurements.

For calculate the error rate between the prosthesis measurement for the human knee and the multibody model (M1) Fig 4.12:

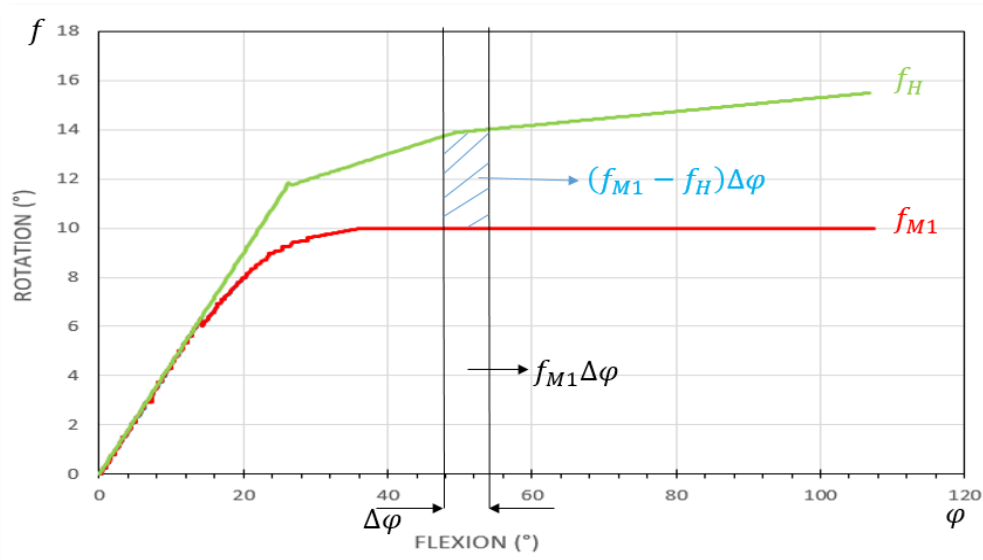


Fig.4.12 Normalized error between the average of the human knee and multibody model

As we can see the deferent between the human knee average and numerical results of virtual model (M1) presented by $(f_{M1} - f_H)\Delta\varphi$.

Calculate the error rate:

$$\Delta = \frac{\sqrt{\sum \left[\left(\frac{f_H - f_{M1}}{f_{M1}} \right) \Delta\varphi \right]^2}}{\varphi} = \frac{\sqrt{687,18}}{106,02} = 0,2472 = 24,72\% \quad (4.2)$$

That is mean the error rate between the original multibody model M1 and measurement of the human knee: 24, 72%.

4.2. The Virtual Multibody M2

In this part of study we change the geometry of the model M1 with new geometry to create new model M2, so we change the cylindrical joint with spherical joint, trying to get deferent results maybe it will be better.

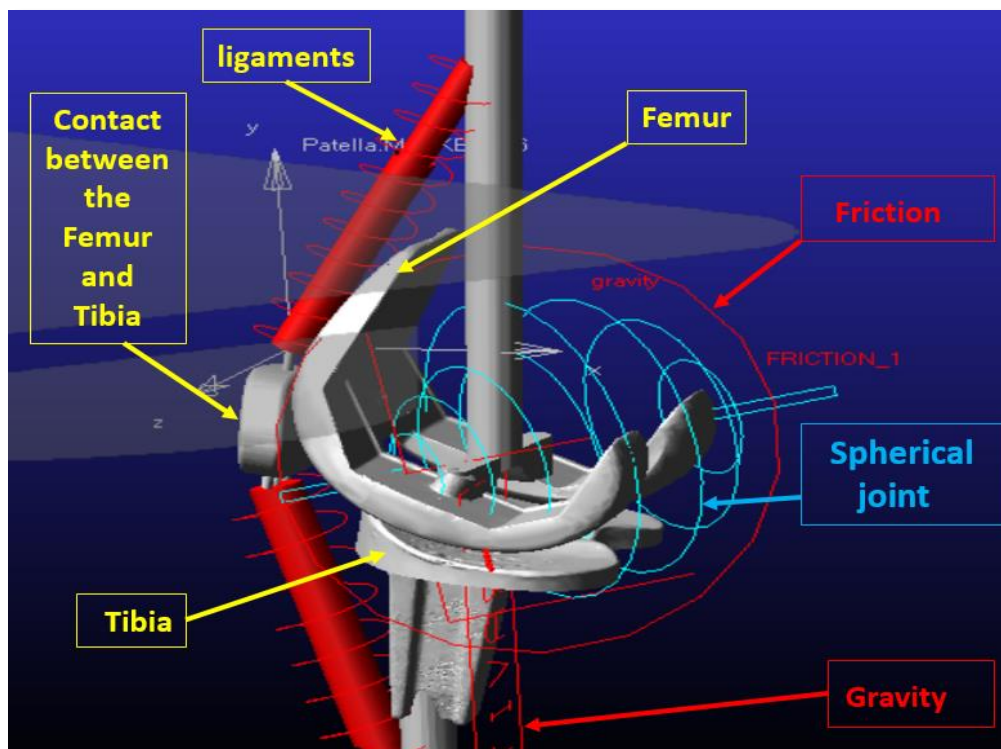


Fig 4.13. Our multibody M2 in the MSC.ADAMS.

After simulated model (M2) is shown in Fig 4.13. The graph of rotation against flexion is illustrated in Fig. 4.14. It was noticed that the angle of rotation varies linearly with respect to the flexion. It was observed that the sudden increase in the rotational angle was offset by an increase in the angle of curvature. A sharp rise in the flexion angle till 120° was seen beyond the rotational angle of 9° . The maximum elevation of flexion against the angle of rotation was found to be 120° .

4. RESULTS AND DISCUSSION

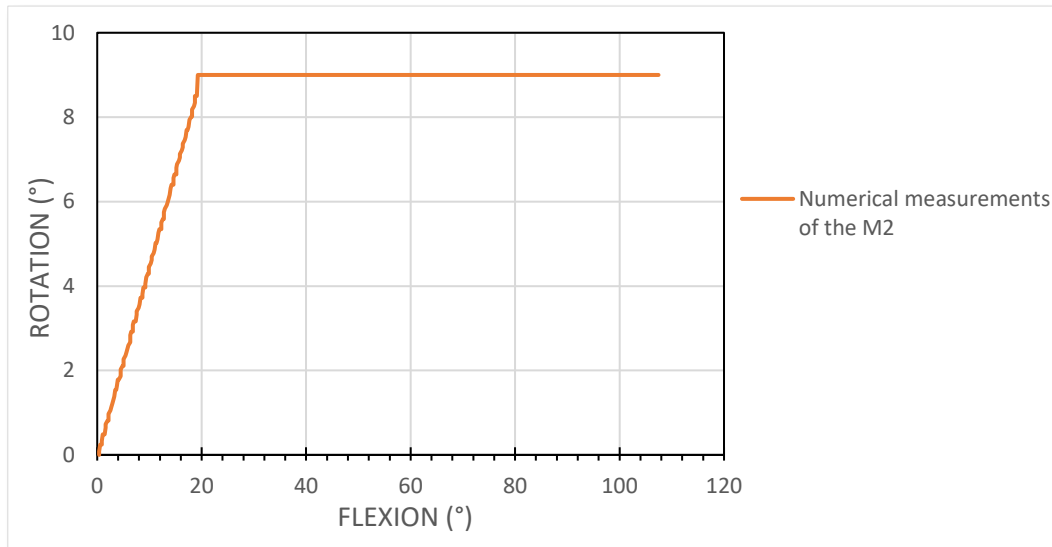


Fig 4.14. A graph of rotation against flexion of our virtual M2.

In order to validate the results from the numerical studies, we compared our virtual numerical model (M2) with the prostheses joints that have been tested using with the test machine in the Hungarian University of agriculture engineering and life science. The average values are plotted together against the virtual numerical model, as shown in Fig 4.15. The close similarity between the two curves indicates that this virtual model can replace the measurement by the test machine of the Hungarian University of Agriculture Engineering and Life Science.

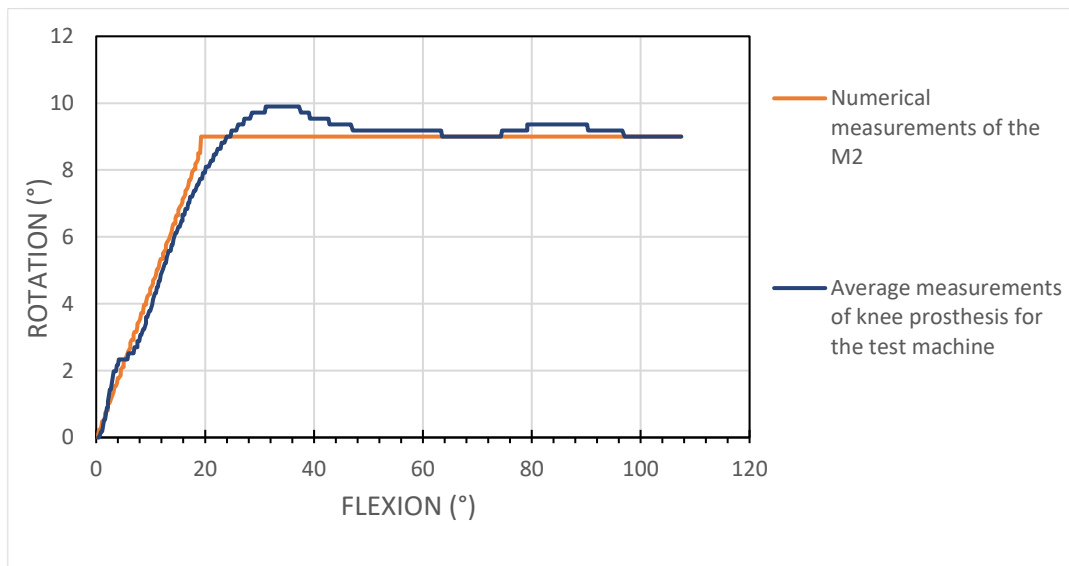


Fig 4.15. Verification results of our virtual M2 with the prosthesis developed with a test machine.

4. RESULTS AND DISCUSSION

So after comparing the new model (M2) we have to find the error rate between the between the average of the test machine results and multibody model M2

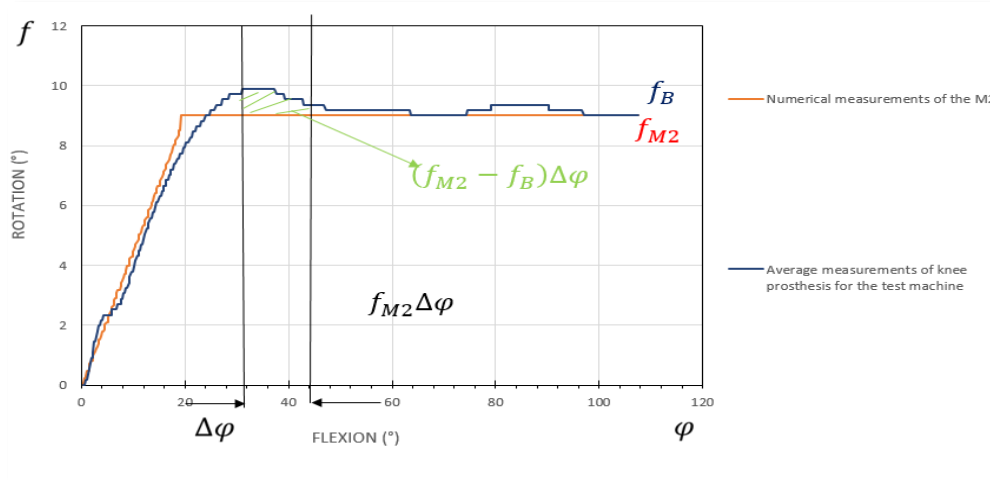


Fig.4.16 Normalized error between the average of the test machine results and multibody model M2.

As we can see (Fig4.16) the deferent between the measurements of the knee prosthesis for test machine and numerical results of virtual model (M2) presented by $(f_{M2} - f_B)\Delta\varphi$.

Calculate the error rate:

$$\Delta = \frac{\sqrt{\sum \left[\left(\frac{f_{M2} - f_B}{f_B} \right) \Delta\varphi \right]^2}}{\varphi} = \frac{\sqrt{34.978}}{106,02} = 0,0557 = 5,57\% \quad (4.1)$$

That is mean the error rate between the original multibody model (M2) and measurement of the knee prosthesis for test machine: 5, 57 %.

Table2: Comparing between the cylindrical joint and spherical joint

	Error rate comparing with measurement of the knee prosthesis for test machine (Balassa)
Using cylindrical joint	7,2%
Using spherical joint	5,57%

As we can see the different between the joints (geometry of the model) results and the measurements of the knee prosthesis for the test machine, that show us the best joint can give us the less error rate to be more close to the test machine in this study.so we will say that the best joint to make the best version of the multibody model it is spherical joint.

4.3 Developing the kinematic motion of Multibody model M2 for the knee prosthesis geometry

ADAMS Software is the most widely used multibody dynamics and motion analysis software in the world. Adams helps engineers study the dynamics of moving parts, how loads and forces are distributed throughout mechanical systems, and improve and optimize their products' performance (Fig 4.19).

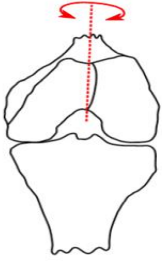
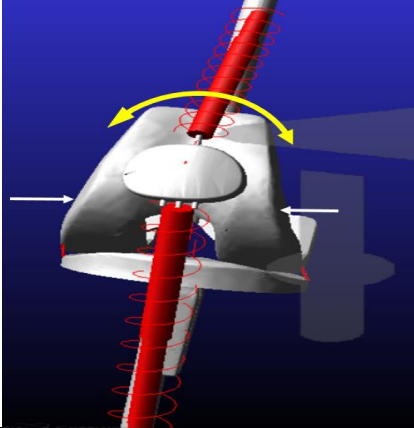
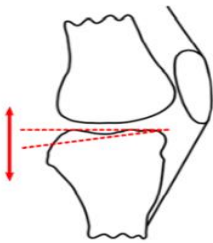
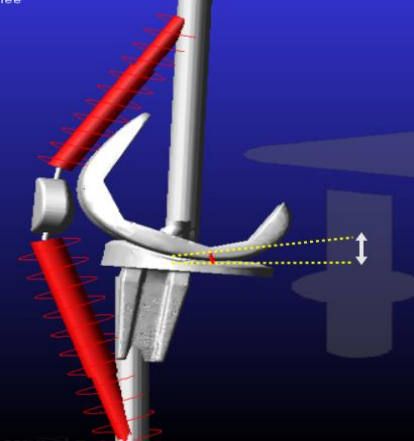
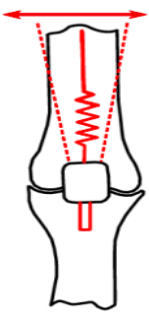
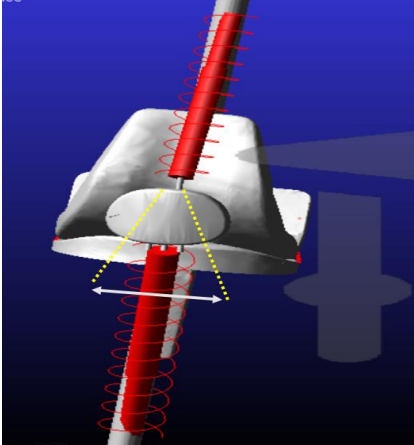
		<p>Femur [0° ↔ 5°]</p> <p>Tibia [0°]</p> <p>Quadriceps [0° ↔ 10°]</p>
		<p>Femur [0°]</p> <p>Tibia [0° ↔ 10°]</p> <p>Quadriceps [0° ↔ 10°]</p>
		<p>Femur [0°]</p> <p>Tibia [0°]</p> <p>Quadriceps [0° ↔ 10°]</p>

Fig 4.19 This diagram shows the specific movement measurements of our model, for the rotation degree of the femur and tibia and quadriceps.

4. RESULTS AND DISCUSSION

Table 3: Position 1 of the multibody model in the first measurement.

<i>The femur curve</i>	<i>Tibia leans back</i>	<i>Quadriceps</i>
5°	0°	10°

To validate the results from the numerical studies, we compared our virtual numerical model specifically for rotation of the femur and Tibia with the prosthesis joint that has been tested using the test machine at MATE University (Csizmadia, 2017)(can you cite the work done on the test machine at MATE University). The average values were plotted together against the virtual numerical model, as shown in Fig 4.19. The close similarity between the two curves indicates that this virtual model can replace the measurement with the MATE University test machine with a more appropriate way without cost and several measurements. It was also found that the rotation angle was increased as the flexion angle varied from 0° to 110° . And this study was under the following conditions with quadriceps at 10° , and femur curve at 5° and while Tibia leans back at the 0° . We noticed there are similar results between the proposed model and other prostheses. In this case, our new model has been created that enables us to make multiple measurements of a knee prosthesis. As a result, we can change the angles of artificial joints, make them more accessible, and obtain faster results without many calculations.

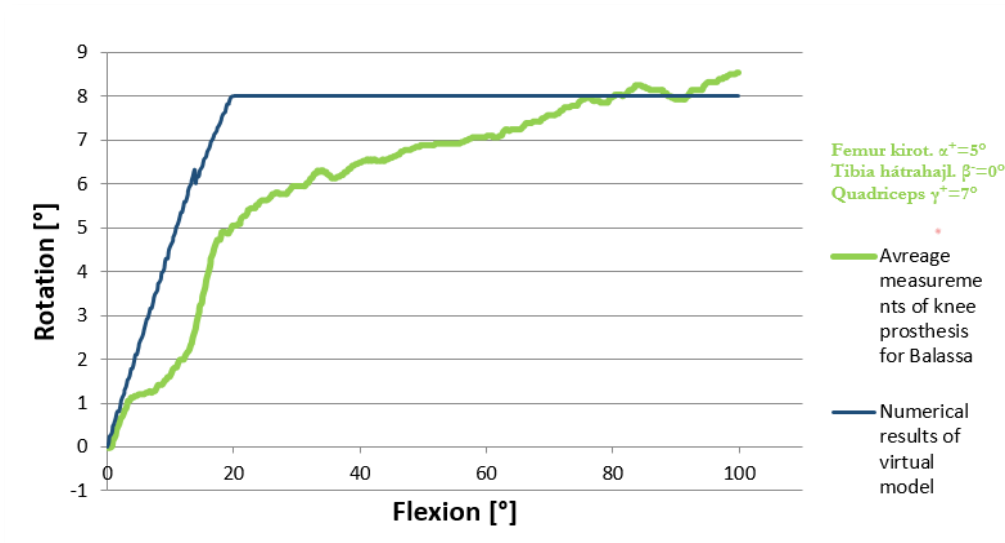


Fig. 4.20 Prosthesis measurement at the position 1 for the test machine and measurement of the multibody model.

For calculate the error rate between the prosthesis measurmnt at the postion 1 for the test machine and the multibody model (M1)Fig 4.21:

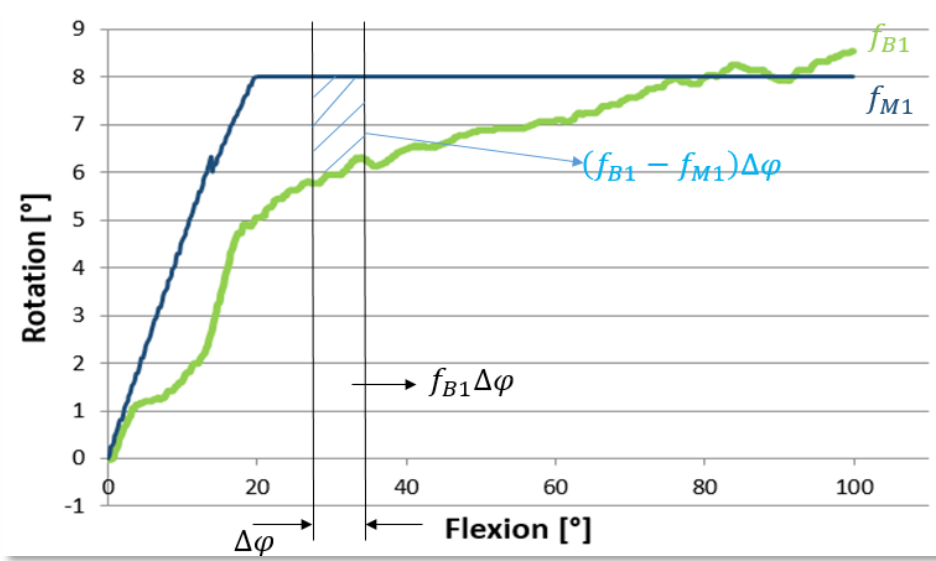


Fig.4.21 Normalized error between Balassa results and multibody model.

As we can see Fig 4.21 the deferent between the measurements of the knee prosthesis for test machine and numerical results of virtual model in position 1 presented by $(f_{B1} - f_{M1})\Delta\varphi$.

Calculate the error rate:

$$\Delta = \frac{\sqrt{\sum \left[\left(\frac{f_{B1} - f_{M1}}{f_{B1}} \right) \Delta\varphi \right]^2}}{\varphi} = \frac{\sqrt{175,148}}{106,02} = 0,1248 = 12,48\% \quad (4.3)$$

That is mean the error rate between the original multibody model and measurement of the measurements of the knee prosthesis for test machine: 12, 48%.

Table 4: Position 2 of the Multibody model in the second measurement

<i>The femur curse</i>	<i>Tibia leans back</i>	<i>Quadriceps</i>
5°	10°	3°

To validate the results from the numerical studies, we compared our virtual numerical model specifically for rotation of the femur and Tibia with the prosthesis joint that has been tested using the test machine at MATE University, The average values are plotted together against the virtual numerical model, as shown in Fig 4.22. The close similarity between the two curves indicates that this virtual model can replace the measurement with the MATE University test machine. It was also found that the rotation angle decreased marginally as the flexion angle varied from 0° to 15° and after the 20° we

4. RESULTS AND DISCUSSION

noticed a significant increase for rotation until 110°. And it was this study with quadriceps 3°, and femur curve degree at 5° and 10° for Tibia leans back.

Similar results have been noticed between the proposed model and other prostheses (Csizmadia, 2017). In this case, our new model has been created that enables us to make multiple measurements of a knee prosthesis geometry (Kheireddine and Oldal, 2021). As a result, we can change the angles of artificial joints, make them more accessible, and obtain faster results without many calculations.

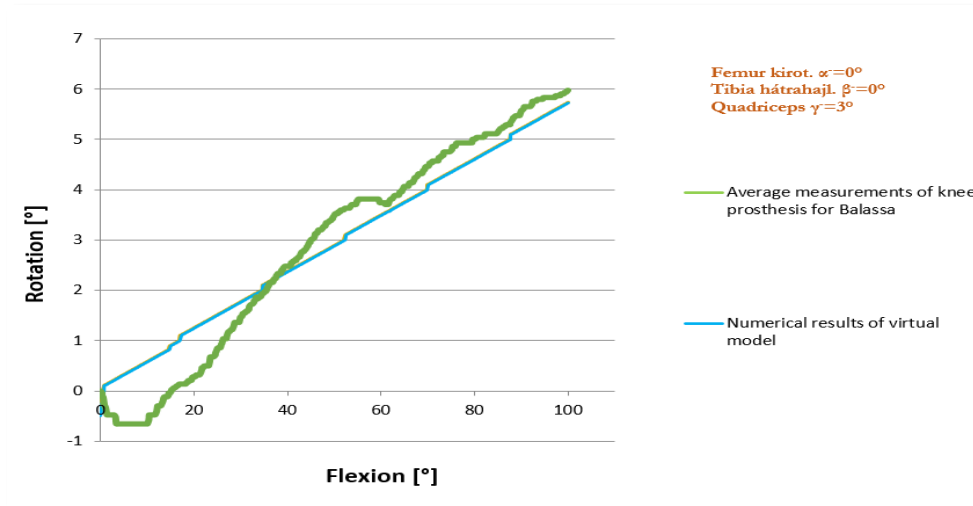


Fig. 4.22 Prosthesis measurement 2 for test machine results and measurement of the multibody model.

For calculate the error rate between the prosthesis measurement at the position 2 for the test machine and the multibody model (M2) Fig 4.23:

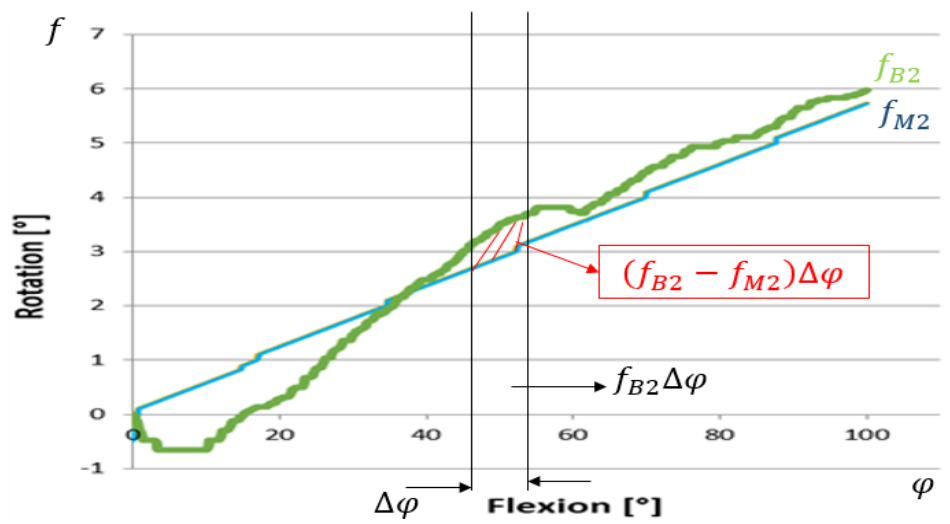


Fig.4.23 Normalized error for the test machine results and multibody model at the 2 position.

As we can see Fig 4.23 the different between the measurements of the knee prosthesis for test machine and numerical results of virtual model in position 2 presented by $(f_{B2} - f_{M2})\Delta\varphi$.

4. RESULTS AND DISCUSSION

Calculate the error rate:

$$\Delta = \frac{\sqrt{\sum \left[\left(\frac{f_{B2} - f_{M2}}{f_{B2}} \right) \Delta \varphi \right]^2}}{\varphi} = \frac{\sqrt{41,751}}{106,02} = 0,0609 = 6,09\% \quad (4.4)$$

That is mean the error rate between the original multibody model and measurement of the human knee: 6,09 %.

Table 5: Position 3 of the Multibody model in the third measurement

<i>The femur cruse</i>	<i>Tibia leans back</i>	<i>Quadriceps</i>
5°	10°	7°

It was also found that the rotation angle was stable as the flexion angle varied from 0° to 25°. Thus, our model's close agreement with other prosthetic joints is established in the flexion range of 25° to 110°. And it was this study with quadriceps 7° and femur cruse at 5° and 10° for tibia leans back (Fig 4.19). We noticed the same results between the proposed model and other prostheses. In this case, our new model has been created that enables us to make multiple measurements of a new model. As a result, we can change the angles of artificial joints, make them more accessible, and obtain faster results without many calculations Fig 4.24.

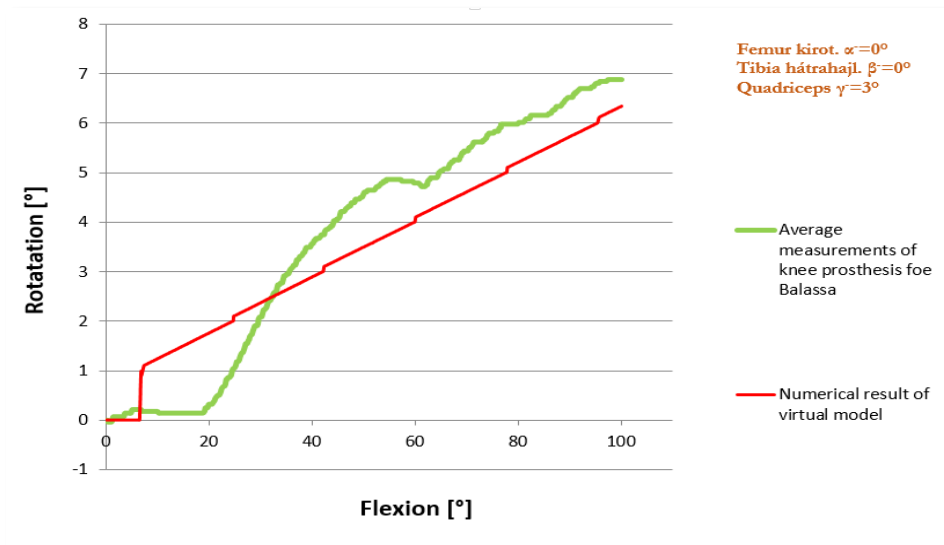


Fig 4.24 Prosthesis measurement 3 for the test machine and measurement of the multibody model.

4. RESULTS AND DISCUSSION

For calculate the error rate between the prosthesis measurmnt at the postion 3 for the test machine and the multibody model (M2)Fig 4.25:

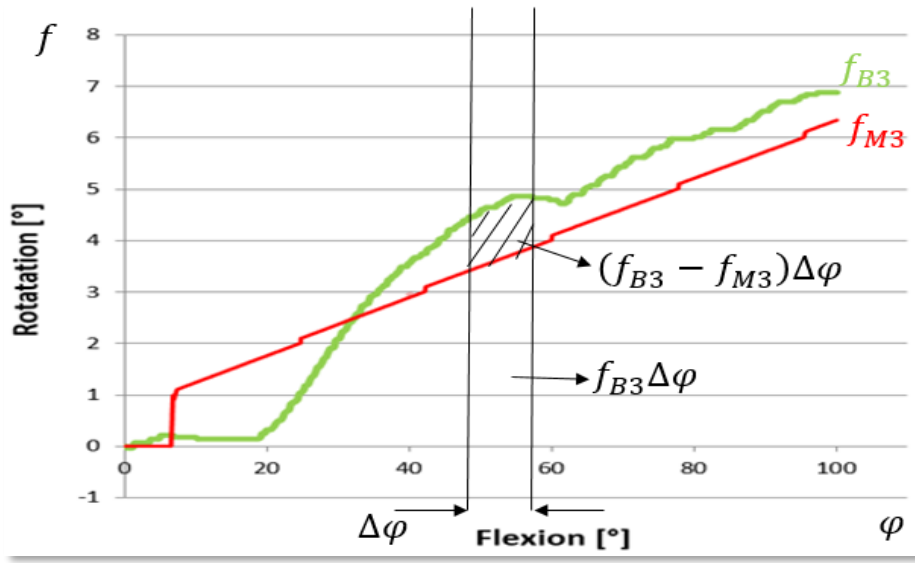


Fig.4.25 Normalized error between the test machine results and multibody model results at the 3 position.

As we can see Fig 4.25 the deferent between the measurements of the knee prosthesis for test machine and numerical results of virtual model in position 3 presented by $(f_{B3} - f_{M3})\Delta\varphi$.

Calculate the error rate:

$$\Delta = \frac{\sqrt{\sum \left[\left(\frac{f_{B3} - f_{M3}}{f_{B3}} \right) \Delta\varphi \right]^2}}{\varphi} = \frac{\sqrt{76,148}}{106,02} = 0,0823 = 8,23\% \quad (4.5)$$

That is mean the error rate between the original multibody model and measurement of the test machine results: 8, 23 %.

Table 6: Position 4 of the multibody model in the fourth measurement

<i>The femur curse</i>	<i>Tibia leans back</i>	<i>Quadriceps</i>
0°	0°	3°

It was also found that the rotation angle was significantly increased as the flexion angle varied from 0° to 17°. After that, we noticed some vibrations between 17° to 40°, and after 40°, we saw a decrease in rotation until 70° of flexion. Then, after 70° to 85°,

4. RESULTS AND DISCUSSION

rotation increases, and after 85° of flexion, we noticed that decrease again for rotation (Fig 4.26).

This part of the study was about making rotation for multibody model like Balassa did that with his test machine at MATE university we did the same study to compare our model with his results and has been determined multibody model range between 25° to 110° this for the flexion and for the rotation of the femur and tibia it was at 0° and it was this study as well under terms of quadriceps at 3°. Thus, our model's close agreement with other prosthetic joints was established in the flexion range of 25° to 110° with quadriceps fixed at 3°, femur curve at 0° and the Tibia leans back also at 0°.

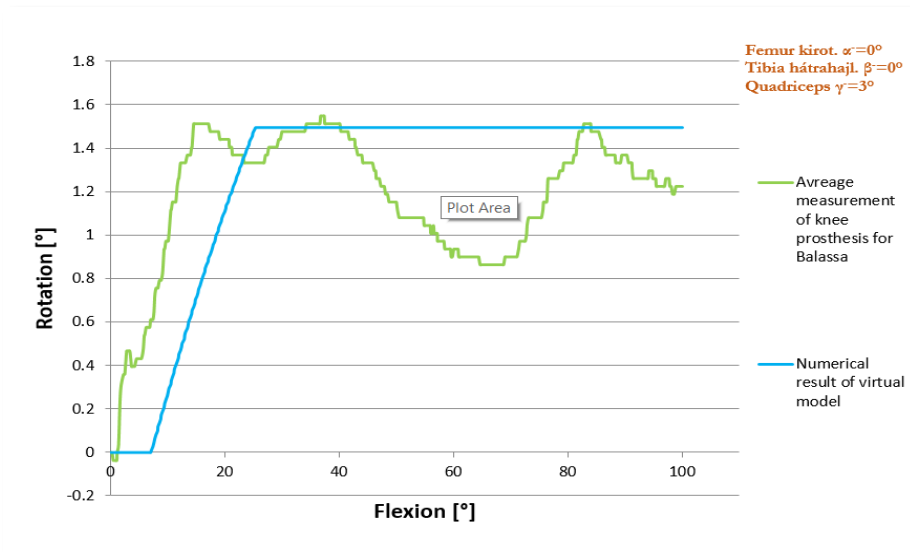


Fig 4.26 Prosthesis measurement 4 for the test machine results and measurement of the multibody model at the 4 position.

For calculate the error rate between the prosthesis measurement at the position 4 for the test machine and the multibody model (M2) Fig 4.27:

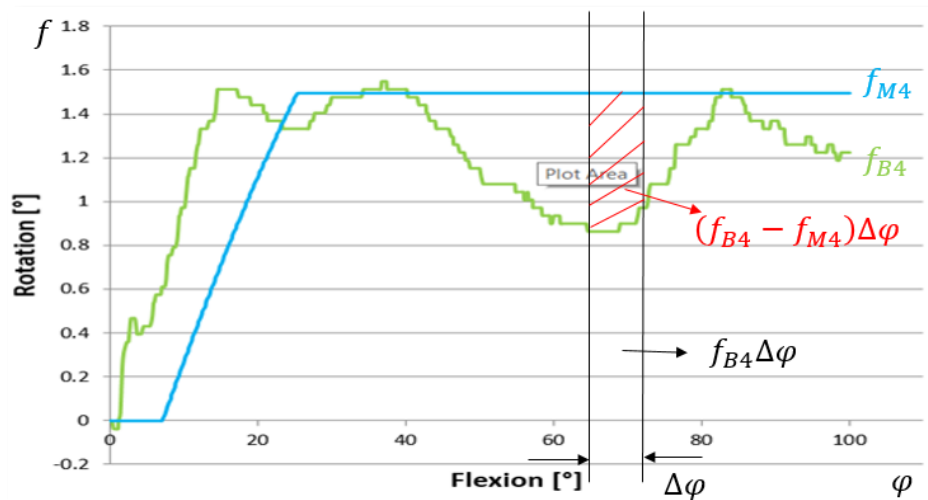


Fig.4.27 Normalized error between the test machine results and the multibody model results at the 4 position.

4. RESULTS AND DISCUSSION

As we can see Fig4.27 the deferent between the measurements of the knee prosthesis for the test machine results and numerical results of virtual model in position 4 presented by $(f_{B4} - f_{M4})\Delta\varphi$.

Calculate the error rate:

$$\Delta = \frac{\sqrt{\sum \left[\left(\frac{f_{B4} - f_{M4}}{f_{B4}} \right) \Delta\varphi \right]^2}}{\varphi} = \frac{\sqrt{312,26}}{106,02} = 0,1666 = 16,66\% \quad (4.6)$$

That is mean the error rate between the original multibody model and measurement of the test machine results: 16, 66 %.

Table 7: Position 5 of the multibody model in the fifth measurement

<i>The femur curse</i>	<i>Tibia leans back</i>	<i>Quadriceps</i>
0°	0°	7°

It was also noticed that there was a rise in the rotation angle as the flexion angle varied from 0° to 20° . And this study was under the following conditions: quadriceps at 7° , femur curse was at 0 degrees and tibia leans back was at 0° . In the final case of the study, we noticed there was a significant increase of the rotation for the multibody model at the beginning and we saw that in the Test machine measurement as well. Our results were at 7° of quadriceps while fixing the femur curse at 0° and the tibia leans back at 0° . But with high degree of quadriceps while fixing the femur and tibia at 0° , as can be seen in (Fig 4.19), there were different results for the multibody model and test machine in this case, so we can say our multibody dos not work well if we fix the femur and tibia while we put the quadriceps at 7° (Fig 4.28).

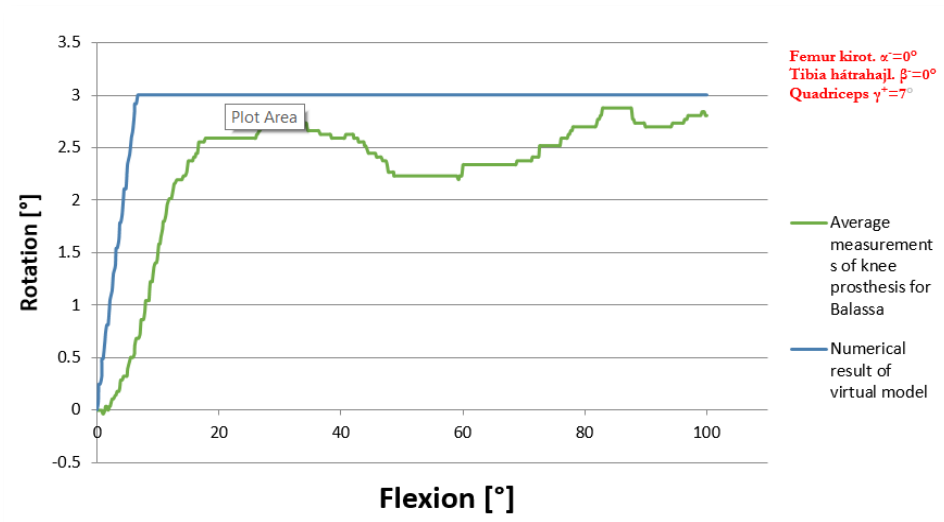


Fig 4.28 Prosthesis measurement 5 for the test machine results and measurement of the multibody model.

4. RESULTS AND DISCUSSION

For calculate the error rate between the prosthesis measurmnt at the postion 5 for the test machine and the multibody model (M2)Fig 4.29:

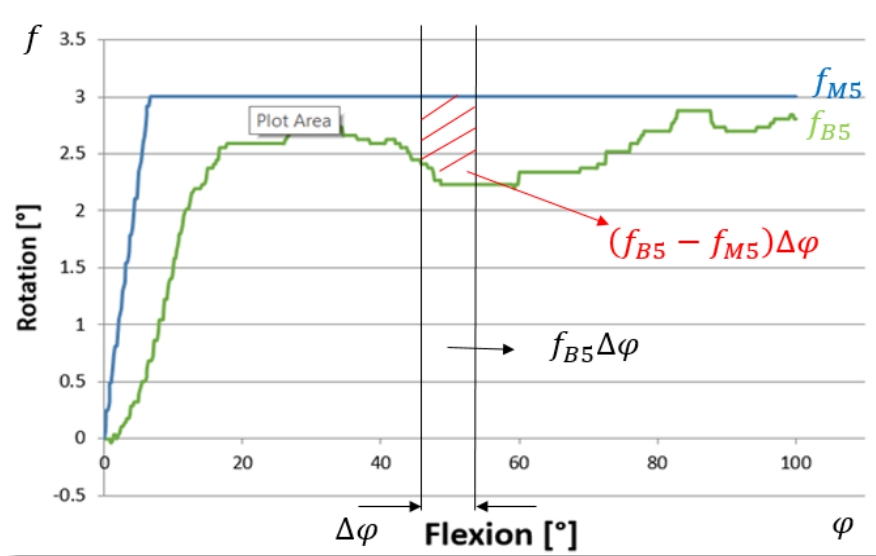


Fig.4.29 Normalized error between the test machine results and the multibody model results at the 5 position.

As we can see Fig4.29 the deferent between the measurements of the knee prosthesis for test machine results and numerical results of virtual model in position 5 presented by $(f_{B5} - f_{M5})\Delta\varphi$.

Calculate the error rate:

$$\Delta = \frac{\sqrt{\sum \left[\left(\frac{f_{B5} - f_{M5}}{f_{B5}} \right) \Delta\varphi \right]^2}}{\varphi} = \frac{\sqrt{455,789}}{106,02} = 0,2013 = 20,13\% \quad (4.6)$$

That is mean the error rate between the original multibody model and measurement of the test machine results: 20, 13 %.

In this case the error is big, so we can say that our model has limit in the case of (Femur =0°, and Tibia = 0°, Quadriceps =7°) do not working like the test machine.

4. RESULTS AND DISCUSSION

Table 7 Errors of the multibody model at different positions.

Position	Position of the model	Error Δ	
1	-Femur curse = 5° -Tibia Leans Back = 0° -Quadriceps = 10°	12,48%	Good
2	-Femur curse = 5° -Tibia Leans Back = 10° -Quadriceps = 3°	6,09%	Good
3	-Femur curse = 5° -Tibia Leans Back = 10° -Quadriceps = 7°	8,23%	Good
4	-Femur curse = 0° -Tibia Leans Back = 0° -Quadriceps = 3°	16,66%	Acceptable
5	-Femur curse = 0° -Tibia Leans Back = 0° -Quadriceps = 7°	20,13%	Not acceptable

The error less than 10% we can say that it is very good results can be close to test machine results, and if the error between the 10% and 20% we can say that it is acceptable, but if the error more than 20% that results is not good because of the different results between the test machine and the multibody model so big.

So we conclude form that table our multibody model can work like the test machine with less error at 4 position as showed in the table 7, but there are one case shown us big number of error between the test machine and our multibody model at the position number 5. When we put the femur at 0° and tibia at 0° as well and quadriceps at 7° do not work like the test machine, and given us big error.

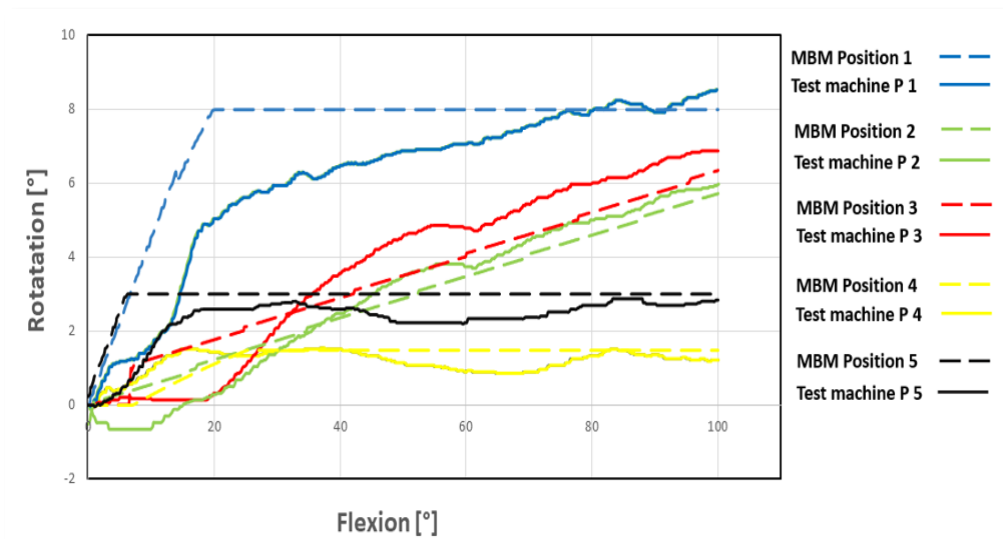
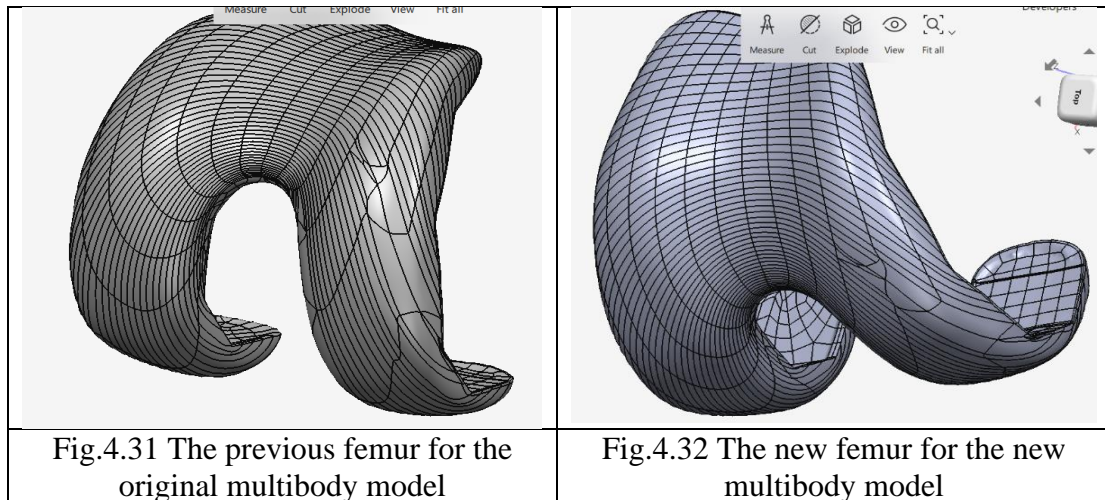


Fig 4.30 Verification results of our virtual model with the prosthesis developed with

a test machine by making several prosthesis measurements.

To validate the results from the numerical studies, we compared our virtual numerical model specifically for rotation of the femur and Tibia with the prosthesis joint that has been tested using the test machine at MATE University in different positions. We noticed there is a slight difference in the error rate between the test machine results and our multibody model in first 4 specific position, but there is one case do not work perfectly as the test machine table7. In this case, we validate the new model that enables us to make multiple measurements of a rotation of the knee. As a result of test machine with slight error rate, and we can change the materials made of artificial joints, more accessible, and obtain faster results without many calculations.

4.4 Developing the new prosthesis geometry



With using Solidworks we made some changing at the femur structure Figs 4.31 and 4.32, with these modification we let the femur moving more effected, and some changes in length width and thickness.

4. RESULTS AND DISCUSSION

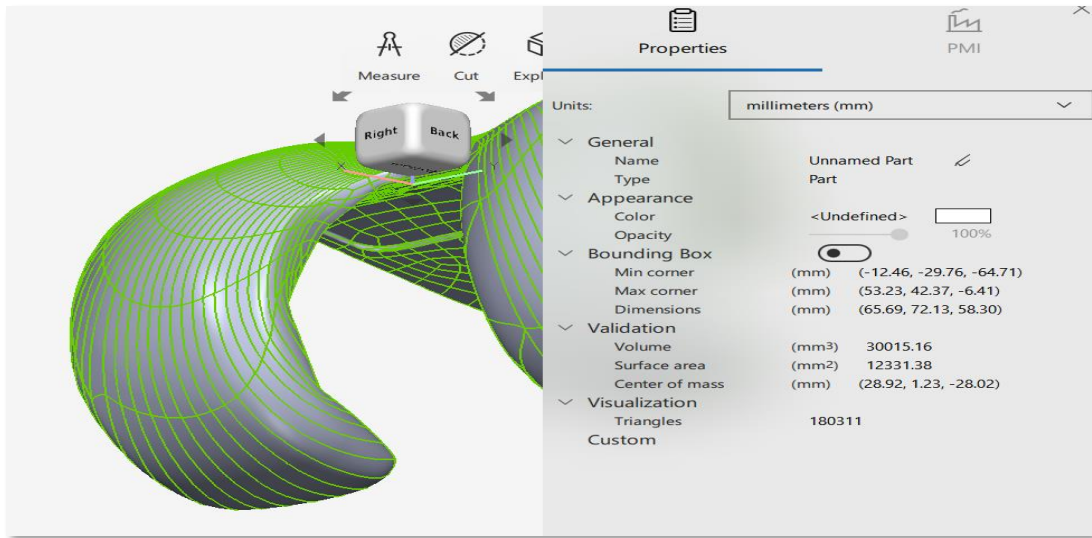


Fig.4.33 Femur of the original multibody model

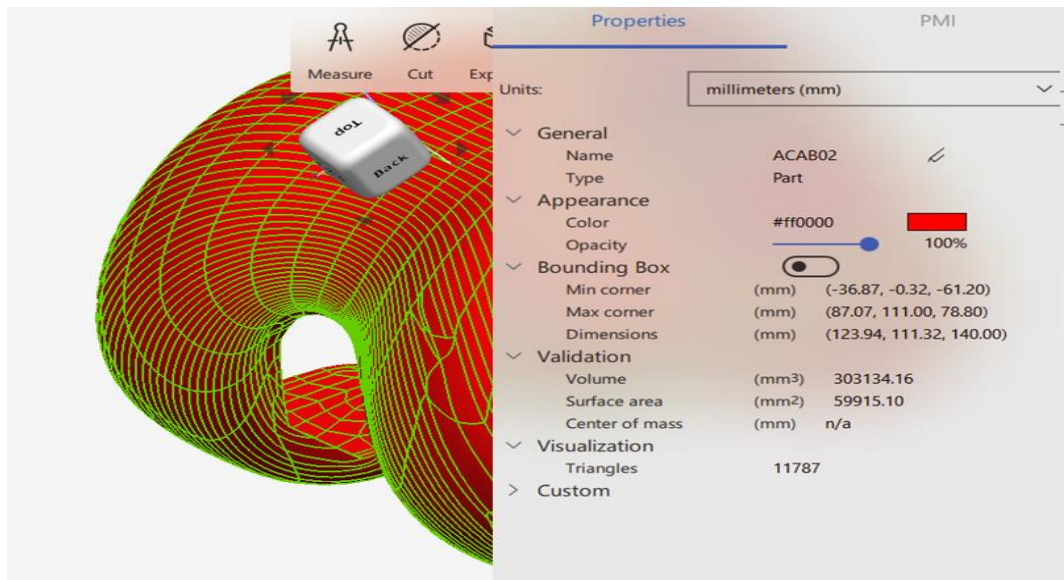


Fig.4.34 Femur of the new multibody model

Femur femoral size for original multibody model	Femur femoral size for new multibody model
---	--

4. RESULTS AND DISCUSSION

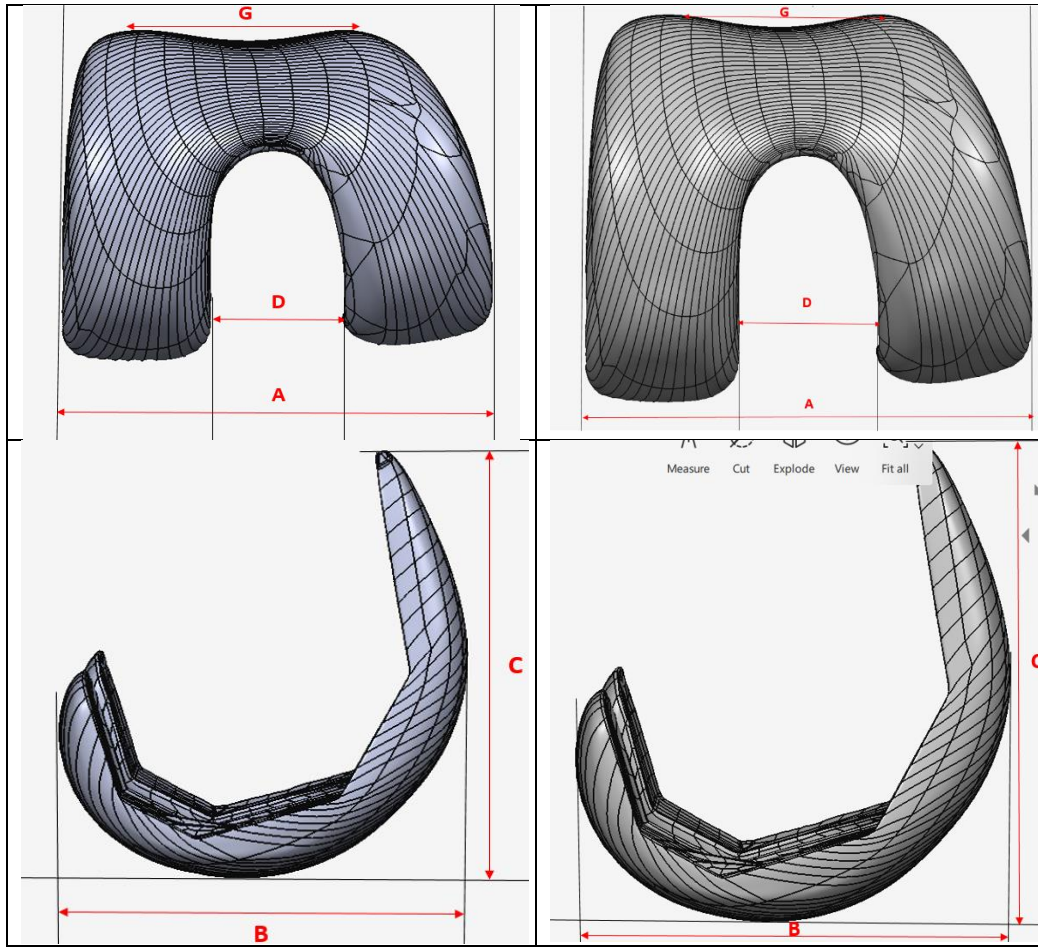


Fig.4.35 Femoral size for the femur

Table 8: Size specifications of the femoral component of total knee replacement.

Femoral size	A	B	C	D	G
Femur of the original multibody model	71,13mm	72,13mm	58,3mm	28,92mm	28,02mm
Femur of the new multibody model	87,07mm	78,8mm	61,2mm	36,2mm	29,51mm

As we can see the table presented the specifications femoral size that have been changed Fig4.35, so we change the width A to 87,07mm and the length C to 61,2 mm and thickness D to 36,2mm. With these changing at the Table 8 we got the new Multibody model Fig 4.36.

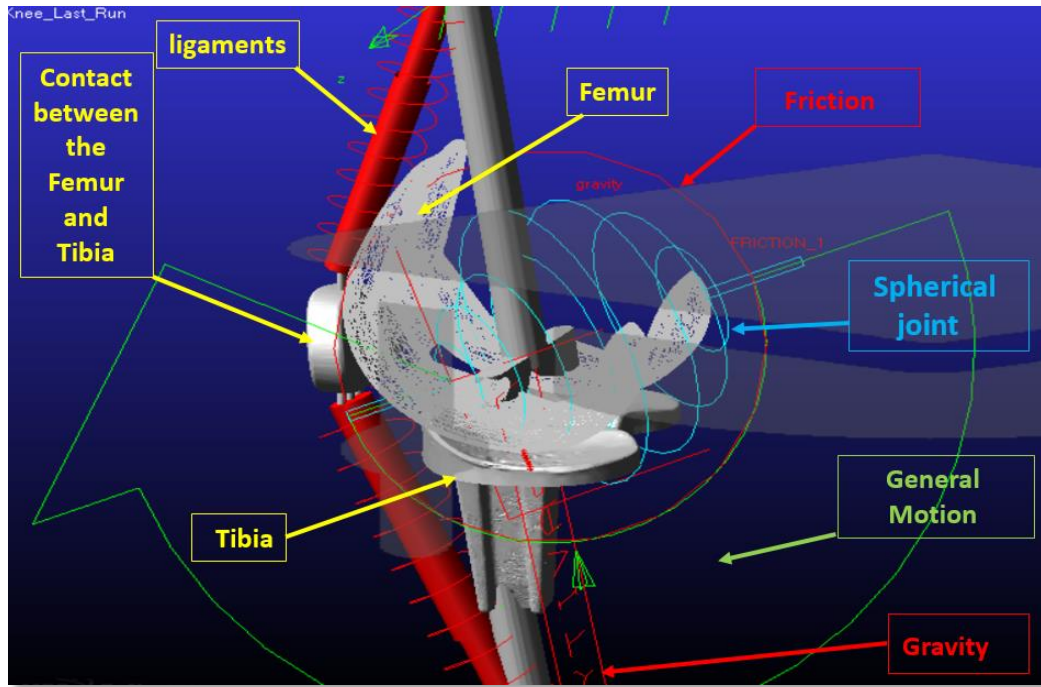


Fig 4.36. Our new multibody model in the MSC.ADAMS.

4.4.1. Boundary conditions for the simulation

After the geometrical model was obtained, the MSC ADAMS program was used to build the multibody model. First, the following boundary conditions were applied to our model (prosthesis geometry):

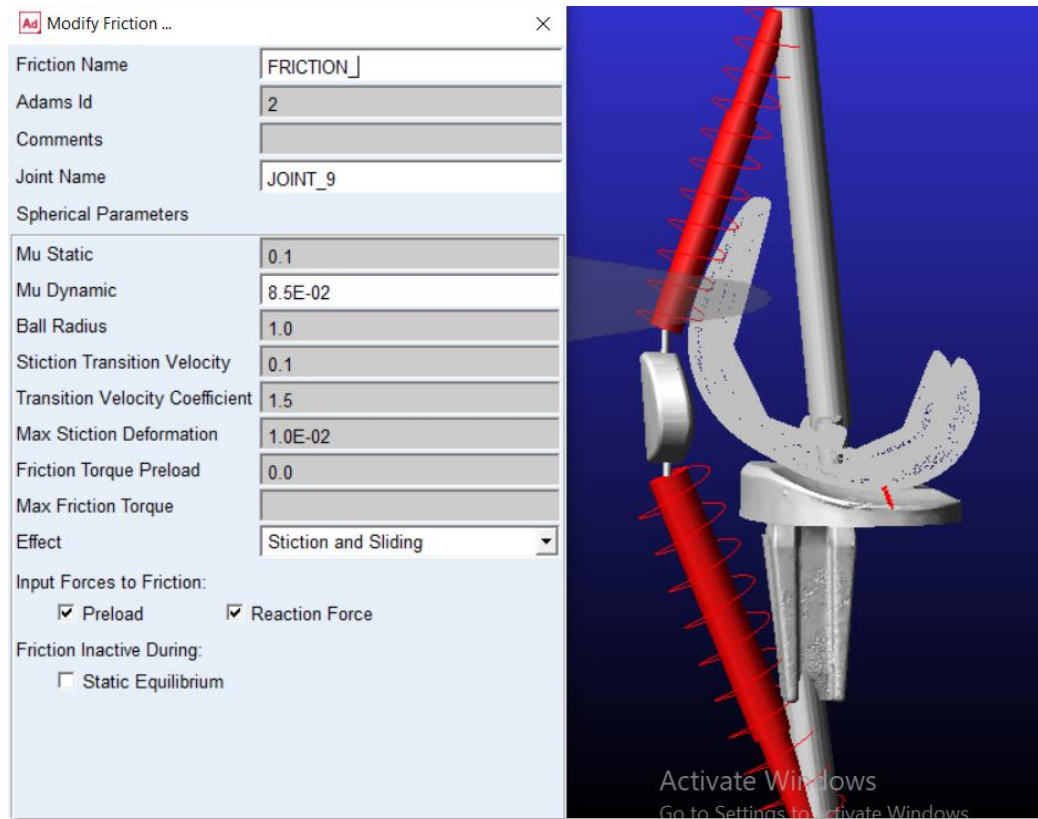


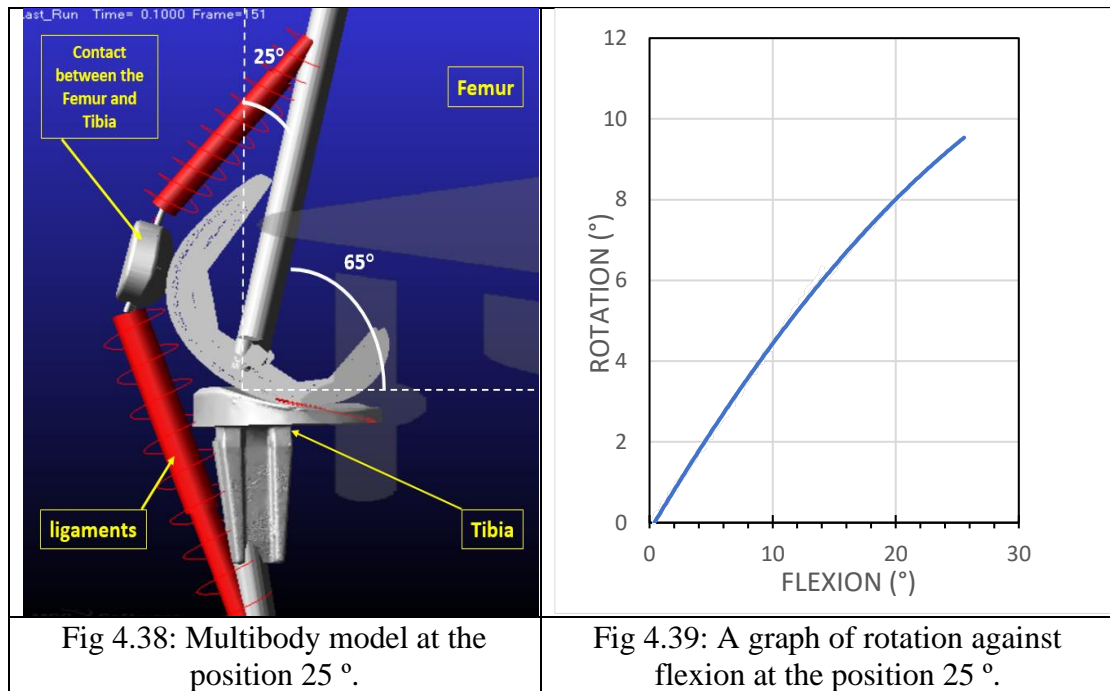
Fig 4.37. Parameters for friction multibody model.

4.4.2. Simulation of the multibody model in different positions

4.4.2.1. Simulation of the Multibody model at the position of 25°.

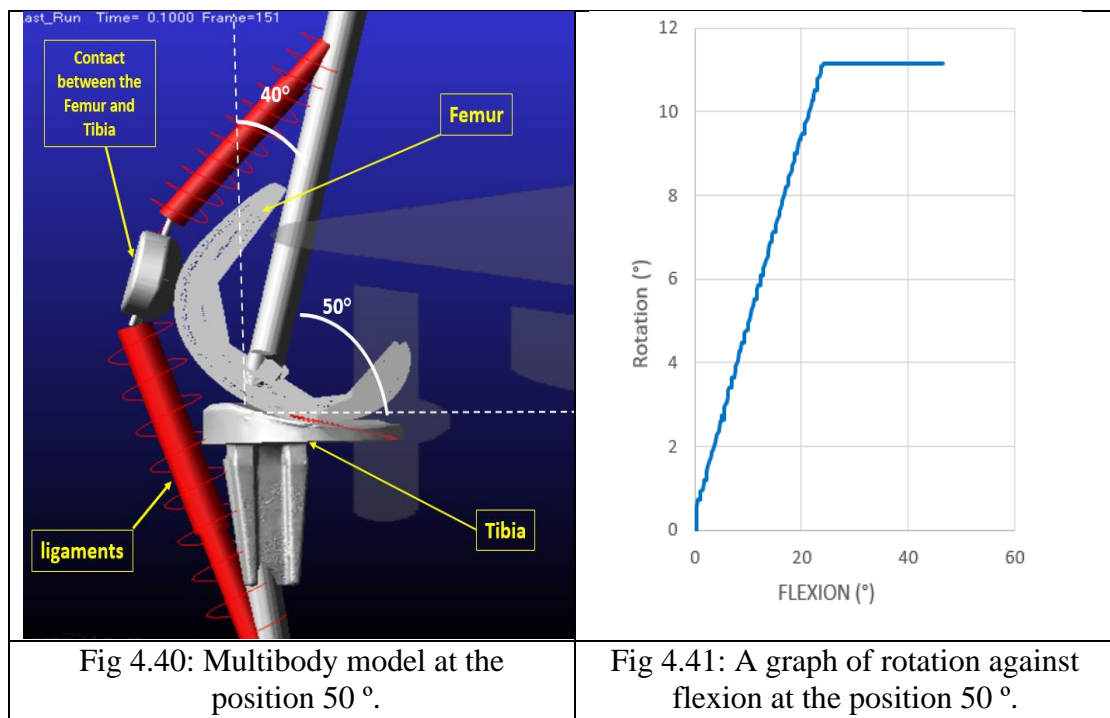
The simulated model is shown in Fig 4.38. The graph of rotation against flexion is illustrated in Fig. 4.39. It was noticed that the angle of rotation varies linearly concerning the flexion. It was observed that the sudden increase in the rotational angle was offset by an increase in the angle of curvature. A sharp rise in the flexion angle till 25° was seen beyond the rotational angle of 20°. The maximum elevation of flexion against the angle of rotation was found to be 25°.

4. RESULTS AND DISCUSSION



4.4.2.2. Simulation of the Multibody model at the position of 50 °.

The simulated model and the graphical representation of the rotational angle with flexion are depicted in Figs 4.40 and 4.41, respectively. It was observed that there was an increase in the degree of rotation (virtual axis) from 0° to 9.5°, whereas the flexion (horizontal axis) varies until 50°. Furthermore, the flexion angle's relative variation was five times bigger than the rotational angle, which indicates that the onset of sliding between the tibia and the femur in the knee occurs in the range of 20°-30° of flexion angle, which conforms to the movement range of the normal human knee.



4.4.2.3. Simulation of the multibody model at the position of 100 °

The pictorial representations of the model at the angles of 0° and 100° of flexion are shown in Figs 4.42 and 4.43. The relationship between the angles of rotation and flexion is illustrated in Fig 4.44. It is observed that the sudden increase in the rotational angle was offset by an increase in the angle of curvature. A sharp rise in the flexion angle till 35° was seen beyond the rotational angle of 20°, which indicates the onset of sliding between the tibia and the femur in the knee. Similarly, the flexion angle in the range of 20°-30° originates the joint prone to rolling. In contrast, the rotational angle's stability for the flexion angle lies in the range of 30° to 110°. The increasing flexion angle indicates that the tendency of sliding is predominant.

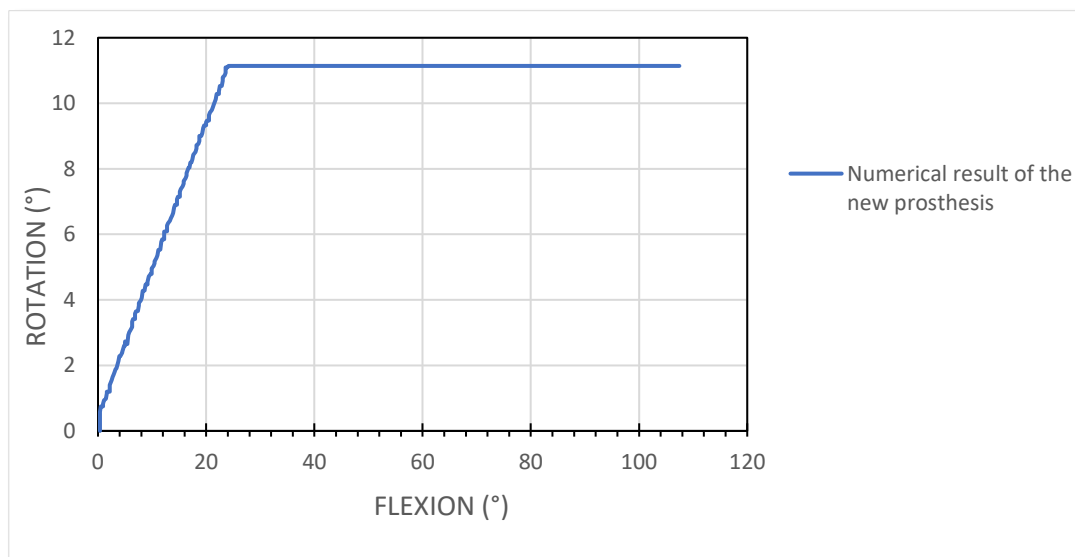
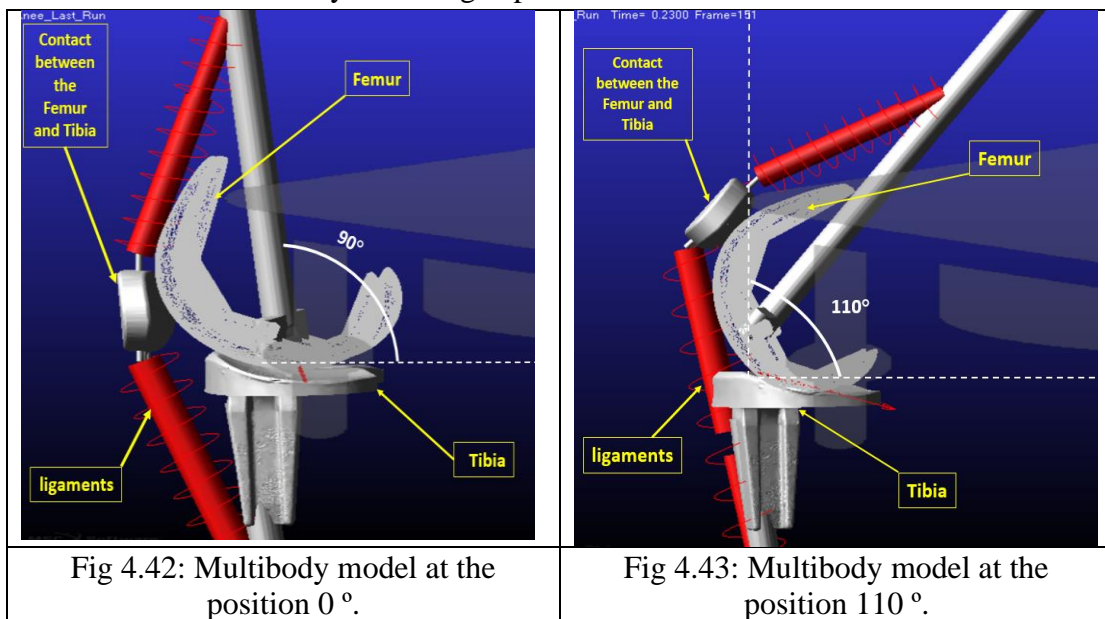


Fig 4.44. A graph of rotation against flexion of our virtual model.

4.4.3. Comparing the current study results of the new prosthesis geometry with a previous results from my previous multibody model M2.

To validate the results from the numerical studies, we compared our virtual numerical model with the prostheses joints that have been tested using the test machine in MATE University. The average values are plotted together against the virtual numerical model, as shown in Fig 4.45. The close similarity between the two curves indicates that this virtual model can replace the measurement with the MATE University test machine.

It was also found that there was a rise in the rotation angle as the flexion angle varied from 0° to 30° . Thus, our model's good value agreement with other prosthetic joints is established in the flexion range of 30° to 110° .

We noticed there are the same results between the proposed model and other prostheses. In this case, we created a new model that enables us to make multiple measurements of a new model. As a result, we can change the materials made of artificial joints, more accessible, and obtain faster results without many calculations.

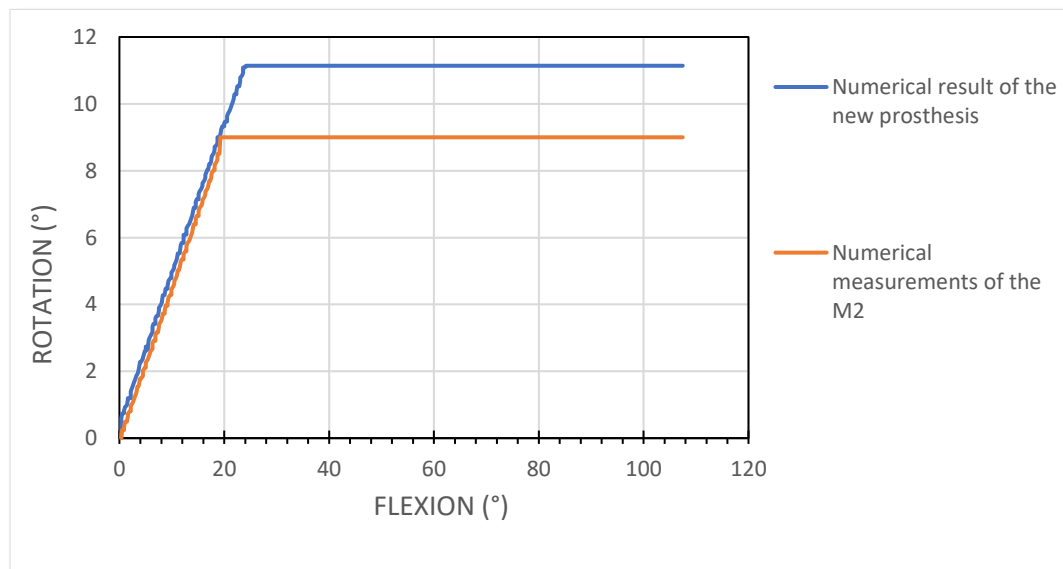


Fig 4.45. Comparing results of our virtual new model with our previous virtual model.

4. RESULTS AND DISCUSSION

For calculate the error rate between the human knee measurements and the numerical results of the original model (M2) Fig 4.46:

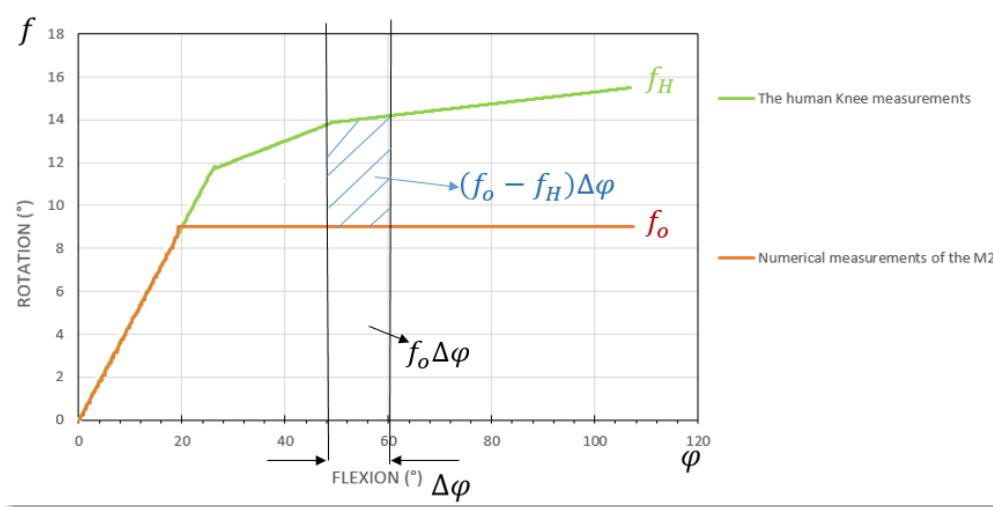


Fig.4.46 Normalized error between the human knee measurements and the original model.

As we can see Fig 4.46 the deferent between the numerical measurements of the original multibody model and the human knee measurements presented by $(f_o - f_H)\Delta\varphi$.

Calculate the error rate:

$$\Delta = \frac{\sqrt{\sum \left[\left(\frac{f_o - f_H}{f_o} \right) \Delta\varphi \right]^2}}{\varphi} = \frac{\sqrt{1085.547}}{106,02} = 0,3106 = 31,06\% \quad (4.7)$$

That is mean the error rate between the original multibody model and the human knee measurements: 31,06 %.

4. RESULTS AND DISCUSSION

Comparing our new prosthesis model with human knee results, as shown in Fig 4.47, we noticed that still there are big different to reach the best results can allowed us to say that we got good results to be more close to the range of the human knee measurements,

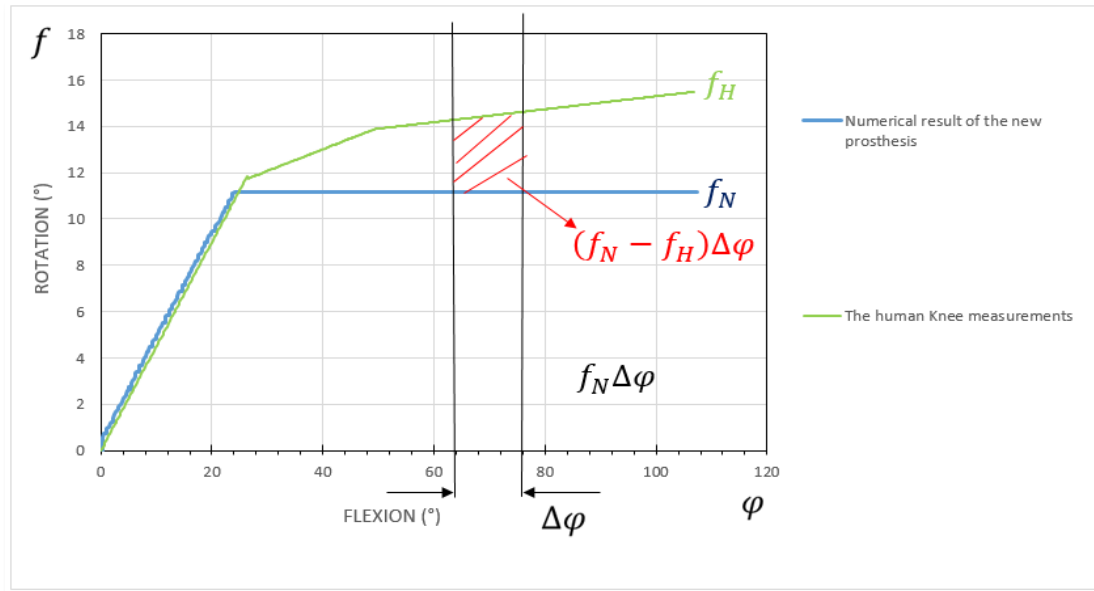


Fig.4.47 Normalized error between the new multibody model and a human knee

As we can see Fig 4.47 the deferent between the measurements of the human knee and numerical measurements of the new multibody model presented by $(f_N - f_H)\Delta\varphi$.

Calculate the error rate:

$$\Delta = \frac{\sqrt{\sum \left[\left(\frac{f_N - f_H}{f_N} \right) \Delta\varphi \right]^2}}{\varphi} = \frac{\sqrt{499,258}}{106,02} = 0,2107 = 21,07\% \quad (4.8)$$

That is mean the error rate between the measurements of the human knee and numerical measurements of the new multibody model: 21, 07 %.

At the end of this part of study, we will say that our new prosthesis geometry is good enough and show us can reach good results better than the original knee prosthesis model.

4. RESULTS AND DISCUSSION

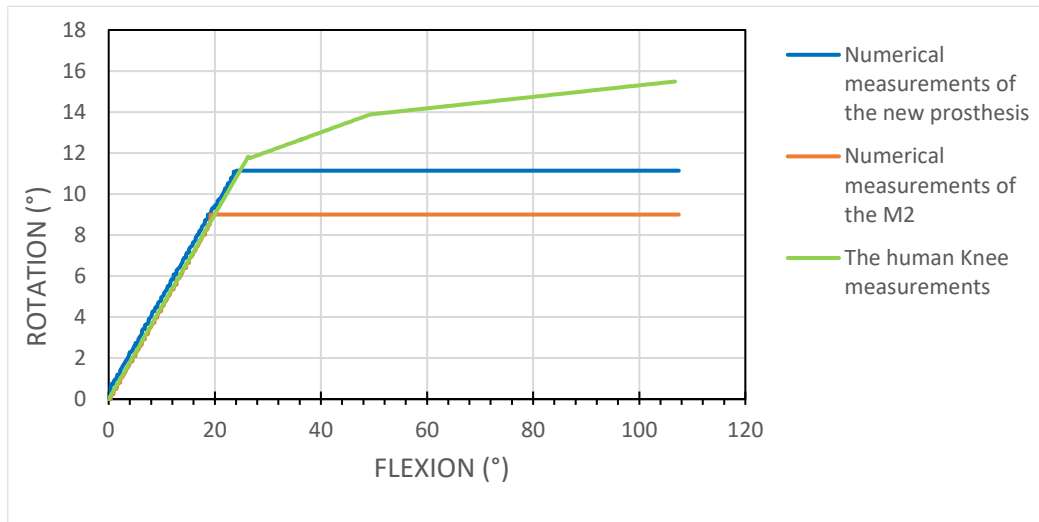


Fig 4.48. Comparing results of our new virtual model with the previous virtual model M2 and with the human knee measurements.

In the end, to validate the results from the numerical studies, we compared our original virtual numerical model with new virtual model with the prostheses joints that have been tested using the test machine in the MATE University. The average values are plotted against the virtual numerical models (new and original geometry), as shown in Fig 4.48. It was also found that there was a rise in the rotation angle as the flexion angle varied from 0° to 30°. Thus, our models (new and previous) are good value agreement with other prosthetic joints is established in the flexion range of 30° to 110°.

We noticed the same results between the proposed models (new and original) and other prostheses. In this case, we created new models (new and original) that enable us to make multiple measurements of new models. As a result, we can change the materials made of artificial joints, more accessible, and obtain faster results without many calculations. And without cost, we can make several measurements for a person's knee size to be repaired.

5. NEW SCIENTIFIC RESULTS

1. *New multibody model and numerical method for knee prosthesis*

I have been create the new multibody model of the knee prosthesis geometry by using MSC.ADAMS program, the ADAMS programmer could compute the forces directly. At first, we saved it as PARASOLID, and we imported it into the MSC.ADAMS. The flexion angle was derived by combining the femur and tibia's angular velocities about the x-axis. This was done considering that the model was at 20 degrees for the sliding and rolling at the start of the movement. The angles were divided into three to tackle the three-dimensional movement. To be able to describe all the coordinates, we have restricted the distal femur by the general point motion, as shown in the results. The knee model was restricted by a cylindrical joint, which allows the flexion process between a femur and tibia. Simple linear springs are designed as the boundary between the rectus femur and the patellar tendon. With this model I developed the numerical measurement if the knee prosthesis geometry which fulfils the mechanical requirements of the human knee. The MSC.ADAMS programmer was applied to demonstrate the movement of the human knee joint in terms of rotation and flexion.

2. *Limits of the kinematic motion of multibody model for the knee prosthesis geometry*

I developed the kinematic motion of multibody model for the knee prosthesis geometry and this part of the study was about making rotation for Multibody model like Balassa did that with his test machine at MATE university we did the same study to compare our model with his results and has been determined Multibody model range between 25° to 110° this for the flexion and for the rotation of the femur and tibia it was at 0 degrees and it was this study as well under terms of quadriceps at 3°. Thus, our model's close agreement with other prosthetic joints was established in the flexion range of 25° to 110° with quadriceps fixed at 3 degrees, femur curve at 0 degrees and the Tibia leans back also at 0 degrees.

3. *New knee prosthesis geometry*

I developed the new multibody model of the knee prosthesis geometry and I developed the new numerical measurement and I got the good result better than the previous one so with these results we can replace the previous model with new model, and the results was close to the normal human knee, so the new model can be the best solution to use the numerical measurement of the knee prosthesis geometry, and using the new Multibody model for the new prosthesis with better results and better than the previous model and the test machine method.

6. CONCLUSIONS AND SUGGESTIONS

The MSC.ADAMS programme was applied to determine the human knee joint's movement in terms of rotation and Flexion. The relationship between these two processes was also described. The changes that occur between the condyles of the developed multibody of the prosthesis are also investigated concerning the flexion angle ranging from 20 to 120 degrees. The boundary conditions were determined, and simulations were performed using the ADAM's programme. Three-dimensional geometry was applied in the new virtual model, taking into account the influence of the condyles and collateral. The multibody modelling was used to measure the degree of Flexion and rotation of the knee concerning its position, like extension or Flexion or rotation, as well as inserting a spring between the tibia and femur while observing its effects on the performance of the knee. A slip ration which is higher than 0.45, as was the limit in literature, was achieved. Applying our model, an average value of 0.7 was reached with the maximum getting up to 0.79, and also obtaining an angle between 110° and 120° for the flexion angle. The generated virtual model was used to measure the knee pros-thesis size before its creation. This virtual model could be used to measure the knee prosthesis size before creating it because it saves time, money, and effort instead of using 3D printing technology, and CNC milling consumes our time, money and effort.

At the end we have to compare all the results together between 2 models that have been created by ADAMS program and the test machine measurements and the human knee average Fig 6.1.

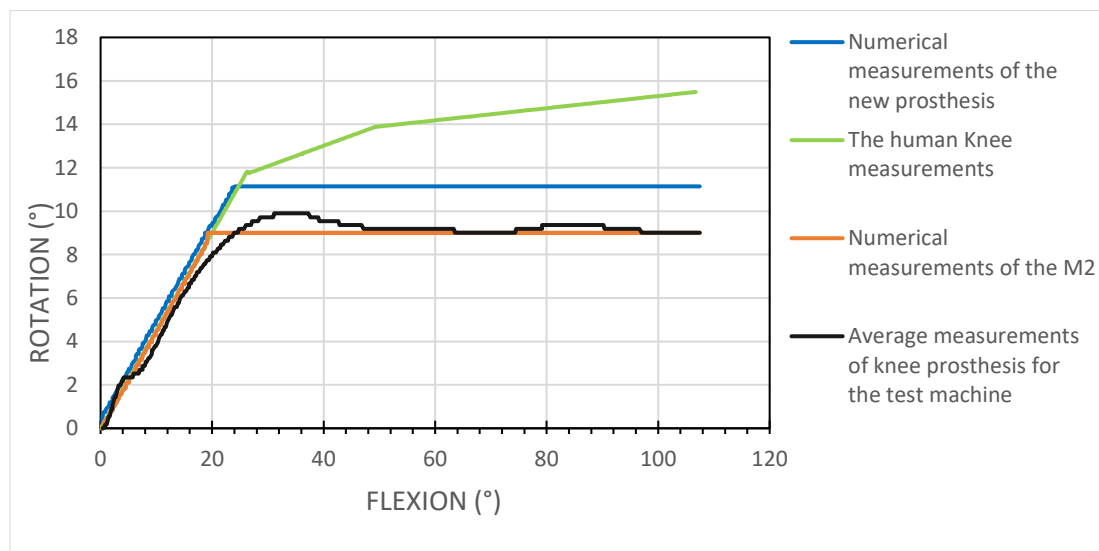


Fig 6.1. Verification results of our new virtual model with the previous virtual model comparing with the human knee measurements and the test machine results.

6. CONCLUSIONS AND SUGGESTIONS

As we can see there are 2 types of our multibody model for the knee prosthesis geometry comparing with the human knee measurements and the average measurements of knee prosthesis for Balassa,

To know exactly how much different between the lines we will applied the integral equation :

$$\Delta = \frac{\sqrt{\sum \left[\left(\frac{f_0 - f_1}{f_0} \right) \Delta \varphi \right]^2}}{\varphi} \quad (6.1)$$

- Comparing between the numerical results of original multibody model and the human knee prosthesis measurements:

$$\Delta = \frac{\sqrt{\sum \left[\left(\frac{f_0 - f_H}{f_0} \right) \Delta \varphi \right]^2}}{\varphi} = \frac{\sqrt{1085,547}}{106,02} = 0,3106 = 31,06\% \quad (6.2)$$

That is mean the error rate between the original multibody model and the human knee measurements: 31, 06 %.

- Comparing between the human knee prosthesis results with the new multibody model error rate:

$$\Delta = \frac{\sqrt{\sum \left[\left(\frac{f_N - f_H}{f_N} \right) \Delta \varphi \right]^2}}{\varphi} = \frac{\sqrt{499,258}}{106,02} = 0,2107 = 21,07\% \quad (6.3)$$

That is mean the error rate between the measurements of the human knee and numerical measurements of the new multibody model: 21, 07 %.

- Comparing between the original multibody model(M1) and measurement of the knee prosthesis for Balassa:

$$\Delta = \frac{\sqrt{\sum \left[\left(\frac{f_{M1} - f_B}{f_B} \right) \Delta \varphi \right]^2}}{\varphi} = \frac{\sqrt{58,25}}{106,02} = 0,072 = 7,2\% \quad (6.4)$$

That is mean the error rate between the original multibody model and measurement of the knee prosthesis for Balassa: 7, 2%.

- Comparing between the multibody model(M2) and measurement of the knee prosthesis for Balassa:

$$\Delta = \frac{\sqrt{\sum \left[\left(\frac{f_{M2} - f_B}{f_B} \right) \Delta \varphi \right]^2}}{\varphi} = \frac{\sqrt{34,978}}{106,02} = 0,0557 = 5,57\% \quad (6.5)$$

That is mean the error rate between the original multibody model (M2) and measurement of the knee prosthesis for test machine: 5, 57 %.

6. CONCLUSIONS AND SUGGESTIONS

So at the end we will say that with this rate of error between the original model with test machine we can the original model can replace the test machine with just 5,57% of error rate but with faster results and without cost, and we can make several measurements for a person's knee size to be repaired.

It can be said that the application of the multibody model saves time as there is no involvement of the tibia and femur, as needed for the knee prosthesis. More importantly, as the application of the test machine is omitted in our process, our model's approximations to a human knee are carried out directly. Thus, we can make several measurements for a person's knee size to be repaired without cost and we develop another knee prosthesis in ADAMS program by changing the femur as mentioned Figs 4.31, 4.35, and we got new results that can be better than the original model for the rotation part of the movements of the knee prosthesis.

In future work, we will try to create an Ankle virtual model in order to get a new virtual model for the complete human leg with the knee and ankle and all required movements. Furthermore, analysis of the anatomical angles such as the different rotations as human full legs, abduction, and adduction will be conducted.

7. SUMMARY

IMPROVEMENT OF KNEE PROSTHESIS GEOMETRY

In summary, the human knee joint usually suffers progressive deterioration with time. The conventional cure of this issue is to replace it with an alternate knee by applying the prosthesis implant. The reason is that the process causes the abrasion of the different materials rather than just sliding or rolling. This study aims to develop the numerical measurement of the knee prosthesis's geometry, which fulfils the mechanical requirements of the human knee. The MSC.ADAMS programme was applied to demonstrate the movement of the human knee joint in terms of rotation and flexion. The changes between the condyles of the developed multibody of the prosthesis related to the flexion angle ranging from 20–120° were investigated and presented. The boundary conditions were determined, and simulations performed using the ADAM's programme. An average value of 0.7 was reached for the slip ration, with the maximum getting up to 0.79. An angle between 110–120° for the flexion angle was obtained. Three-dimensional geometry was applied in the new virtual model, taking into account the influence of the condyles and collateral. The multibody modelling was used to measure the degree of flexion and rotation of the knee concerning its position, like extension, flexion or rotation, and insert a spring between the tibia and femur while observing its effects on the performance of the knee.

It can be said that the application of the multibody model saves time as there is no involvement of the tibia and femur, as needed for the knee prosthesis. More importantly, as the application of the test machine is omitted in our process, our model's approximations to a human knee are carried out directly. Without cost, we can make several measurements for a person's knee size to be repaired.

A slip ration, which is higher than 0.45, was achieved as was the limit in literature. Applying our model, an average value of 0.7 was reached, with the maximum reaching up to 0.79 and obtaining an angle between 110–120° for the flexion angle. The generated virtual model was used to measure the knee prosthesis size before its creation.

Finally, this virtual model could be used to measure the knee prosthesis size before creating it because it saves time, money, and effort instead of using 3D printing technology, and CNC milling consumes our time, money, and effort. So we can say that The multibody model method measurement created can replace the test machine for doing measurement of the prosthesis. Therefore it can serve as a basis for further scientific research. We proved in our method that the factors of the knee prosthesis have a significant influencing effect on the resulting joint kinematics. The ranges recommended by specialists for each prosthesis parameter were confirmed by measurements.

7. ÖSSZEFOGLALÁS (SUMMARY IN HUNGARIAN)

TÉRDPROTÉZIS GEOMETRIA JAVÍTÁSA

Összefoglalva, az emberi térdízület általában idővel fokozatosan romlik. Ennek a problémának a hagyományos gyógymódja az, hogy protézis implantátumot alkalmazunk. Ennek egyik problémája lehet, hogy a nem megfelelő geometria miatt a használat közben a csúszva gördülésre tervezett a protézis anyag további igénybevételt kap, ami kopást, kilazulást okozhat. A tanulmány célja a térdprotézis geometriájának numerikus mérésének kidolgozása, amely megfelel az emberi térd mechanikai mozgásviszonyainak. Az MSC.ADAMS programot alkalmaztam az emberi térdízület mozgásának bemutatására rotáció és hajlítás szempontjából. Megvizsgáltam és bemutattam a protézis kifejlesztett többtestének condylusai között a 20-120°-os hajlítási szöggel kapcsolatos változásokat. A peremfeltételek meghatározása és szimulációi az ADAM program segítségével történtek. A csúszás aránya 0,7-es átlagértéket értek el, a maximum pedig 0,79-re emelkedett. A hajlítási szög 110-120° közötti szöget vett fel. Az új virtuális modellben háromdimenziós geometriát alkalmaztam, figyelembe véve a condylusok és a kollaterális hatását. A többtest modellezést arra használtam, hogy megmérjem a térd hajlításának és elfordulásának mértékét a helyzetére vonatkozóan, mint például a nyújtás, hajlítás vagy elforgatás, és rugót helyeztem be a sípcsont és a combcsont közé, miközben megfigyeltem annak a térd kinematikájára gyakorolt hatását.

Elmondható, hogy a többtest modell alkalmazása időt takarít meg, mivel a térdprotézis vizsgálatához nem szükséges a sípcsont és a combcsont fizikai modellje. Ennél is fontosabb, hogy mivel a tesztgép alkalmazását kihagyjuk a folyamatunkból, a modellünk emberi térdre való közelítését közvetlenül hajtjuk végre. Többletköltség nélkül több mérést is elvégezhetünk a újabb térdprotézis geometriákkal.

0,45-nél nagyobb csúszási arányt értem el, ahogy az irodalomban is megengedett. Modellemet alkalmazva 0,7-es átlagértéket értem el, a maximum elérte a 0,79-et és 110-120° közötti szöget kaptunk a hajlítási szögre. A generált virtuális modellt a térdprotézis kinematikájának mérésére használtam annak legyártása előtt.

Végül ezzel a virtuális modellel megmérhetjük a térdprotézis mozgását a gyártás előtt, amivel időt, pénzt és erőfeszítést takaríthatunk. Nincs szükség sem a 3D nyomtatási technológia sem a CNC marás segítségével létrehozott fizikai modellre, ami időt, pénzt és erőforrásokat emésztene fel. Így elmondhatjuk, hogy a megalkotott többtest modell módszerrel végzett mérés helyettesítheti a protézis mérésére szolgáló tesztgépet. Ezért további tudományos kutatások alapjául szolgálhat. Módszerünkkel igazoltuk, hogy a térdprotézis geometriája jelentős mértékben befolyásolja a kialakuló ízületi kinematikát. A szakemberek által az egyes protézisparaméterekre javasolt tartományokat mérésekkel igazoltuk

8. APPENDICES

A1: Bibliography

- 1 Ardestani, M.M., Moazen, M., Jin, Z., 2015. The Knee Contribution of geometric design parameters to knee implant performance : Conflicting impact of conformity on kinematics and contact mechanics. *The Knee* 22, 217–224. <https://doi.org/10.1016/j.knee.2015.02.011>
- Balassa, G.P., 2019. Development and examination of a knee prosthesis geometry. *Műszaki Tudományos Közlemények* 11, 27–30. <https://doi.org/https://doi.org/10.33895/mtk-2019.11.03>
- Barber, C.E.H., Marshall, D.A., Mosher, D.P., Akhavan, P., Houghton, K., Batthish, M., Levy, D.M., Schmeling, H., Tibollo, H., Grant, S., Khodyakov, D., Lacaille, D., Barber, C.E.H., Marshall, D.A., Mosher, D.P., Akhavan, P., Tucker, L., Houghton, K., Batthish, M., Levy, D.M., Schmeling, H., Ellsworth, J., Tibollo, H., Grant, S., Khodyakov, D., Lacaille, D., 2016. Development of System-level Performance Measures for Evaluation of Models of Care for Inflammatory Arthritis in Canada Development of System-level Performance Measures for Evaluation of Models of Care for Inflammatory Arthritis in Canada. <https://doi.org/10.3899/jrheum.150839>
- Barzan, M., Modenese, L., Carty, C.P., Maine, S., Stockton, C.A., Sancisi, N., Lewis, A., Grant, J., Lloyd, D.G., Brito da Luz, S., 2019. Development and validation of subject-specific pediatric multibody knee kinematic models with ligamentous constraints. *Journal of Biomechanics* 93, 194–203. <https://doi.org/10.1016/j.jbiomech.2019.07.001>
- Bert, J.M., 2005. Unicompartmental knee replacement. *Orthopedic Clinics of North America*. <https://doi.org/10.1016/j.ocl.2005.05.001>
- Beverland, D.E., Sheridan, G.A., 2021. Arthroplasty Today Knee Flexion Angle Measurement Using Virtual Assessment Tools : Correct Procedure and Potential Pitfalls. <https://doi.org/10.1016/j.artd.2021.11.012>
- Bonasia, K., Sekeres, M.J., Gilboa, A., Grady, C.L., 2018. Title : Prior Knowledge Modulates the Neural Substrates of Encoding and Retrieving Naturalistic Events at Short and Long Delays Neurobiology of Learning and Memory Prior knowledge modulates the neural substrates of encoding and retrieving naturalistic eve. *Neurobiology of Learning and Memory* 0–1. <https://doi.org/10.1016/j.nlm.2018.02.017>
- Bull, A.M.J., Kessler, O., Alam, M., Amis, A.A., 2008. Changes in knee kinematics reflect the articular geometry after arthroplasty. *Clinical Orthopaedics and Related Research*. <https://doi.org/10.1007/s11999-008-0440-z>
- Christiansen, B.A., Anderson, M.J., Lee, C.A., Williams, J.C., Yik, J.H.N., Haudenschild, D.R., 2012. Musculoskeletal changes following non-invasive knee injury using a novel mouse model of post-traumatic osteoarthritis. *Osteoarthritis and Cartilage* 20, 773–782. <https://doi.org/10.1016/j.joca.2012.04.014>
- Chui, C.S., Leung, K.S., Qin, J., Shi, D., Augat, P., Wong, R.M.Y., Chow, S.K.H., Huang, X.Y., Chen, C.Y., Lai, Y.X., Yung, P.S.H., Qin, L., Cheung, W.H., 2020. Population-Based and Personalized Design of Total Knee Replacement Prosthesis for Additive Manufacturing Based on Chinese anthropometric Data. *Engineering*. <https://doi.org/10.1016/j.eng.2020.02.017>

- Crane, C.D., 2016. Joint Angle Measurement Using Strategically Placed Accelerometers and Gyroscope 8, 1–7. <https://doi.org/10.1115/1.4031299>
- Csizmadia, M., 2017. érdprotézisek kinematikai vizsgálatához kifejlesztett vizsgálóberendezés összefoglaló bemutatása Balassa Gábor Péter, M. Csizmadia Béla. <https://doi.org/10.17489/biohun/2017/1/05>
- Damsgaard, M., 2006. Analysis of musculoskeletal systems in the AnyBody Modeling System 14, 1100–1111. <https://doi.org/10.1016/j.simpat.2006.09.001>
- Delp, S.L., Loan, J.P., Hoy, M.G., Zajac, F.E., Topp, E.L., Rosen, J.M., 1990. An Interactive Graphics-Based Model of the Lower Extremity to Study Orthopaedic Surgical Procedures. *IEEE Transactions on Biomedical Engineering* 37, 757–767. <https://doi.org/10.1109/10.102791>
- DeMers, M.S., Pal, S., Delp, S.L., 2014. Changes in tibiofemoral forces due to variations in muscle activity during walking. *Journal of Orthopaedic Research* 32, 769–776. <https://doi.org/10.1002/jor.22601>
- Feder, S.M., Levy, M.S., 1992. LOCATION-DEPENDENT VARIATIONS IN THE MATERIAL PROPERTIES OF THE ANTERIOR CRUCIATE LIGAMENT 25.
- Fekete, G., Wahab, M.A., Baets, P. De, 2011. Analytical and Computational Estimation of Patellofemoral Forces in the Knee Under Squatting and Isometric Motion. *Sustainable Construction and Design* 246–257.
- Flores, P., 2008. Kinematics and Dynamics of Multibody Systems with Imperfect Joints ► Presents suitable methodologies for the dynamic analysis of multibody mechanical systems with joints ► Studies and case studies of real and imperfect joints. *Book multibody* 34, 6221.
- Freeman, M.A.R., Pinskerova, V., 2005. The movement of the normal tibio-femoral joint. *Journal of Biomechanics* 38, 197–208. <https://doi.org/10.1016/j.jbiomech.2004.02.006>
- Frigo, C., Pavan, E.E., Brunner, R., 2010. A dynamic model of quadriceps and hamstrings function. *Gait and Posture*. <https://doi.org/10.1016/j.gaitpost.2009.09.006>
- Gabriel, M.T., Eric, I., Woo, S.L., Yagi, M., Debski, R.E., 2004. Distribution of in situ forces in the anterior cruciate ligament in response to rotatory loads 22, 8–12.
- Gill, R.H.S., 2016. Biomechanics of the lower limb. *Surgery* 1–9. <https://doi.org/10.1016/j.mpsur.2016.06.007>
- Girase, H., Nyayapati, P., Booker, J., Lotz, J.C., Bailey, J.F., Matthew, R.P., 2021. Automated assessment and classification of spine , hip , and knee pathologies from sit-to-stand movements collected in clinical practice. *Journal of Biomechanics* 128, 110786. <https://doi.org/10.1016/j.jbiomech.2021.110786>
- Guerin, B., Jouvion, A., Brier, M.G. De, Trappier, T., Thefenne, L., 2013. Hunting prosthesis for a upper limb amputation Posters English version Coupled analysis of the kinetic data of gait and functional MRI of the amputee . A case of brain plasticity and late acquisition of gait from a patient with congenital lower limbs atro. *Annals of Physical and Rehabilitation Medicine* 56, e31–e32. <https://doi.org/10.1016/j.rehab.2013.07.190>
- Guillemin, F., Rat, A.C., Mazieres, B., Pouchot, J., Fautrel, B., Euller-Ziegler, L., Fardellone, P., Morvan, J., Roux, C.H., Verrouil, E., Saraux, A., Coste, J., 2011. Prevalence of symptomatic hip and knee osteoarthritis: A two-phase population-based survey1. *Osteoarthritis and Cartilage* 19, 1314–1322. <https://doi.org/10.1016/j.joca.2011.08.004>
- Hroncová, D., Delyová, I., Frankovský, P., 2014. Kinematic analysis of mechanisms

- using MSC Adams. *Applied Mechanics and Materials* 611, 83–89.
<https://doi.org/10.4028/www.scientific.net/AMM.611.83>
- Hu, G., Wang, W., Chen, B., Zhi, H., Li, Y., Shen, Y., Wang, K., 2021. Concurrent validity of evaluating knee kinematics using Kinect system during rehabilitation exercise ☆. *Medicine in Novel Technology and Devices* 11, 100068.
<https://doi.org/10.1016/j.medntd.2021.100068>
- Hughes, H. V, Tj, J., 2020. Proteomic comparison of osteoarthritic and reference human menisci using data-independent acquisition mass spectrometry *Osteoarthritis* 28, 1092–1101. <https://doi.org/10.1016/j.joca.2020.05.001>
- Hyodo, K., Kanamori, A., Kadone, H., 2020. Arthroplasty Today Gait Analysis Comparing Kinematic , Kinetic , and Muscle Activation Data of Modern and Conventional Total Knee Arthroplasty. *Arthroplasty Today* 6, 338–342.
<https://doi.org/10.1016/j.artd.2020.03.011>
- Id, H.A.L., 2021. Prise en charge des douleurs articulaires : exemples de l ’ arthrose et des douleurs post traumatiques Océane Mahé To cite this version : HAL Id : hal-03297909 soutenance et mis à disposition de l ’ ensemble de la Contact : ddoc-thesesexercice-contact@uni.
- Imhauser, C.W., Kent, R.N., Boorman-Padgett, J., Thein, R., Wickiewicz, T.L., Pearle, A.D., 2017. New parameters describing how knee ligaments carry force in situ predict interspecimen variations in laxity during simulated clinical exams. *Journal of Biomechanics* 64, 212–218.
<https://doi.org/10.1016/j.jbiomech.2017.09.032>
- Jones, C.D.S., Grimshaw, P.N., 2010. *The Biomechanics of the Anterior Cruciate Ligament and Its Reconstruction*.
- K. Markolf, Mensch, & Amstutz, 1976; Nielsen, Rasmussen, Ovesen, & Andersen, 1984, n.d. *Medial-Side Injury of the Knee*.
- Katona, G., M. Csizmadia, B., Andrónyi, K., 2015. Determination of reference function to knee prosthesis rating. *Biomechanica Hungarica*.
<https://doi.org/10.17489/biohun/2013/1/31>
- Kheireddine, Z., Oldal, I., 2021. Numerical measurement of a virtual model for the knee prosthesis geometry. *Applied Sciences (Switzerland)* 11.
<https://doi.org/10.3390/app11062541>
- Kierkegaard, S., Jørgensen, P.B., Søballe, K., Mechlenburg, I., 2015. Pelvic movements are restored to reference values during stair climbing but not during stepping one year after uni-compartmental knee arthroplasty - A secondary analysis of a randomized controlled trial. *Osteoarthritis and Cartilage* 23, A111–A112. <https://doi.org/10.1016/j.joca.2015.02.830>
- Klein, F., Sommerfeld, A., 2014. *The Theory of the Top. Volume IV. The Theory of the Top. Volume IV*. <https://doi.org/10.1007/978-0-8176-4829-9>
- Komdeur, P., Pollo, F.E., Jackson, R.W., 2002. Dynamic Knee Motion in Anterior Cruciate Impairment: A Report and Case Study. *Baylor University Medical Center Proceedings* 15, 257–259.
<https://doi.org/10.1080/08998280.2002.11927850>
- Komistek, R.D., Mahfouz, M.R., Bertin, K.C., Rosenberg, A., Kennedy, W., 2008. In Vivo Determination of Total Knee Arthroplasty Kinematics A Multicenter Analysis of an Asymmetrical Posterior Cruciate Retaining Total Knee Arthroplasty 23, 41–50. <https://doi.org/10.1016/j.arth.2007.01.016>
- Lenz, M., Acklin, Y.P., Kasper, L.A., Mischler, D., Varga, P., Zderic, I., Gehweiler, D., Klos, K., Gueorguiev, B., Stoffel, K., 2021. Biomechanical evaluation of the docking nail concept in periprosthetic fracture fixation around a stemmed total

- knee arthroplasty. *Journal of Biomechanics* 115, 110109.
<https://doi.org/10.1016/j.jbiomech.2020.110109>
- Lepoutre, J.P., 2007. Modélisation biomécanique du mouvement : Vers un outil d'évaluation pour l'instrumentation en orthopédie. These.
- Merkher, Y., Sivan, S.S., Etsion, I., 2006. A rational human joint friction test using a human cartilage-on-cartilage arrangement a rational friction test using a human cartilage on cartilage arrangement. *Tribology Letters*.
<https://doi.org/10.1007/s11249-006-9069-9>
- Mesfar, W., 2005. Biomechanics of the knee joint in flexion under various quadriceps forces 12, 424–434. <https://doi.org/10.1016/j.knee.2005.03.004>
- Mommersteeg, T.J.A., Blankevoort, L., Huiskes, R., Kooloost, J.G.M., 1996. CHARACTERIZATION OF THE MECHANICAL KNEE LIGAMENTS : APPROACH OF 29, 151–160.
- Moreno, J.C., Lima, E.R. De, Brunetti, F.J., Pons, L., 2006. Design and implementation of an inertial measurement unit for control of artificial limbs : Application on leg orthoses 118, 333–337.
<https://doi.org/10.1016/j.snb.2006.04.039>
- NAGY, D., SZENDRŐ, P., NAGY, J., BENSE, L., 2015. Synergy 2015 International Conference, in: Research & Development. pp. 21–28.
- Nguyen, H.C., Paul, W., Egmond, N. Van, Weinans, H., Slump, C.H., Sackers, R.J.B., Custers, R.J.H., 2021. The need for a standardized whole leg radiograph guideline : The effects of knee flexion , leg rotation , and X-ray beam height. *Journal of Cartilage & Joint Preservation* 1, 100022.
<https://doi.org/10.1016/j.jcjp.2021.100022>
- Niitsu, M., n.d. of the 569–570.
- Nomura, E.U., Horiuchi, Y., Kihara, M., 2000. Medial patellofemoral ligament restraint in lateral patellar translation and reconstruction 1–7.
- Of, V., Of, A.T.M., Knee, T.H.E., 1996. TECHNICAL NOTE VALIDATION OF A THREE-DIMENSIONAL MODEL OF THE KNEE 29, 955–961.
- Olinski, M., Gronowicz, A., Handke, A., Ceccarelli, M., 2016. Design and characterization of a novel knee articulation mechanism. *International Journal of Applied Mechanics and Engineering* 21, 611–622. <https://doi.org/10.1515/ijame-2016-0037>
- Paelinck, L., 2018. Automatic Segmentation of the Lower Limb Anatomy Automatic Segmentation of 2016–2018.
- Pataky, T.C., Koseki, M., Cox, P.G., 2016. Probabilistic biomechanical finite element simulations: Whole-model classical hypothesis testing based on upcrossing geometry. *PeerJ Computer Science* 2016, 1–21. <https://doi.org/10.7717/peerj-cs.96>
- Pearcy, M., 1999. A three-dimensional definition for the flexion / extension and abduction / adduction angles 37, 440–444.
- Penney, L.M., David, E., Witt, L.A., 2011. A review of personality and performance: Identifying boundaries, contingencies, and future research directions. *Human Resource Management Review* 21, 297–310.
<https://doi.org/10.1016/j.hrmr.2010.10.005>
- Petersen, W., Sekiya, J.K., 2006. Anterior cruciate ligament anatomy and function relating to anatomical reconstruction 982–992. <https://doi.org/10.1007/s00167-006-0076-z>
- Phruetthiphat, O., Zampogna, B., Vasta, S., Tassanawipas, B., Gao, Y., Callaghan, J.J., 2021. TKR after posttraumatic and primary knee osteoarthritis : a

- comparative study 8, 1–8.
- Popescu, A.L., 2009. Mechanisms of gustatory coding in *Spodoptera littoralis* To cite this version : HAL Id : pastel-00004445.
- Postolka, B., Schütz, P., Fucentese, S.F., Freeman, M.A.R., Pinskerova, V., List, R., Taylor, W.R., 2020. Tibio-femoral kinematics of the healthy knee joint throughout complete cycles of gait activities. *Journal of Biomechanics* 110, 109915. <https://doi.org/10.1016/j.jbiomech.2020.109915>
- Preliminary, A., 1982. THE TOTAL FEMORAL PROSTHESIS.
- Price, A.J., Alvand, A., Troelsen, A., Katz, J.N., Hooper, G., Gray, A., Carr, A., Beard, D., 2018. Hip and knee replacement 2 Knee replacement. *The Lancet* 392, 1672–1682. [https://doi.org/10.1016/S0140-6736\(18\)32344-4](https://doi.org/10.1016/S0140-6736(18)32344-4)
- Quinlan, N.D., Wu, Y., Chiamonti, A.M., Guess, S., Barfield, W.R., Yao, H., Pellegrini, V.D., 2020. Functional Flexion Instability After Rotating-Platform Total Knee Arthroplasty. *The Journal of bone and joint surgery* 102, 1694–1702. <https://doi.org/10.2106/JBJS.19.01403>
- Richards, C., Higinson, J.S., 2010. Knee contact force in subjects with symmetrical OA grades: Differences between OA severities. *Journal of Biomechanics* 43, 2595–2600. <https://doi.org/10.1016/j.jbiomech.2010.05.006>
- Ristaniemi, A., Torniainen, J., Paakkonen, T., Stenroth, L., Finnilä, M.A.J., Tanska, P., Töyräs, J., Korhonen, R.K., 2021. Biomechanical , biochemical , and near infrared spectral data of bovine knee ligaments and patellar tendon. *Data in Brief* 36, 106976. <https://doi.org/10.1016/j.dib.2021.106976>
- Sciences, E.D., Mouvement, D.U., Cnrs, I.S.M.U.M.R., Royer, P., Argenson, J., 2019. UNIVERSITE D ' AIX-MARSEILLE Jean-Baptiste RENAULT.
- Seel, T., Raisch, J., Schauer, T., 2014. IMU-Based Joint Angle Measurement for Gait Analysis 6891–6909. <https://doi.org/10.3390/s140406891>
- Society, I., Conference, S., Activities, O., 2020. A PRACTICAL OPEN-SOURCE COMPARISON OF DISCRETE AND CONTINUOUS BIOMECHANICAL ANALYSIS TECHNIQUES Stuart A . McErlain-Naylor 180–183.
- Steckel, H., Starman, J.S., Baums, M.H., Klinger, H.M., Schultz, W., Fu, F.H., 2007. The double-bundle technique for anterior cruciate ligament reconstruction : a systematic overview 99–108. <https://doi.org/10.1111/j.1600-0838.2006.00600.x>
- Subit, D., 2005. Mod ´ elisation de la liaison os-ligament dans l ´ articulation du genou To cite this version :
- Takahashi, A., Sano, H., Ohnuma, M., 2012. Patellar morphology and femoral component geometry influence patellofemoral contact stress in total knee arthroplasty without patellar resurfacing 1787–1795. <https://doi.org/10.1007/s00167-011-1768-6>
- Tang, J., Zhao, J., 2021. Simultaneous Anterior Cruciate Ligament, Posterior Cruciate Ligament, Posteromedial Corner, and Posterolateral Corner Reconstruction of the Knee. *Arthroscopy Techniques* 10, e2723–e2731. <https://doi.org/10.1016/j.eats.2021.08.019>
- Taylor, A.J., Carpenter, W., Runner, R.P., 2021. Arthroplasty Today Staged Bilateral Total Knee Arthroplasty for Neglected Blount Disease Using a Gap Balancing Technique. *Arthroplasty Today* 11, 25–31. <https://doi.org/10.1016/j.artd.2021.07.009>
- Thelen, D.G., Chumanov, E.S., Best, T.M., Swanson, S.C., Heiderscheit, B.C., 2005. Simulation of biceps femoris musculotendon mechanics during the swing phase of sprinting. *Medicine and Science in Sports and Exercise* 37, 1931–1938. <https://doi.org/10.1249/01.mss.0000176674.42929.de>

- Tørholm, S., Rasmussen, J., Damsgaard, M., Christensen, S.T., 2000. Inverse-inverse dynamics simulation of musculo-skeletal systems.
- Vince, K.G., 2014. The problem total knee replacement systematic, comprehensive and efficient evaluation. *The bone and joint journal* 96, 105–111. <https://doi.org/10.1302/0301-620X.96B11.34531>
- Wang, F., Xue, H., Ma, T., Yang, T., Wen, T., Tu, Y., 2021. Prosthesis size distribution in Oxford phase III unicompartmental knee arthroplasty - Based on more than 1900 Chinese patients. *Journal of Orthopaedics* 25, 230–236. <https://doi.org/10.1016/j.jor.2021.05.019>
- Warren, R.F., 2017. Ligament Injury Is More Common Than We Thought. *Arthroscopy: The Journal of Arthroscopic and Related Surgery* 33, 2182–2183. <https://doi.org/10.1016/j.arthro.2017.09.010>
- Weiss, J., 2014. Computational Modeling of Ligament Mechanics Computational Modeling of Ligament Mechanics. <https://doi.org/10.1615/CritRevBiomedEng.v29.i3.20>
- Williams, A., Logan, M., 2004. Understanding Tibio-Femoral motion. *Knee* 11, 81–88. <https://doi.org/10.1016/j.knee.2003.12.004>
- Winter, D.A., Winter, D.A., 2013. Biomechanics of Normal and Pathological Gait : Implications for Understanding Human Locomotor Control University of Waterloo either surgically , biochemically or electrically , human gait has not been search Council of Canada (Grant MT4343), the Nationa 37–41. <https://doi.org/10.1080/00222895.1989.10735488>
- Wolf, A., Wartzack, S., 2018. PARAMETRIC MOVEMENT SYNTHESIS : TOWARDS VIRTUAL OPTIMISATION OF MAN- MACHINE INTERACTION IN ENGINEERING DESIGN 941–952.
- Z. KHEIREDDINE, I.O., 2019. Virtual Testing Method of Human Knee Prosthesis 4, 386–392. <https://doi.org/10.21791/IJEMS.2019.1.48.fibula>
- Zanasi, S., 2011. Innovations in total knee replacement : new trends in operative treatment and changes in peri-operative management. *Eur Orthop Traumatol* 21–31. <https://doi.org/10.1007/s12570-011-0066-6>
- Zatsiorsky, V.M., Motion, H., 2005. Book review 38, 1371–1372. <https://doi.org/10.1016/j.jbiomech.2004.07.001>
- Zeng, Y.M., Yan, M.N., Li, H.W., Zhang, J., Wang, Y., 2020. Does mobile-bearing have better flexion and axial rotation than fixed-bearing in total knee arthroplasty? A randomised controlled study based on gait. *Journal of Orthopaedic Translation* 20, 86–93. <https://doi.org/10.1016/j.jot.2019.07.009>
- Zheng, L., Carey, R., Thorhauer, E., Tashman, S., Harner, C., Zhang, X., 2017. In vivo tibiofemoral skeletal kinematics and cartilage contact arthrokinematics during decline walking after isolated meniscectomy. *Medical Engineering and Physics* 0, 1–8. <https://doi.org/10.1016/j.medengphy.2017.10.014>
- Zhong, Y., Wang, Y., Wang, H., Rong, K., Xie, L., 2011. Stress changes of lateral collateral ligament at different knee flexion with or without displaced movements: a 3-dimensional finite element analysis. *Chinese Journal of Traumatology English Edition* 14, 79–83. <https://doi.org/10.3760/cma.j.issn.1008-1275.2011.02.003>
- Zhou, F., Xue, F., Zhang, S., 2020. The application of 3D printing patient specific instrumentation model in total knee arthroplasty. *Saudi Journal of Biological Sciences* 27, 1217–1221. <https://doi.org/10.1016/j.sjbs.2020.02.017>

A2: Publications related to the dissertation

Refereed papers in foreign languages:

1. **Zehouani Kh**, Boukhari A, (2018), study of Rayleigh Bernard convection by lattice Boltzmann method, Modern environmental science and engineering, New York, USA, 4 (9), 867-871, *Doi: 10.15341/mese(2333-2581)/09.04.2018/001*.
2. **Zehouani Kh**, Oldal I,(2019), Virtual testing method of human knee prosthesis, International Journal of Engineering and Management Sciences (IJEMS), Debrecen, Hungary, Vol.4,386-392. *DOI: 10.21791/IJEMS.2019.1.48*.
3. **Zehouani Kh**, Oldal I,(2021), Developing of Knee Prosthesis in ADAMS Program, Mechanical Engineering Letters, Godollo, Hungary, HU ISSN 2060-3789.
4. **Zehouani Kh**, Oldal I,(2021), Study of Heat Transfer in a Cylinder Subject to Robin's Conditions, Mechanical Engineering Letters, Godollo, Hungary, HU ISSN 2060-3789.
5. **Zehouani Kh**, Oldal I,(2021), Numerical Measurement of a Virtual Model for the Knee Prosthesis Geometry, Applied sciences, Basel, Switzerland, 11(6), 2541 <https://doi.org/10.3390/app11062541>.
6. **Zehouani Kh**, Oldal I,(2021), Improvement of the test machine for knee prosthesis, Open Journal of Polymer Chemistry, Hong Kong, China, under prosering.
7. **Zehouani Kh**, Oldal I,(2022), Developing the kinematic motion of Multibody model for the knee prosthesis geometry, International Journal for Engineering Modelling, Zagreb, Croatia, under reviewer.

International conference proceedings:

8. **Zehouani Kh**, Oldal I, study of Rayleigh Bernard convection by lattice Boltzmann method,23rd workshop on energy and environment, Gödöllő, Hungary.2017
9. **Zehouani Kh.**, Oldal I,Virtual testing method of human knee prosthesis, International Scientific Conference On Advances In Mechanical Engineering, Debrecen, Hungary, October 11-13, 2018.
10. **Zehouani Kh.**, Oldal I, flexion-rotation angle of the new model of the knee prosthesis in ADAMS program. BPS Conference in Mechanical Engineering, Gödöllő, Hungary.2019.
11. **Zehouani Kh.**, Oldal I, Multi-body model of the knee prosthesis in ADAMS program, International Conference on Engineering & Technology (ICET-19),Ottawa,Canada.2019

International conference abstracts:

12. **Zehouani Kh.**, Oldal I, Study of Heat Transfer in a Cylinder, Synergy international conferences-engineering, Agriculture and green industry innovation, Gödöllő, Hungary, October 12-15,2017.
13. **Zehouani Kh.**, Oldal I,Test machine of knee prosthesis geomtry, 24rd workshop on energy and environment, Gödöllő, Hungary,2018.

9. ACKNOWLEDGEMENTS

This PhD work has been accomplished at Institute for Mechanical Engineering Technology, Faculty of Mechanical Engineering, MATE University- Gödöllő, between October 2017 and January 2022.

The PhD program including the present research is supported by Stipendium Hungaricum Scholarship Program.

I would like to acknowledge my most profound gratitude to my supervisors Dr. Oldal Istvan for his valuable recommendations, advice, excellent guidance and continuous encouragement during my PhD research. This dissertation would not have been possible without his considerable academic support and it was my pleasure to work under his supervision and learn the sober scientific research ways. Additionally, I desire to extend my sincere gratitude to all the team of Institute for Mechanical Engineering Technology.

In addition, I would like to express my thanks and gratitude to the head of Doctoral School of Mechanical Engineering Prof. Dr. Gábor Kalácska for his valuable advice and fatherly dealing throughout my research years which has dramatically contributed to facilitate the completion of the doctoral degree.

This scientific work is dedicated to my family, in particular, my father Ammar Zehouani and my mother Samira Houideg for their financial and moral support.

Kheireddine Zehouani

Gödöllő, 2022